



UNIVERSIDAD AUTÓNOMA DE SAN LUIS POTOSÍ

FACULTAD DE CIENCIAS QUÍMICAS

CENTRO DE INVESTIGACIÓN Y ESTUDIOS DE POSGRADO

**ESTUDIO DE LA ESTABILIZACIÓN QUÍMICA DE PEROVSKITAS
PARA SU POTENCIAL APLICACIÓN EN CELDAS
FOTOVOLTAICAS EN CONDICIONES AMBIENTALES**

TESIS QUE PARA OBTENER EL GRADO DE
DOCTOR EN CIENCIAS EN INGENIERIA QUIMICA

PRESENTA

MC CESAR MANUEL DEL ANGEL OLARTE

DIRECTOR DE TESIS

DRA ALMA GABRIELA PALESTINO ESCOBEDO



SAN LUIS POTOSÍ, SLP MAYO 2021

El programa de maestría en Ciencias de la Ingeniería Química de la Universidad Autónoma de San Luis Potosí pertenece al Programa Nacional de Posgrados de Calidad (PNPC) del CONACYT, registro 000897, en el nivel Consolidado.

Número de registro de la beca otorgada por CONACyT: 635246



ESTUDIO DE LA ESTABILIZACIÓN QUÍMICA DE PEROVSKITAS PARA SU POTENCIAL APLICACIÓN EN CELDAS FOTOVOLTAICAS EN CONDICIONES AMBIENTALES por César Manuel Del Ángel Olarte se distribuye bajo una [Licencia Creative Commons Atribución-NoComercial-SinDerivadas 4.0 Internacional](https://creativecommons.org/licenses/by-nc-nd/4.0/).

*To my beloved father,
this is a piece of what your son can do,
thank you for everything.*

ACKNOWLEDGEMENTS

Everything started in Manchester, UK. It was just a vague idea about something I wanted to create. I did not know nothing about perovskites or solar cells. Then, I talked with the first person who believed in my skills to perform something different. Dra. Gabriela Palestino. Who She became my tutor for the second time, now in a Ph.D. project. Thanks to her, I could make possible the idea I had in mind, develop my research skills by myself and continue learning about this exciting research world.

Moreover, she gathered a group of specialists who guided me during these four years. Thanks to them, I did not lose my direction during the development of the project. Dr. Ángel Gabriel Rodríguez Vázquez, Dra. Guadalupe Cárdenas, Dr. Antonio Méndez, Dra. Estela Calixto Rodríguez, Dr. Luis Felipe Cházaro, Dra. Harumi Moreno, all of you represented a real challenge to me, and I thank you for the ideas, suggestions, and direction in the past four years.

During the development of the project, I also learned from other students. Gerardo Bucrin helped me in a summer course to establish the first parameters for substrate preparation and film deposition. Thank you for sharing your ideas. I hope you also learned from me during your short staying. To the students: Raul Itzae, Karla Gallegos, and Ivana Ortega, who made possible the electrical characterization of the material and additional microscopic assessments. And Erick Joshua Martínez, my adventure buddy, stayed for a year helping me synthesize thin-films. With his help I develop the set-up for thin-film deposition, solve technical issues, and try every idea to obtain every day, a better film. Thank you for everything!

I would like to thank the technicians Fernando Rodríguez and Gregorio Balderas for helping me in the microscopic characterization of the films, scanning electron, and atomic force microscopy, respectively. And the technicians' Rosa Lina Tovar and Claudia Hernández for their help in the crystallographic characterization.

I also counted on my great friends, who supported me in many different ways: Miguel Olvera and Jorge Huerta, I have many stories with you, and I thank you for encouraging me to finish what I started. Felipe Garay always shared an opinion related to research doubts, material preparation, and writing issues.

And my beloved wife, Melina Matus, thank you for encouraging and supporting me in every moment, for understanding the path of a research student, and for sharing this journey with me. I love you.

RESUMEN

La eficiencia, el costo y la estabilidad son las tres características más importantes que un dispositivo fotovoltaico debe cumplir para poder considerarse como posible producto comercial. En los últimos años un nuevo tipo de celdas ha captado el interés de la comunidad científica, cuyo componente principal es una perovskita híbrida orgánica-inorgánica. Los dispositivos estudiados han logrado eficiencias hasta de 20%, empleando métodos de depósito sencillos. Estos grandes avances se han logrado con el empleo de la perovskita $\text{CH}_3\text{NH}_3\text{PbI}_3$ como material absorbedor de radiación, sin embargo, debido a su naturaleza, estas celdas carecen de una estabilidad confiable. En este trabajo se emplea la técnica de blow-drying como un método alternativo para obtener películas delgadas de $\text{CH}_3\text{NH}_3\text{PbI}_3$ a partir de soluciones con diferente concentración, empleando aire caliente (25% humedad relativa, 90 °C) como gas de arrastre y condiciones de humedad controlada durante la formación de los depósitos. Mediante FTIR se verificó la química superficial de los depósitos, los cuales mostraron cierta hidratación cuando se empleó aire a 25 °C, misma que fue eliminada al emplear aire caliente. Además, los depósitos obtenidos por esta técnica consistieron en estructuras entrecruzadas conformadas por pequeños gránulos, de acuerdo con lo observado mediante MEB. La cobertura de los sustratos estuvo influenciada por la concentración de las soluciones empleadas para obtener los depósitos, obteniendo un mejor recubrimiento al emplear una solución de concentración 0.434 M. Por otro lado, se estudió la estabilidad de los depósitos obtenidos al ser expuestos a ambientes con humedades de 25%. En esta prueba destacó la estabilidad de los depósitos obtenidos empleando una solución 0.434 M, cuya resistencia a la degradación se extendió a más de 12 días en ambientes con 25% de humedad.

Palabras clave: perovskita, película delgada, blow-drying, celdas solares

ABSTRACT

Stability is still a property that limits the commercialization of perovskite solar cells. Thus, with the development of continuous deposition methods, it is essential to determine their feasibility in terms of stability and the efficiency of the devices produced. In this work, a hot air blow-drying (HABD) method is proposed as an alternative for the deposition of $\text{CH}_3\text{NH}_3\text{PbI}_3$ (MAPbI) perovskite thin-films. The ability of HABD to produce homogeneous and stable thin-films was systematically studied and compared with those produced with air at standard conditions (25 °C, 25% relative humidity). The MAPbI thin-films were characterized by infrared spectroscopy and X-ray diffraction revealing that air temperature rules the film hydration. Partial degradation after using air at standard conditions was observed in contrast with the stable and pure perovskite phase obtained when using air heated at 90 °C. The influence of solution concentration on the surface coverage was determined by scanning electron and atomic force microscopies. It was found that 4 μL of precursors solution (0.434 M) produced a homogeneous MAPbI thin-film with ~ 180 nm thickness and smooth surface ($R_q \sim 29$ nm) covering a 6.25 cm² area. Moreover, the outstanding optical and electrical properties of MAPbI were not affected by the deposition procedure. Remarkably, degradation tests demonstrate that our HABD method is capable of producing stable MAPbI thin-films with excellent resistance to degradation at ambient conditions (up to 15 days), which makes it a promising low-cost and easy to use method for the continuous fabrication of perovskite solar cells.

Keywords: perovskite, thin-films, blow-drying, solar cells

Contents

ACKNOWLEDGEMENTS	iv
RESUMEN	vi
ABSTRACT	vii
1. GENERAL INTRODUCTION	1
1.1 The perovskite compounds.	2
1.2 Hybrid perovskites.....	3
1.3 Perovskite solar cells.....	7
2. MOTIVATION OF THE PROJECT	11
2.1 Hypothesis.....	11
2.2 General Objective.....	12
2.3 Specific objectives.....	12
3. HYBRID PEROVSKITE MATERIALS: FUNDAMENTAL ASPECTS AND APPLICATIONS	14
3.1 Hybrid perovskite materials	14
3.2 Synthetic routes for perovskite thin-films	19
3.2.1 Coordination solvents	20
3.2.2 Deposition methodologies from solutions	22
3.2.2.1 Spin coating.....	23
3.2.2.2 Doctor blade	24
3.2.2.3 Slot-die coating[32].....	24
3.2.2.4 Spray-coating[33]	25
3.2.2.5 Blow-drying.....	26
3.2.3 Post-treatments.....	27
3.3 Properties of hybrid perovskites	29
3.3.1 Physical properties.....	29
3.3.1.1 Optical properties	29
3.3.1.2 Electrical properties.....	31
3.3.2 Chemical properties	33
3.3.2.1 Chemical stability	34

3.3.2.2 Thermal stability	36
3.4 Solar cells.....	38
3.4.1 Working principle of solar cells.....	39
3.4.2 Characteristics of solar cells[70]	41
3.4.3 State of the art of perovskite solar cells	46
4.4.3.1 High-efficiency perovskite solar cells.....	47
3.4.3.2 Large area perovskite solar cells.....	49
3.4.3.3 Stable perovskite photovoltaic devices.....	51
3.5 Conclusions and outlook	55
4. ONE-STEP METHOD FOR THE FABRICATION OF HIGH-QUALITY PEROVSKITE THIN-FILMS UNDER AMBIENT CONDITIONS: STABILITY, MORPHOLOGICAL, OPTICAL AND ELECTRICAL EVALUATION	57
4.1. Introduction.....	57
4.2 Thin Film Preparation	59
4.2.1 Materials and precursor solutions	59
4.2.2 Deposition procedure.....	59
4.3 Photovoltaic device preparation	60
4.4 Thin-film characterization	61
4.4 Results and discussion.....	62
4.4.1 Chemical composition.....	62
4.4.2 Crystallography	64
4.4.3 Thin Film Morphology	66
4.4.4 Textural properties	72
4.4.5 Optical properties.....	74
4.4.6 Chemical stability	76
4.4.7 Electrical properties	79
4.4.8 Photovoltaic performance	80
4.5 Conclusions.....	84
5. GENERAL CONCLUSIONS.....	87
APPENDIX. CHARACTERIZATION TECHNIQUES	89
Electromagnetic radiation	89

Optical absorption spectroscopy	91
Fourier Transformed Infrared Spectroscopy	92
X-ray diffraction	94
Scanning electron microscopy.....	96
Atomic force microscopy	97
Hall-effect measurement	99
I-V curve measurement	101
6. BIBLIOGRAPHY	104

Index of Figures

Figure 1 ABX ₃ perovskite structure and composition: a) the corner-sharing octahedra composed of B cations (in blue) and X anions (colored in red) enclosing the A cation (in gray), b) elements that can be combined to prepare a perovskite compound, each color corresponds to a specific site[1].....	2
Figure 2 Compositional and structural differences between the inorganic perovskite (a) and the hybrid perovskite (b) compound[2].....	3
Figure 3 External factors that affect the stability of a hybrid perovskite compound[3].	5
Figure 4 Comparison of the increase in photovoltaic efficiency for various thin-film technologies[4].....	8
Figure 5 Perovskite materials and their different properties, along with the corresponding crystal structure of the representative perovskite material[5].	14
Figure 6 Crystallographic information of perovskites: a) crystal structure showing the positions of the ions and b) tolerance factor and the effect of its value on the crystal structure, r_A , r_B , and r_X are the ionic radii of the corresponding ions.	16
Figure 7 Evolution of perovskite application in solar cells: a) a comparison in thickness reduction between dye-sensitized solar cells (DSSC), mesoporous (MSSC and solid states solar cells[11]; b) cross-sectional view of a “p-i-n” perovskite solar cell[12].	17

Figure 8 Ion library for the synthesis of hybrid perovskite materials, the “A” cation includes ammonium (M), cesium(Cs), hydroxylammonium (HA), hydrazinium (DA), methylammonium (MA), formamid (FM), formamidinium (FA), ethylammonium (EA), guanidine amine (GA) and dimethylamine (DEA). For the “B” site, metalloids from the group IV: Ge, Sn and Pb are considered. Halogens Cl, Br and I are selected for the “X” site. Squares in red indicate a more common combination while gray squares denote either an abandoned or unexplored compound, some features considered for the selection are stability, energy gap, effective electron-hole masses (m_e^* m_h^*), exciton binding energy, and defect tolerance. Lead-free compounds are separated in a yellow line in the last row[13]..... 18

Figure 9 Types of thin-film perovskite deposition: a) wet-chemical deposition employing precursor solutions or "inks" and b) vapor phase deposition by evaporating the reagents under a vacuum environment[18]..... 20

Figure 10 Coordination solvents employed to disperse perovskite precursors: dimethylformamide (DMF), dimethylsulfoxide (DMSO) and N-2-methyl,pyrrolidone (NMP) along with the reported mechanisms that involve the perovskite formation[23]..... 22

Figure 11 Perovskite thin-film deposition methods by employing precursor solutions[13]..... 23

Figure 12 Continuous perovskite deposition by slot-die coating in flexible substrates[13] 25

Figure 13 Optical properties of hybrid perovskites: a) absorbance spectra of different perovskite materials and b) comparison of absorption coefficient between a perovskite compound and several inorganic compounds employed in solar cells[54] 30

Figure 14 Bonding diagram of a $[PbI_6]^{-4}$ cluster: a) zero-dimensional system and a 3D perovskite structure [55], b) the models depict the composition of the top valence band (TVB) and the bottom conduction band (BCB) in accordance with the bonding diagram, as obtained from molecular simulation[56] 31

Figure 15 Steady-state photoconductivity and Hall effect measurements in $CH_3NH_3PbI_3$ films: a) μ_{Hall} in a vapor-grown 100 nm thick polycrystalline $CH_3NH_3PbI_3$ film measured at different photoexcitation densities, is narrowly constant (the dashed lines show an average $\approx 8 \text{ cm}^2\text{V}^{-1}\text{s}^{-1}$, b)

photoconductivity and Hall carrier density measured as a function of absorbed photon density[58]	32
Figure 16 Physical appearance of perovskite thin-films before and after degradation: a) photographs of the as-synthesized CH ₃ NH ₃ PbI ₃ /FTO film and (b,c) the degraded films after the exposure with moisture. (d) optical micrograph of the as-grown perovskite film and (e) the degraded CH ₃ NH ₃ PbI ₃ film[61]. (f) degradation of perovskite thin-films kept in dark at room temperature with 90% relative humidity and a pristine PbI ₂ film.[14] (g) moisture stability of a perovskite solar cell measured with a humidity of 45 %[62]......	35
Figure 17 Thermal behavior of CH ₃ NH ₃ PbI ₃ perovskite : a) TGA heating curve and corresponding 1st derivative of a perovskite powder obtained with an equimolar ratio of precursors PbI ₂ and CH ₃ NH ₃ I in DMF[63], b) X-ray diffractograms of TCO/TiO ₂ /MAPbI ₃ films that were subjected to 85 °C for 24 h in different ambient[64], c) crystal phase transitions of MAPbI ₃ perovskite, the PbI ₆ octahedra are depicted in blue, and the iodide ions are in red[65]	37
Figure 18 Structures of solar cells with different configurations: a) structure of a silicon solar cell, composed by a thick p-type semiconductor which absorbs most of the incident light and most of the power is generated. After radiation absorption, the minority carriers (electrons) diffuse to the junction, where they are swept cross by a strong built-in electric field. The electrical current is extracted by metal contacts at the front and back of the cell. b) structure of a p-i-n junction, this cell contains a layer of intrinsic semiconductor that separates the p-type and n-type semiconductors. Generation of charge carriers occurs mainly within the space charge region. Additionally, the built-in electric field enhances the charge separation, which is reflected in the collection efficiency. Usually transparent conducting oxide (TCO) and a metal layers are used as contacts at the top and back of the solar cell[70].	38
Figure 19 Schematic representation of a solar cell, the close-up shows the depletion zone around the junction between the n-type and p-type layers [71]......	39
Figure 20 Band diagram with different processes occurring in perovskite solar cells: a) main process: (1) generation, (2) charge transport and (3) charge extraction, b) undesirable processes (marked in red): (4) recombination of the photogenerated species, (5,6) back charge transfer at the interfaces of ETL and HTL and (7) charge recombination between the ETL and HTL [72]......	41

Figure 21 The equivalent circuit of an ideal solar cell (full lines). Nonideal components are shown by the dotted line [70].	42
Figure 22 characteristics of a solar cell: a) current density-potential measurement of a solar cell that consists of a fundamental diode with dark saturation current $j_0 = 4.34 \times 10^{-11}$ mA/cm ² , the short circuit current and open circuit voltage are noted by circles. b) The electrical power supplied by the solar cell as a function of voltage. The power is normalized at 100 mW/cm ² (corresponding to 1 sun of light intensity). The maximum power is noted by a circle [73].	43
Figure 23 The I-V characteristic of the solar cell in the two-diode model for three values of the ratio I_{02}/I_{01} [70].	45
Figure 24 The effect of series (a) and parallel (b) resistance on the I-V characteristics of a solar cell[70].	46
Figure 25 An overview of publications of perovskite solar cells. Data is taken from Scopus in March 2021 using the keywords "perovskite solar cells".	47
Figure 26 Historical evolution of the power conversion efficiency (PCE) of perovskite solar cells (PSCs), the graphic is composed by the data in Table 2. (b) Different device architectures in PCSs: the mesoscopic, which contains a mesoporous electron-transporting material (ETM) layer, the normal-planar, and the inverted-planar structure[75].	48
Figure 27 Progress of the efficiency of recently reported large-area perovskite solar cells fabricated by various deposition methods[80].	51
Figure 28 Scheme with the most important studies relating the stability of perovskite materials. At the base, there are localized studies focused on the material and understanding of the nature of stability. Followed by studied on operating cells and finally module-level studies at the pinnacle. The terms at the right represent key aspects of studies at each level[82].	54
Figure 29. Perovskite preparation by blow-drying deposition under room conditions	60
Figure 30 Infrared spectra: a) Methylammonium Iodide powder and MAPbI thin-film obtained by blow-drying methodology using b) air at 25 °C, and c) hot air at 90 °C.	63

- Figure 31 Crystalline structures of MAPbI thin-films obtained by blow-drying, a) calculated diffraction pattern, b) MAPbI perovskite synthesized with air at 25 °C and 25 %R.H. and c) MAPbI thin-film obtained at 90 °C with low humidity atmosphere (<25 %). Schemes of the MSPbI perovskite crystalline structure d) oriented in the 110 direction, and e) partially degraded. 64
- Figure 32 Surface morphology of perovskite thin-films obtained by blow-drying deposition methodology using: a) regular air(25 °C,25 %R.H.), and hot air(90 °C)..... 67
- Figure 33 Photographs of MAPbI perovskite thin-films obtained by hot air blow-drying method (air-flow = 10 m/s, T = 90 °C) at different solutions' volume and precursors' concentration: a) degree of transparency, b) mirror-like appearance denoting the macroscopic homogeneity..... 69
- Figure 34 Morphology of MAPbI perovskite thin-film related with the crystal orientation obtained by XRD. The crystal grows in the z-direction resulting in a needle-like morphology observed by SEM. 70
- Figure 35 Effect of concentration and volume of precursor solutions in the morphology of MAPbI thin-films. Morphology obtained with 3 μL of: a) 0.216 M, b) 0.32 M, and c) 0.434 M precursor concentration, d) 4 μL, and e) 5 μL of 0.434 M precursor solution. 71
- Figure 36 Textural analysis carried out by AFM. Perovskite films (a-c) obtained with 3 μL, 4 μL and 5 μL of precursor solution, respectively. 3D perspective (d-f) of the thin-films. Cross-sectional height in three different areas of the same thin-films (g-i). The solution concentration was 0.434 M. 74
- Figure 37 Optical properties of synthesized MAPbI thin-films by blow-drying methodology, using hot-air at 90 °C: a) Absorbance spectra of different sections of the thin-film and b) calculated absorption coefficient of MAPbI compared with the silicon..... 75
- Figure 38 Degradation study under 25 %R.H. of perovskite thin-films. a) Degradation kinetics followed by measuring the UV-Vis absorbance of the thin-films, b) effect of the precursor concentration on the perovskite degradation following the absorption intensity at 750 nm, c) degradation rate of thin films obtained with different volumes of a 0.434 M precursor solution. 77

Figure 39 Perovskite thin-films degraded under controlled conditions (25 °C, 25% R.H.): a) as-synthesized MAPbI thin-films obtained by HADB method (air at 90 °C) b) degraded thin-films after several days of exposure at the controlled atmosphere..... 78

Figure 40 Photovoltaic performance of perovskite solar cells with MAPbI thin-films: a) comparison of the photovoltaic efficiency depending on the type of deposition technique, standard blow-drying, and HADB; b) shunt characterization $g(V)$ and c) $r(J)$ used to obtain R and A factors for the solar cell assembled by HADB methodology. The architecture of the solar cell was TCO/CdS/MAPbI/Graphite-Ag. The measurements were carried out under ambient conditions. 81

Figure 41. Types of electromagnetic radiation by wavelength range and energy[125] 90

Figure 42. Interactions of electromagnetic radiation with matter[126]. 91

Figure 43. Molecular vibrations and the range in which they are detected over the infrared spectrum[127]. 94

Figure 44. Schematic representation of the Bragg’s Law[128] 95

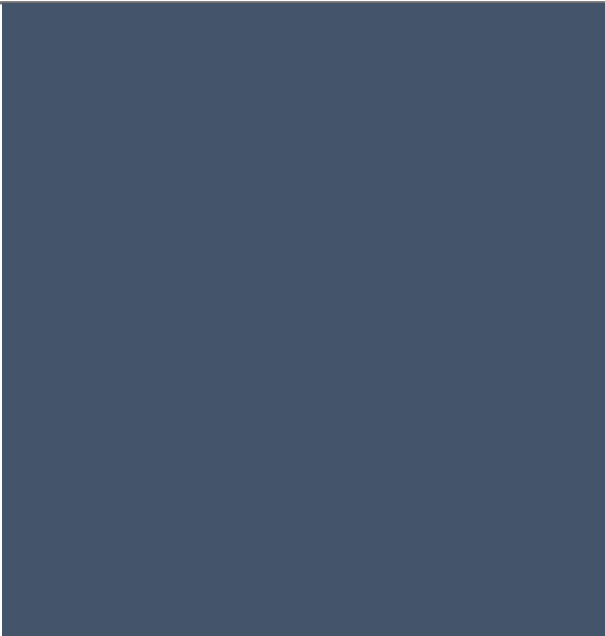
Figure 45. Differences between the optical microscopy and scanning electron microscopy[129]. 97

Figure 46. AFM operation principle: a) attraction/repulsion forces experimented by the tip measured by AFM and b) the feedback loop of an AFM equipment to construct the analyzed surface[130]. 98

Figure 47. Hall effect experimented by a bar sample of a conducting material[131]. 99

Figure 48. Film sample prepared for the Van der Paw resistivity and Hall measurements[132]. 101

Figure 49. Circuit diagram for a current-voltage (I-V) measurement of a solar cell[133]. 102



Chapter 1

General Introduction

CESAR MANUEL DEL ANGEL OLARTE

1. GENERAL INTRODUCTION

Nowadays, environmental concerns are a real trend. As the population grows, more energy is required to sustain human activities, resulting in over-exploiting natural resources, and generating excessive waste. Moreover, the world still depends on fossil fuels to satisfy the energy demand, not to mention that the world economy strongly depends on this issue. However, there is no way to stop fossil fuel consumption without risking the economy, so the strategy to stop the environmental pollution is reducing this fuel consumption and recurring to alternative energy sources to complement the energy demand.

In this sense, solar energy is one of the best choices among the renewable energy sources available, as it can be transformed into heat or electricity. Solar energy results in a convenient energy source directly transformed into electricity through special devices known as solar cells. For this reason, several countries have relied on electricity generation through solar cells. Additionally, there is a constant technological enhancement regarding solar cells.

Thanks to technological development, there are various generations of solar cells. One of the most recent involves the development of solar cells employing materials that promise to surpass the current efficiencies. To make possible the commercialization of photovoltaic devices, intense research is still in progress regarding efficiency, scalability, and stability.

In this thesis, one of the materials trending in the photovoltaic research field is studied, the perovskite. Perovskites are known for their electrical and optical properties, which make possible the generation of high-efficiency solar cells, the simplicity of the procedures to synthesize these materials, and also are recognized for their stability issues.

1.1 The perovskite compounds.

Perovskite is the name of a family of compounds which share the formula ABX_3 . Where the “A” site is usually occupied by a small cation, the “B” position corresponds to a heavy metal and the “X” site belongs to a non-metal ion. This formula comes from the $CaTiO_3$ compound, which is referred as the model of a perovskite compound. Perovskites are known for its peculiar crystal arrangement which characterizes for a corner-sharing BX_6 octahedra enclosing the A cation. Figure 1 depicts the crystal structure of the ideal perovskite along with the possible elements that can be employed to synthesize a perovskite compound. Due to the versatility of the formula, almost every element from the periodic table is a good candidate to prepare a perovskite.[1]

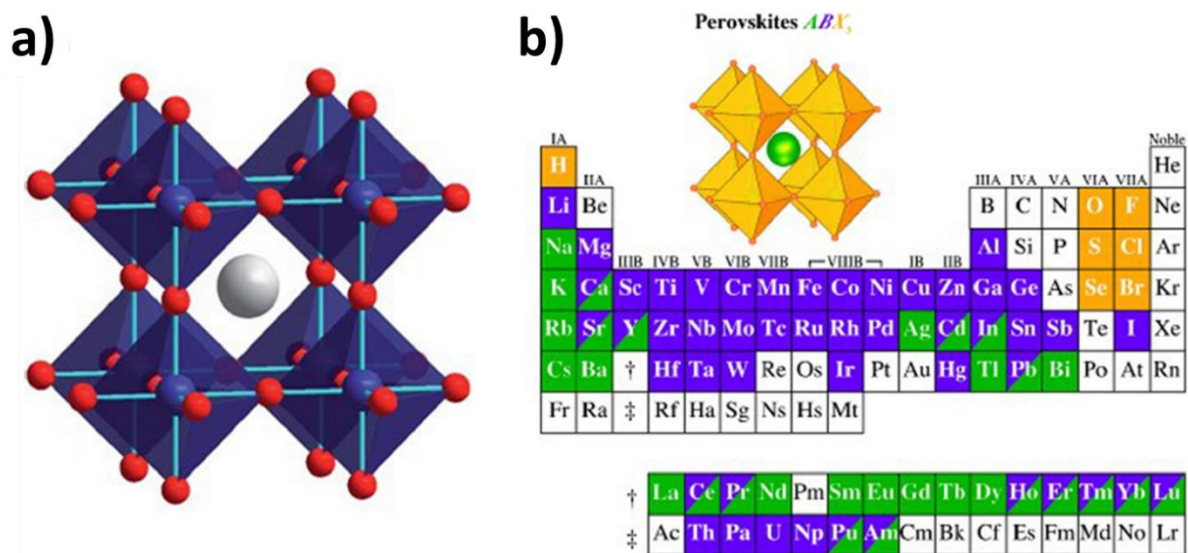


Figure 1 ABX_3 perovskite structure and composition: a) the corner-sharing octahedra composed of B cations (in blue) and X anions (colored in red) enclosing the A cation (in gray), b) elements that can be combined to prepare a perovskite compound, each color corresponds to a specific site[1].

Apart from the inorganic perovskites, there are hybrid perovskites, which are composed of an organic cation placed in the “A” position, expanding the catalog of

perovskite compounds. This kind of perovskites plays a crucial role in the research field since they were identified as promising compounds for photovoltaic applications.

1.2 Hybrid perovskites

Hybrid perovskites replace the inorganic cation for a suitable organic cation in the “A” site. Figure 2 displays the main differences between an inorganic perovskite and a hybrid compound. The “A” site is usually occupied by an organic cation like the methylammonium (see Figure 2b). Hybrid perovskites in general, involve the use of lead ions and halide elements which build the octahedral structure. Moreover, due to the size of the organic cation employed to synthesize hybrid perovskites, structural distortions occur to adjust the space for the components[2].

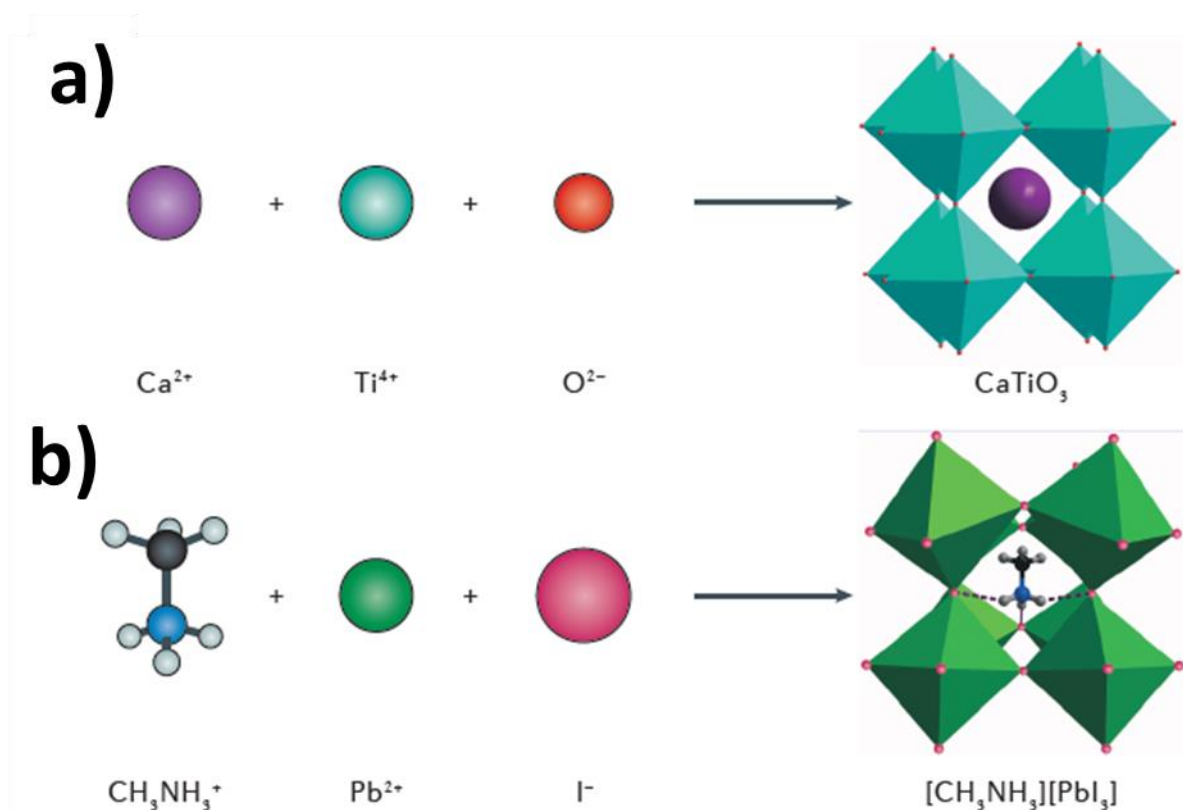


Figure 2 Compositional and structural differences between the inorganic perovskite (a) and the hybrid perovskite (b) compound[2].

For the case of hybrid perovskite compounds, the methylammonium lead iodide is recognized as the reference. Several modifications taking this molecule as the basis can be performed, whether changing the organic part, employing mixtures of organic molecules, interchanging the lead ion for an equivalent heavy metal, or changing the composition of the “X” anion by mixtures of halogens. These modifications can lead to hybrid perovskite with different properties to overcome certain issues in photovoltaic applications. In this work, the methylammonium lead iodide was selected as the material of study because it is considered the base material. We employed this characteristic to establish a synthetic methodology that could be adapted to different perovskite compositions.

Hybrid perovskites characterize for their optical and electrical properties, which is one of the reasons they are considered promising materials for high-efficiency solar cells. Taking the methylammonium lead iodide as a reference, it can absorb an important fraction of the electromagnetic spectrum. With an energy gap of 1.56 eV its optical absorption covers from the ultraviolet region to the near-infrared section. Additionally, the absorption range can be modulated by changing the composition of the “X” anion.

Along with its optical absorption modulation, the electrical properties make possible the transport of electrical species in thin-films, which is an advantage compared with other materials employed in solar cells, like silicon. Over the years, important features like the diffusion length of electrical species, the binding energy, and the sensitivity of the conductivity have been studied, allowing the correlation between the high efficiencies in photovoltaic applications and the physical properties.

Despite the signs of progress made on understanding the physical properties, it is still not possible to visualize the application of hybrid perovskite materials in real-life photovoltaic devices. The main disadvantage of hybrid perovskites is stability, which is an essential factor that needs to be assured in order to develop a solar cell. Figure 3

depicts some of the external factors that compromise the stability of a perovskite compound. As can be seen, some of the factors are highly related with real-life applications, like moisture and heat. Recalling that a solar cell is an outdoor device that must resist direct exposition to weather conditions.

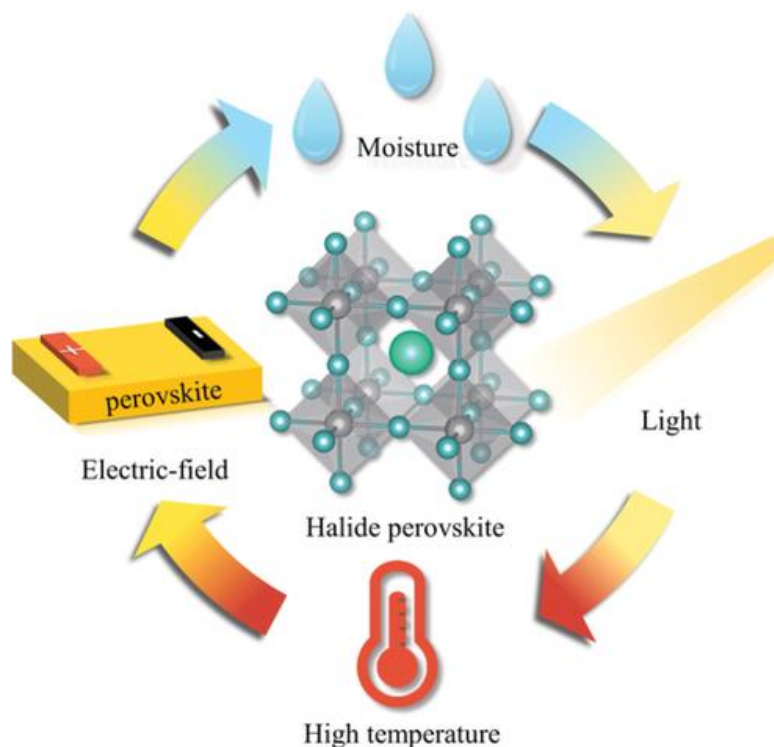


Figure 3 External factors that affect the stability of a hybrid perovskite compound[3].

The stability issues have become the main problem for these compounds, encouraging the researchers to find alternatives and develop strategies to obtain stable hybrid perovskites. This has given a result not only partially stable compounds but also the development of synthetic methodologies under environmental conditions.

In the early stages of hybrid perovskite development, the synthesis of methylammonium iodide strictly included inert atmosphere due to the risk of premature degradation of the compound. During this time, the spin coating deposition technique was the most employed methodology to obtain perovskite thin films. The simplicity of

the method allowed the possibility of synthesizing thin films in an inert atmosphere box. However, the films needed to be stored under the same conditions until its characterization.

Although spin-coating allowed the obtention of high-quality thin-films, the procedure was limited to small area deposition, which was the second problem to be overcome during the early stages of development. New deposition methods were required to achieve large-area depositions, or that could be scalable, in order to offer possible commercialization of perovskite photovoltaic devices.

As a result, several methods were developed to obtain hybrid perovskite thin-films in large-area substrates. Some examples are the slot-die coating, the spray-coating, or the roller-coating technique. These methodologies, in combination with certain strategies to obtain more stable perovskite compounds make possible the adaptation of the synthesis to a continuous deposition of hybrid perovskite thin-films. In this work, a supporting method known as blow-drying was employed as the main deposition technique. Blow-drying consists in usually blowing an inert gas over the as-synthesized thin-film to eliminate residual solvent from the film and complete the perovskite formation. Most of the times this is a secondary methodology which comes after a spin-coating or slot-die deposition. However, it has the potential to be employed to synthesize perovskite materials itself.

All the advances mentioned above were achieved because of the possibility of synthesizing hybrid perovskite materials from precursor solutions. Another recognized advantage of the hybrid perovskite materials is that the reagents are salts that can be dispersed in specific solvents. Clearly, the management of a precursor solution is easier and allows the use of simple deposition methodologies or its adaptation to the solution deposition.

In general, the synthesis of a hybrid perovskite involves the chemical reaction of the organic compound, which is an organic halide, and the inorganic part, which usually is a lead halide salt. In order to disperse the reagents, a coordination solvent is needed. Among the solvents available, N-N, dimethylformamide, and dimethylsulfoxide are the most employed coordination solvents. These molecules have the capacity to coordinate with the lead halide salt and, at the same time, contain the organic cation. The formation mechanism of the perovskite compound involves the substitution of the coordination solvent for the organic cation. This process is promoted by the evaporation of the coordination solvent, which is the objective of the deposition method. In the case of this work, dimethylformamide was chosen as the coordination solvent due to its relatively high boiling point and the ease of coordinating with iodo-plumbates, which constitutes an important step in the formation of perovskite.

Because of the advantages that offer hybrid perovskites, from their synthesis to the application, these materials have become a real trend in the photovoltaic research field—resulting in important advances in high-efficiency devices and stable devices under laboratory tests.

1.3 Perovskite solar cells

Perovskite solar cells are those devices that include in their architecture a hybrid perovskite material. The structure of this kind of cell consists of a p-i-n heterojunction, where the intrinsic semiconductor is the perovskite. In order to achieve the photovoltaic effect, the perovskite needs to be surrounded by different semiconductors on each side so that when the electromagnetic radiation reaches the perovskite film, the exciton species (electrons and holes) are collected by specific semiconductors, avoiding direct recombination within the perovskite film.

In a dye-sensitized solar cell (DSSC), hybrid perovskites were used for the first time, achieving an efficiency of 3.2%. After this application, the use of hybrid perovskites increased considerably, going from DSSC to mesoporous thin-films and finally to solid

thin-films. Along with developing its kind of photovoltaic device, the efficiencies obtained by these devices increased in a matter of years. Figure 4 depicts the efficiency achieved by perovskite solar cells compared to the efficient development of other thin-film devices. To date, the efficiency of a perovskite photovoltaic device is around 23%, which is a significant breakthrough considering that this efficiency was achieved in about ten years from its first application.

The perovskite efficiency increase showed in Figure 4 motivates the researchers to continue improving the photovoltaic device production, implementing continuous deposition techniques, and enhancing the perovskite content to increase stability. It is believed that the new generation of photovoltaic devices can be developed based on hybrid perovskite compounds, although much work still needs to be done to achieve this.

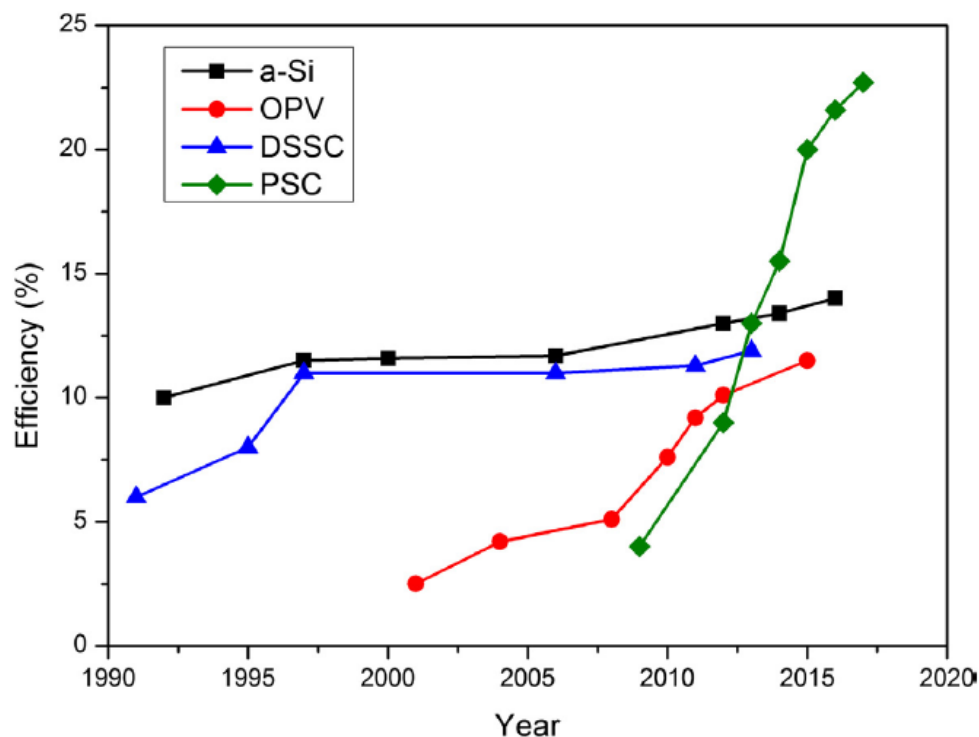
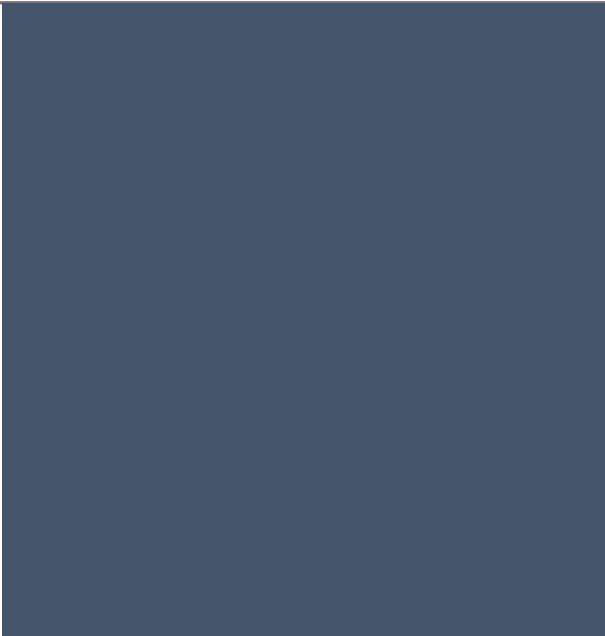


Figure 4 Comparison of the increase in photovoltaic efficiency for various thin-film technologies[4]

Thus, this work is divided into various chapters with the aim of presenting a comprehensive study: in chapter 2, the motivation of the project is stated, along with the objectives of the research work. Chapter 3 is dedicated to a well-documented exploration of the fundamentals, from the material to the solar cell application, closing with the state of the art of perovskite photovoltaics. The development of a thin-film deposition methodology is aboard in chapter 4, along with the corresponding characterization of the perovskite material and its application in a solar cell device. Finally, chapter 5 includes the general conclusions about the project.



Chapter 2

Motivation of the project

CESAR MANUEL DEL ANGEL OLARTE

2. MOTIVATION OF THE PROJECT

Global energy consumption and the current environmental concerns require renewable energy sources to decrease fossil fuel exploitation gradually. As an alternative, photovoltaic devices offer the possibility of transforming solar energy into electricity cleanly. Moreover, new photovoltaic technologies are emerging in the research field, promising the development of more efficient devices. Among them, perovskite materials have shown impressive advances in the development of new generation photovoltaic devices. However, more research is still in progress, focused on the synthesis of thin-films under environmental conditions, using deposition methods that allow continuous production, and looking for alternatives to increase the chemical stability of the materials.

Therefore, this thesis aims to provide an alternative procedure for the production of perovskite thin-films, which can be applied under environmental conditions opening the possibility to be scalable. Additionally, we have contributed by generating comprehensive knowledge on the stability of the materials obtained by the proposed method and the study of properties and application prospects of perovskite thin-films in solar cells.

2.1 Hypothesis

Perovskite thin-films can be developed by the blow-drying deposition method. Moreover, by using hot air instead of air at room temperature, the evaporation rate of the solvent can be increased, enabling the fast perovskite formation and complete elimination of the solvent from the material. Additionally, the environmental conditions do not affect the material purity. The synthesized material is suitable for the construction of a solar cell under ambient conditions.

2.2 General Objective

To synthesize the perovskite $\text{CH}_3\text{NH}_3\text{PbI}_3$ thin-films through the blow-drying deposition method, evaluate the chemical stability of the thin-films, and demonstrate their application in solar cells.

2.3 Specific objectives

To develop the methodology to obtain perovskite thin-films by blow-drying deposition under room temperature conditions.

To synthesize perovskite thin-films under different conditions by varying the concentration and volume of precursor solutions.

To determine the physical and chemical properties of the perovskite thin-films obtained by the different deposition procedures and synthesis parameters.

To evaluate the chemical stability of the perovskite thin-films obtained by blow-drying deposition.

To evaluate the performance of perovskite thin films as part of a photovoltaic device used under room temperature and humidity.



Chapter 3

Hybrid perovskites for photovoltaics: Fundamental aspects and applications

CESAR MANUEL DEL ANGEL OLARTE

3. HYBRID PEROVSKITE MATERIALS: FUNDAMENTAL ASPECTS AND APPLICATIONS

3.1 Hybrid perovskite materials

The name “perovskite” is a common term used to refer to a large family of compounds that share certain crystallographic characteristics. One of the most important to be considered is their composition, which can be described with the formula ABX_3 , where A and B are metal ions and X is a non-metal ion. The term “perovskite” was originally given to the mineral $CaTiO_3$ by Gustave Rose in 1839 in honor of Count Lev Aleksevich von Perovski, a Russian statesman and mineralogist[5].

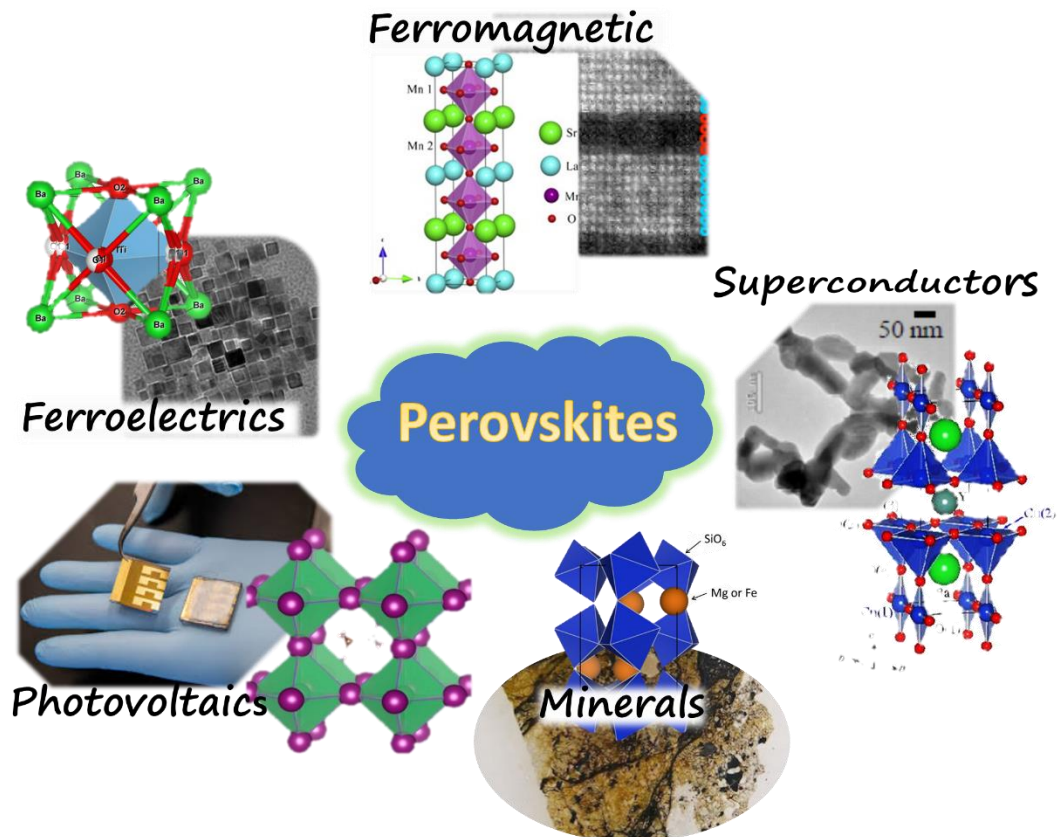


Figure 5 Perovskite materials and their different properties, along with the corresponding crystal structure of the representative perovskite material[5].

Nowadays, there are hundreds of compounds with the same crystalline form which belong to the perovskite family. Most of them are minerals with remarkable properties[6]. Figure 5 depicts some of the most recognized properties of different perovskite compounds and the corresponding crystalline structure of each representative material. Regarding inorganic perovskites, it is important to mention the compound BaTiO_3 , which exhibits critical ferroelectric properties[7]. Moreover, it is possible to synthesize perovskite superlattices with ferromagnetic and conducting properties with the appropriate conditions by using $(\text{La,Sr})\text{MnO}_3$ combinations[8]. One of the most abundant minerals in the lower mantle is a perovskite. The $(\text{Fe,Mg})\text{SiO}_3$ or bridgemanite is the most abundant silicate on earth. Perovskites are still highly studied in these days[1]. In the last 20 years, a new class of perovskites, called hybrid perovskites, has changed the photovoltaic research field, promising to surpass the efficiencies of commercial devices.

Inorganic perovskites crystalize in a well-defined/recognized structure where the components are localized, as shown in Figure 6a. In the ideal structure of perovskite, the divalent metal cation is surrounded by six X anions, which form a BX_6 coordination sphere from the crystallographic view. This coordination sphere takes the form of an octahedron which, in turn, is enclosed by eight A cations, resembling an octahedron inside a cube. Based on this description, the ideal crystalline structure of perovskite is the cubic form. However, natural distortions may occur due to the ionic radius of the atoms which conform to the perovskite compound.

Given the flexibility of the compound formula ABX_3 , several combinations of elements can be used to synthesize a perovskite, resulting in an altered crystallographic form of the ideal perovskite crystal structure. In order to check the compatibility of the ions and predict the deviation from the ideal crystal structure, there is a formula that relates the ionic radius of the elements, known as the tolerance factor. The result explains the deviation from the ideal perovskite structure, where the ideal structure takes the value

of 1. The farther from this value, the more distorted the crystal structure of the compound (see Figure 6b).

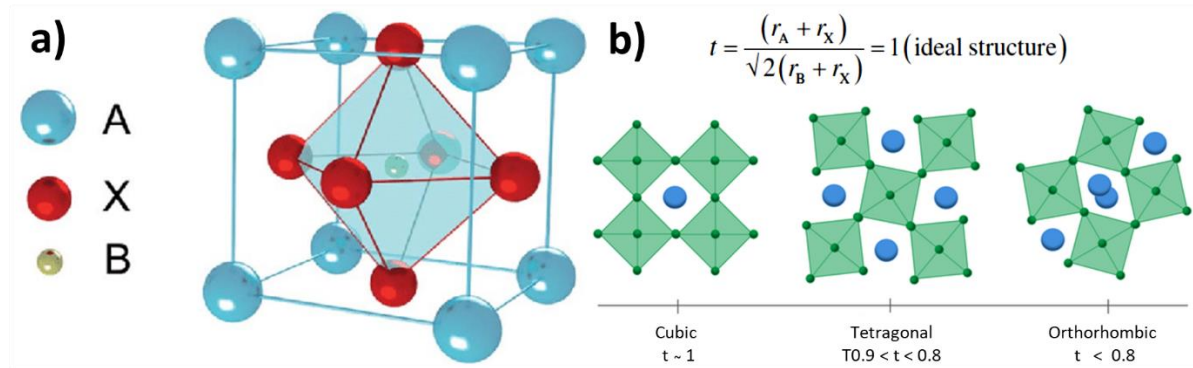


Figure 6 Crystallographic information of perovskites: a) crystal structure showing the positions of the ions and b) tolerance factor and the effect of its value on the crystal structure, r_A , r_B , and r_X are the ionic radii of the corresponding ions.

Additionally, to the flexibility of the ABX_3 formula, not only metallic ions in the A place can be used to create a perovskite compound. With the introduction of an organic cation, a new category of perovskites was introduced, known as hybrid perovskites or organic-inorganic perovskites. This new type of perovskite was first studied by Mitzy et. al.[9]. However, after its application as absorber material in a dye-sensitized solar cell (DSSC) by Miyasaka et. al.[10], this kind of compounds got special attention in the photovoltaic research field.

Figure 7 depicts the evolution of hybrid perovskite materials in solar cells. After its first application, hybrid perovskites rapidly became a recognized material because of its electrical and optical properties, being applied in different ways into a new type of solar cells called perovskite solar cells. In a few years, perovskite solar cells evolved from thick mesoporous solar cells to thin-film perovskite photovoltaic devices, which was possible due to the capacity of the perovskite materials to be synthesized in the form of thin-films. Additionally, the possibility to obtain hybrid perovskites by solution deposition strongly contributed to the rapid development of perovskite solar cells.

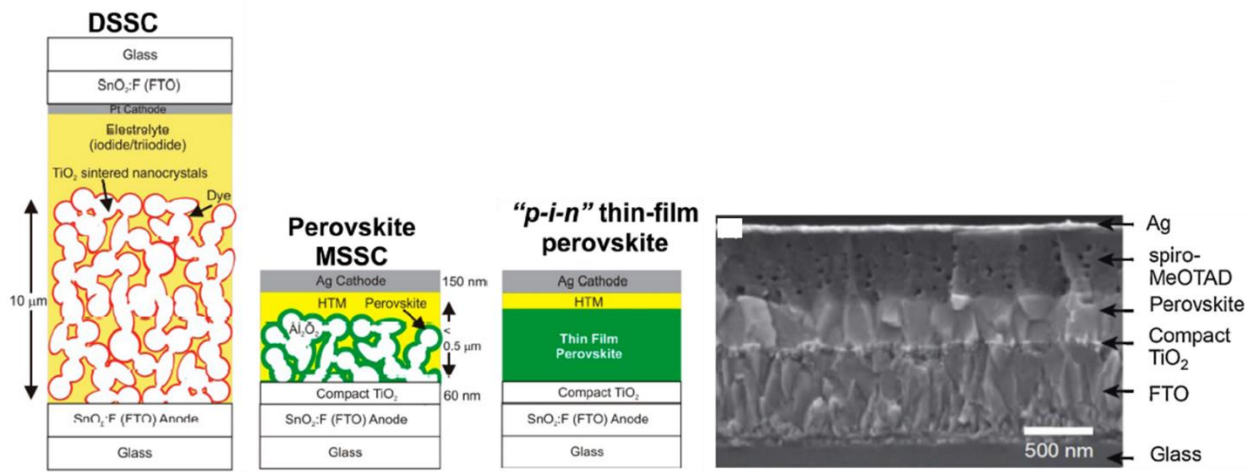


Figure 7 Evolution of perovskite application in solar cells: a) a comparison in thickness reduction between dye-sensitized solar cells (DSSC), mesoporous (MSSC and solid states solar cells[11]; b) cross-sectional view of a “p-i-n” perovskite solar cell[12].

Hybrid perovskites follow the same formula as their inorganic homologous, ABX_3 . Although, in this case, the A cation is an organic compound, the most common is methyl ammonium. Due to the introduction of an organic cation, the octahedra suffer some tilting to adjust the space, causing the distortion of the crystal structure. Because of these reasons, the most common hybrid perovskite, the methyl ammonium lead iodide ($MAPbI_3$), exhibits a tetragonal crystal structure with a tolerance factor of 0.86.

Regarding the hybrid perovskites for photovoltaic applications, several combinations can result in exciting materials for these purposes. Figure 8 depicts a catalog of different ions employed to synthesize perovskites for photovoltaic applications. Usually, the methylammonium (MA) and the formamidium (FA) are the most recurrent A ions. The B cation, on the other hand, focuses on Pb or Sn. Although Sn results in highly unstable compounds, it allows synthesizing lead-free perovskites to address environmental concerns. Finally, Cl, Br, or I can be considered for the X ions. However, the last two are more frequent in hybrid perovskites.

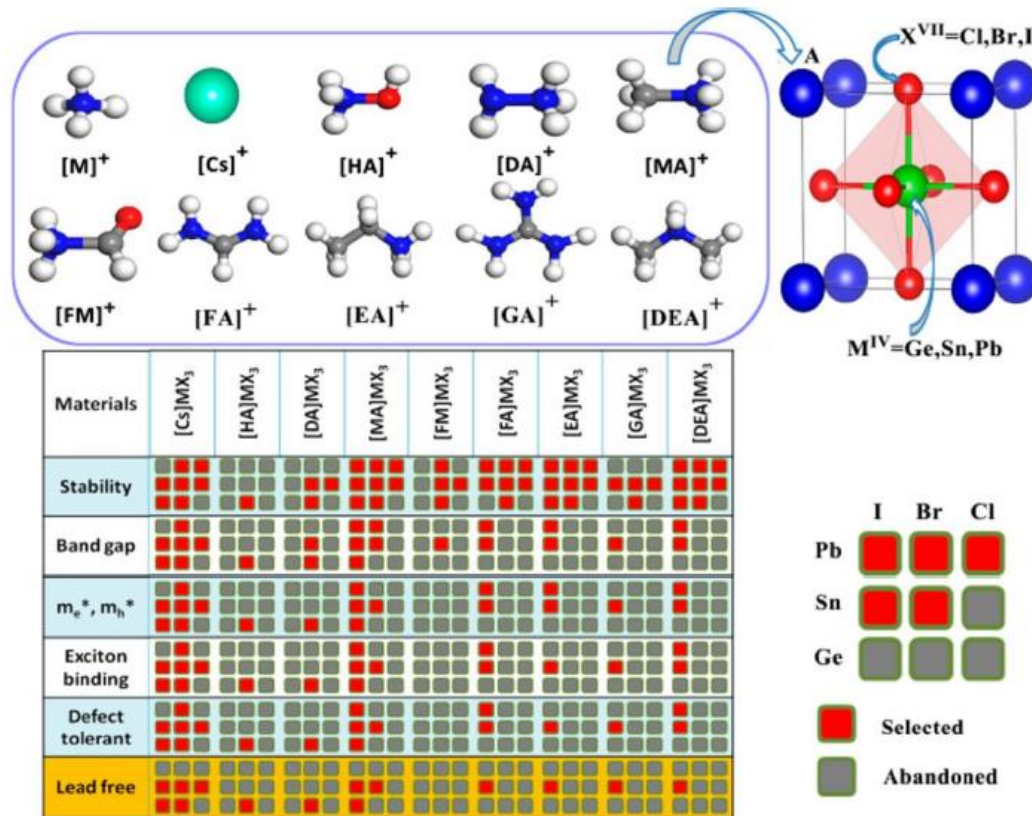
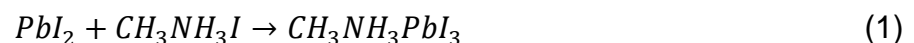


Figure 8 Ion library for the synthesis of hybrid perovskite materials, the “A” cation includes ammonium (M), cesium(Cs), hydroxylammonium (HA), hydrazinium (DA), methylammonium (MA), formamid (FM), formamidinium (FA), ethylammonium (EA), guanidine amine (GA) and dimethylamine (DEA). For the “B” site, metalloids from the group IV: Ge, Sn and Pb are considered. Halogens Cl, Br and I are selected for the “X” site. Squares in red indicate a more common combination while gray squares denote either an abandoned or unexplored compound, some features considered for the selection are stability, energy gap, effective electron-hole masses (m_e^* , m_h^*), exciton binding energy, and defect tolerance. Lead-free compounds are separated in a yellow line in the last row[13].

Exhaustive research is still in progress, exploring more possibilities and combinations to obtain a perovskite material with enhanced electrical properties, long-range optical absorption, and chemical durability, which are desired characteristics for high efficiency and stable solar cells. Moreover, the synthetic routes to obtain perovskite thin films open a wide range of opportunities to, in the near future, scale the production of photovoltaic devices containing these materials.

3.2 Synthetic routes for perovskite thin-films

Hybrid perovskites are considered a strong competitor against other materials for photovoltaic applications. Not only due to their electrical and optical properties but also because of the possibility to synthesize the materials from precursor solutions. These characteristics make possible the use of simple methodologies to generate high-quality thin-film depositions. These advantages are related to the nature of the precursors and the chemical reaction involved in synthesizing a hybrid perovskite material. As an example, equation 1 shows the chemical reaction for the formation of methylammonium lead iodide, the most common hybrid perovskite[14]:



As can be seen from the equation, it is an equimolar reaction between the reagents. Therefore, to obtain a thin film perovskite material, it is important to consider: the purity of precursors, the reaction phase, and the substrate employed for deposition. For the case of the reagents, both lead halide and methyl ammonium iodide are salts, which can be dissolved in a liquid media. This gives an idea of the type of reaction phase.

Since the nature of the reactants is in the form of salt, two approaches can be taken to make the reagents produce a perovskite thin film over a substrate. Those are illustrated in Figure 9: the wet-chemical synthesis and the vapor deposition technique.

The synthesis from solutions (also known as wet-chemical deposition[15] or meniscus coating[16]) has the advantage of managing the reagents in a liquid media. Moreover, the deposition techniques are diverse and require flexible reaction conditions. The thin films obtained from these methods are highly sensitive to the reaction conditions. In some cases, it is challenging to avoid surface defects, such as pinholes and uncovered areas. The gas-phase method[17], on the other hand, offers an excellent quality of the thin-films, usually low roughness and pinhole-free surfaces. However, the method

generally needs vacuum conditions and high energy requirements to evaporate the reagents. Additionally, only small areas of substrate can be treated to obtain a perovskite thin film, which is the main drawback when compared with the solution methods.

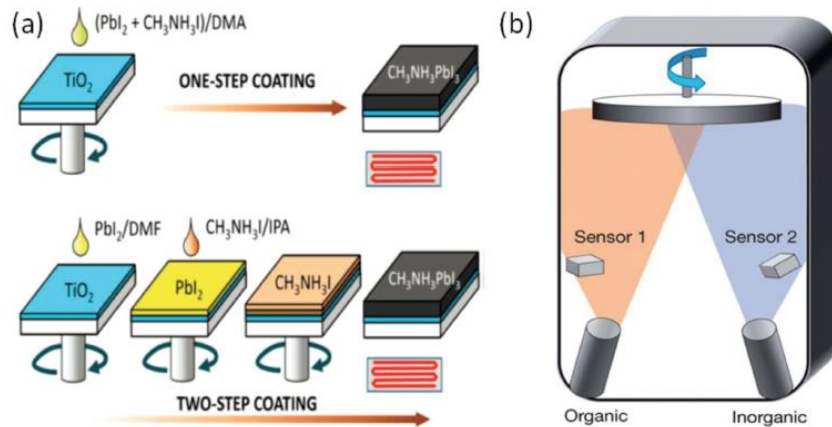


Figure 9 Types of thin-film perovskite deposition: a) wet-chemical deposition employing precursor solutions or "inks" and b) vapor phase deposition by evaporating the reagents under a vacuum environment[18].

As research progress toward more scalable deposition techniques with the aim of a commercial product, the solution-based methods become in the best choice[19]. Moreover, several deposition methods have been developed and improved, achieving large area depositions with good thin-film quality characteristics. Therefore, an appropriate approach to these techniques will be performed hereafter.

3.2.1 Coordination solvents

The synthesis of hybrid perovskite thin films from solutions requires the selection of an adequate liquid media to disperse and contain the reagents[20]. Following this consideration, it is necessary to recall the well-established chemical behavior of lead halide complexes. As a transition metal with an s^2 configuration, lead can easily undergo complexes with halide ions[14,21]. These lead complexes, known as

plumbates, become the precursors in the formation of hybrid perovskite compounds[22].

Prior to the formation of the halide plumbates, lead iodide needs to be prepared for the coordination by interacting with a coordination solvent, such as dimethylformamide (DMF), dimethyl sulfoxide (DMSO), or N-methyl,2 pyrrolidone (NMP)[23]. The characteristic of these solvents is to donate a pair of electrons to form Lewis adducts with the Pb^{2+} ions. After the formation of the Lewis adducts, the halide plumbates generate gradually by introducing halide ions in the solution and evaporating the coordination solvent. This phase has usually been observed as an intermediate complex, as depicted in Figure 10.

Finally, as the coordination solvent completely evaporates, the halide ions take the place of the leaving solvent molecules, occurring a rearrangement of the chemical and crystal structure to form the perovskite compound[24]. Based on this mechanism, the perovskite formation depends on solvent evaporation, which can be modulated by the solvent or combination of solvents or by using solvent additives. These strategies for selecting the appropriate solvent are known as solvent engineering techniques[25]. Once the solvent media is chosen, it is necessary to define the method for evaporating the solvent, the deposition method.

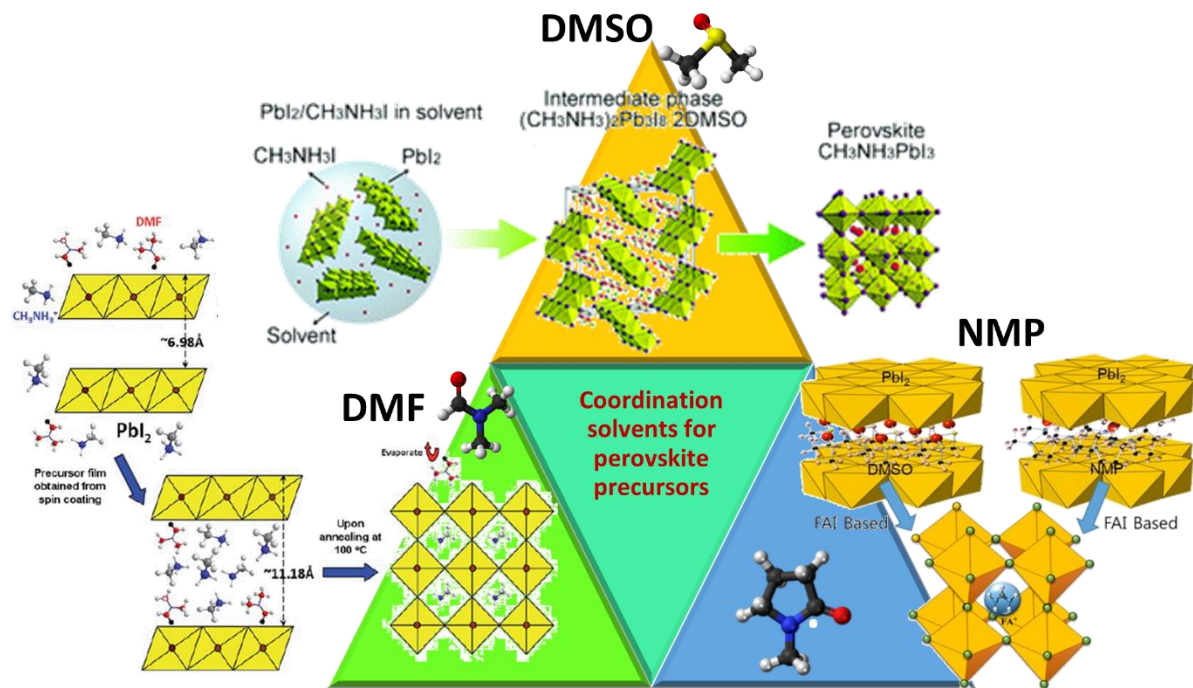


Figure 10 Coordination solvents employed to disperse perovskite precursors: dimethylformamide (DMF), dimethylsulfoxide (DMSO) and N-2-methyl,pyrrolidone (NMP) along with the reported mechanisms that involve the perovskite formation[23].

3.2.2 Deposition methodologies from solutions

There are a lot of methods that allow the elimination of the coordination solvent to promote the perovskite thin-film formation over a substrate. Figure 10Figure 11 depicts some of the most recognized deposition techniques[13,26]. The simplest one consists of evaporating the solvent by heating the substrate[27] (example not shown in Figure 11), however by applying this method, it is difficult to control the film growth[28], and only small areas can be treated. Due to these problems, heating the sample is usually considered an extra treatment employed to eliminate residual solvent molecules trapped in the films. The methods depicted in Figure 11 allow the formation of perovskite thin-films in short times. The method is highly reproducible and involves high substrate areas. The most important characteristics of each one are explained below.

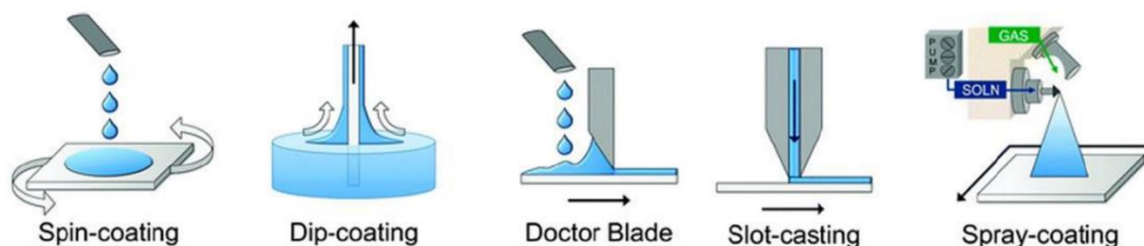


Figure 11 Perovskite thin-film deposition methods by employing precursor solutions[13].

3.2.2.1 Spin coating

Spin-coating is still the most implemented deposition procedure to obtain perovskite thin films. Even though this method implies the deposition over small areas of the substrate, it played a crucial role in the first years of developing perovskite solar cells, allowing the obtention of highly efficient solar cells. For this reason, spin-coating is considered a reliable method to obtain high-quality perovskite thin-films, to be studied in small areas, usually for the determination of physical and chemical properties.

As depicted in Figure 11, the method consists of placing the substrate over a rotative plane. Then the precursor solution is added while the substrate is rotating. The centrifugal force exerted by the rotations scatter the solution and almost instantly expels the solvent, allowing the formation of the perovskite thin-film[29].

There are some variations of this methodology. This deposition method can be applied in one or two steps, as depicted in Figure 9a. Depending on the precursors contained in the solution: if both precursors are contained in the same solution, then a one-step process is applied; on the contrary, if the precursors are contained in separated solutions, a two-step process is carried out. Moreover, this method can be combined with other techniques such as the dip-coating methodology. In this combined method, usually, a PbI_2 film is deposited by spin-coating. After that, the substrate is immersed in a methylammonium iodide solution for some minutes[30]. By exposing the PbI_2 thin-film with the organic halide, it gradually converts to the perovskite compound.

3.2.2.2 *Doctor blade*

This procedure implies the dispersion of the precursors, taking advantage of the rheological properties of the solution. The prepared precursor solution is dropped onto the substrate, then is dispersed by moving a blade positioned at a suitable height. It is important to note that the substrate needs to be at a certain temperature to promote solvent evaporation[31]. So that precursor dropping, blade speed and height, and substrate temperature are the key parameters to achieve perovskite thin-films with the desired quality for photovoltaic applications. This process involves heating the substrate, which was considered an appropriate technique. The use of a blade to disperse the solution and movement of the substrate enhances the thin-films quality. Additionally, the process can be adapted to obtain a continuous deposition over a long substrate, demonstrating its importance as a methodology to be industrialized.

3.2.2.3 *Slot-die coating*[32]

Like doctor-blade, slot-casting or slot-dye coating relies on the dispersion of the precursor solution across the substrate as a function of a moving accessory. An important characteristic of this method is the maximum use of reagents. The setup consists of a slot-die head positioned at a custom distance from the substrate, placed in a horizontal position. The head possesses a narrow slit designed to contain and dispense the precursor solution. The slot is filled by pumping the precursor solution using a syringe pump. As the slot head is positioned to cover the entire width of the substrate, only the necessary solution is injected over the substrate, minimizing the resource waste.

The deposition involves the continual injection of perovskite precursor solution, whether by moving the slot head or the substrate. Moreover, to evaporate the solvent, the substrate needs to be heated during the injection of the solution to provide a rapid formation of the perovskite film. Sometimes a second head is adapted to the system. From this head, an inert gas is blown to drive the solvent evaporation.

Thanks to the development of this method, it was possible to demonstrate the continuous deposition of perovskite thin-films and further the continuous building of perovskite solar cells. Figure 12 shows the continuous deposition of perovskite thin-films over a flexible substrate by using the slot-die method. To make possible the scalation a series of rolls were added to move the substrate. Due to this adaptation, the continuous deposition of thin-films is known as roll-to-roll deposition, and it is considered the best approach to industrialize the obtention of perovskite solar cells.

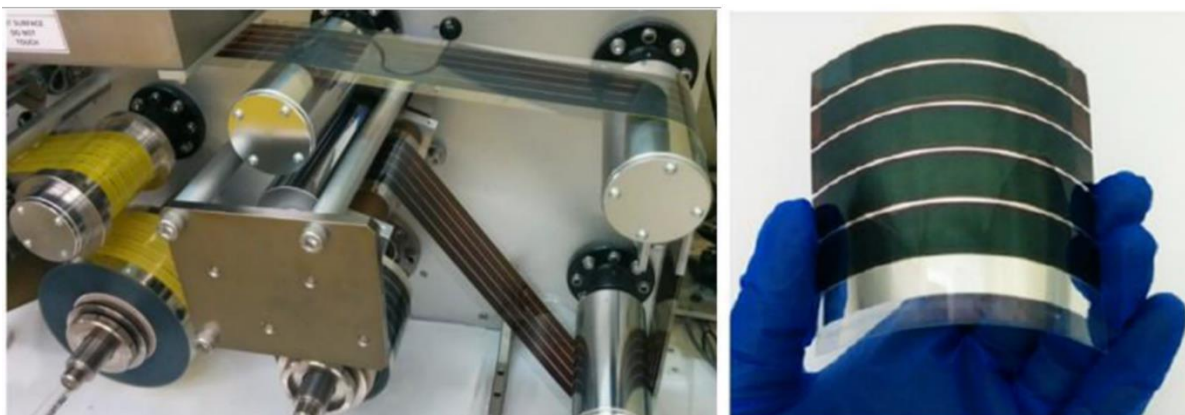


Figure 12 Continuous perovskite deposition by slot-die coating in flexible substrates[13]

3.2.2.4 Spray-coating[33]

The spray-coating is a relatively recent deposition technique, being used for the first time by Barrows et. al.[34] in 2014, has had a fast development over the years, achieving solar cells with efficiencies of 15% in modules of 12 cm². To date the highest efficiency for a solar cell obtained with this method is nearly 20%. This methodology was created mostly for large area deposition, which is a remarkable advantage when compared with other methodologies. Additionally, the spray-coating process is superior in time to obtain a perovskite thin-film, being able to achieve perovskite depositions twice as fast compared with the slot-die coating.

The methodology to obtain perovskites thin-films through this method can be described as follows: the liquid solution of precursors is transformed into micro droplets by means of different procedures (whether pressurizing the solution and pass through a nozzle, ultrasonication, or by applying an electrostatic force). Then a gas flow is applied to direct the solution mist to the substrate. When the solution has reached the surface, a coalescence process takes place, starting the formation of a wet film. The perovskite film is formed when the solvent evaporates. The substrate is commonly kept at a certain temperature to achieve solvent evaporation, although some other alternatives have been applied, such as the anti-solvent bath treatment.

As a relatively recent methodology, improvements are still in progress, especially in the post-treatments. However, this method offers a good perspective for scalable deposition.

3.2.2.5 Blow-drying

The blow-drying deposition is an alternate method for synthesizing perovskite thin films. It is usually applied as a complement during the film formation by spin-coating[35,36], or a post-treatment when the thin-films are synthesized by slot-die or spray coating[37]. However, in only a few reports, blow-drying is applied as the primary deposition technique[38,39], which is a great area of opportunity because the methodology is simple and requires basic equipment to be applied.

The methodology consists of dispersing the precursor solution onto the substrate. After that, an inert gas is blown over the substrate to create a wet film which gradually will transform into a perovskite thin film [40]. Because this procedure is used as a second step in continuous deposition methodologies such as the slot-die coating, the blow-drying can be considered for potential application in scalable technologies to obtain perovskite thin-films. Therefore, more studies are required involving the thin-film deposition by using this methodology.

3.2.3 Post-treatments

So far, the principle of formation of hybrid perovskites has been explained as a complexation between lead halides and halide ions. This process can be carried out in liquid media employing a coordination solvent to separate and contain the lead ions. The formation of the perovskite compound in this case depends on the evaporation of the coordination solvent, which can be achieved by the different methods explained above. However, in most of the cases the solvent evaporation is incomplete, mainly because of the high boiling point of the coordination solvent. As a result, most of the thin-films obtained contain traces of solvent, which damage the final quality of the films. To prevent this inconvenience, some treatments post-deposition are required to obtain pure perovskite thin-films and to enhance the quality of the films. Some of these post-treatments can be applied as a deposition technique itself.

As previously explained, in the annealing process (heat treatment) the as-synthesized perovskite thin-films are exposed in a hot plate for several minutes to eliminate residual solvent molecules[41]. Additionally, it has been observed that after the heat treatment the perovskite thin-film increases its grain size[42] and grain boundaries disappear, leading to smooth surfaces. Temperatures range from 50°C[43] to 150 °C[44,45], and the time of treatment varies from 10 minutes to more than 30 minutes[46].

The blow-drying is also considered a post-treatment, also known as gas quenching[47]. After the deposition has finished, the samples are exposed to different gases which take away the remnant solvent. In this treatment, N₂ or air is the common gases employed to finish the perovskite formation.

Finally, the anti-solvent treatment can be compared with the dip-coating procedure. In this treatment, the as-synthesized thin-films are submerged in a chemical bath containing a molecule with affinity to the solvent but not to the perovskite[48–50],

known as an anti-solvent molecule. Also, the anti-solvent can be dropped onto the as-synthesized thin-film, as reported in some spin-coating procedures[51,52].

There is no rule to define which post-treatment could be applied depending on the deposition method employed. Sometimes a combination of them is applied to assure a good quality of the final thin-films.

3.3 Properties of hybrid perovskites

Since its first application in solar cells, perovskites acquired special attention from researchers, who started improving perovskite photovoltaic devices in a short period of time, supporting this fast development in its electrical and optical properties. Along with the development of efficient solar cells, several groups started studying the properties of hybrid perovskites to reveal their capacity and limitations.

3.3.1 Physical properties

3.3.1.1 Optical properties

One of the most remarkable physical properties which characterizes hybrid perovskites is its optical absorption, Figure 13a depicts the optical absorption of three different perovskites designed for photovoltaic applications. From the picture, the absorption of the most common hybrid perovskite, the MAPbI_3 , characterizes an absorption band edge at ~ 780 nm. This property can be compared with a homologous hybrid perovskite in which the methylammonium iodide is replaced with the formamidinium cation, which exhibits an energy gap of ~ 1.48 eV. Additionally, the FAPbI_3 perovskite is more stable compared with the latter. CsPbI_3 , on the other hand, is considered an alternative for an all-inorganic perovskite which potentially provides long-term stability to the material, reporting a higher energy gap of 1.73 eV.

The energy gap of hybrid perovskites can be tailored not only by changing the cation in the A position but also by gradually replacing or doping with different halides, as reported by Noh et. al.[53] who studied different proportions of Br/I to vary the energy gap from 1.57 eV for pure iodide to 2.29 eV for pure bromide.

Along with optical absorption, the absorption coefficient is a crucial property that defines the capacity of a material for thin-film applications. Figure 13b shows a comparison of the absorption coefficient of different semiconductors employed in photovoltaics. It is important to note the comparison between semiconductors such as

the GaAs or CdTe employed in thin-film solar cells and the MAPbI_3 hybrid perovskite. The absorption coefficient of this perovskite allows a high absorption of radiation by a small thickness film. As a comparison, a layer of ~ 330 nm of a hybrid perovskite can absorb most of the incident radiation, which a $500 \mu\text{m}$ layer of c-Si can only achieve. Considering that the perovskite layers can be obtained from a solution deposition, this is an overwhelming result.

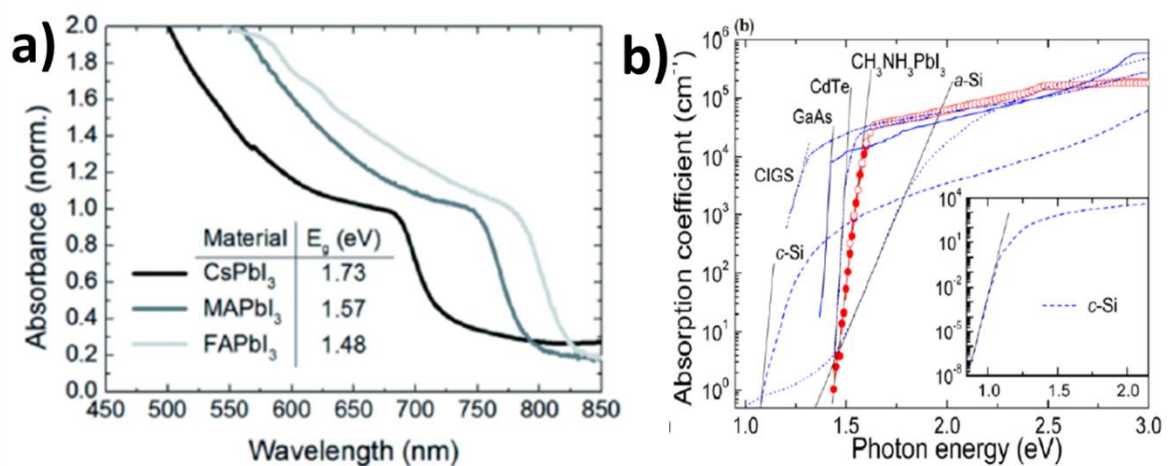


Figure 13 Optical properties of hybrid perovskites: a) absorbance spectra of different perovskite materials and b) comparison of absorption coefficient between a perovskite compound and several inorganic compounds employed in solar cells[54].

The optical absorption of hybrid perovskite materials comes from its electronic band arrangement. Figure 14 shows the bonding diagram for a $[\text{PbI}_6]^{4-}$ cluster studied by Umebayashi et al. [55]. Calculations obtained the electronic arrangement based on the density-functional theory (DFT). Additionally, they extended the approximations to a 3D model (which involves the complete crystal structure of a hybrid perovskite material).

As can it be observed in Figure 14. The top valence band (TVB) on a hybrid perovskite is composed by Pb 6s – I 5p σ -antibonding orbital, while the bottom conduction band (BCB) is composed by Pb 6p – I 5p π -antibonding orbital and Pb 6p – I 5s σ -antibonding

orbital. Figure 14b depicts the described band structure obtained by molecular simulation.

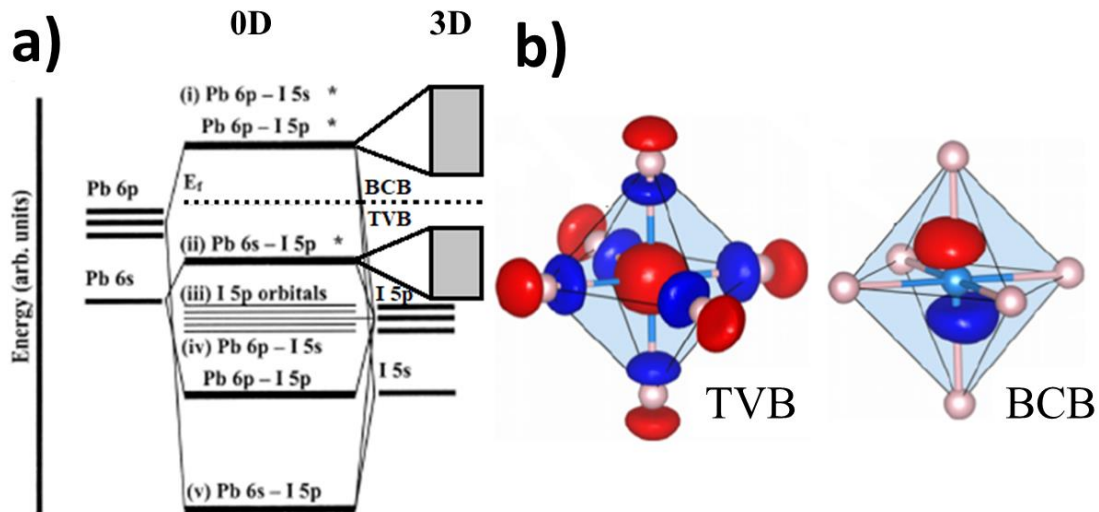


Figure 14 Bonding diagram of a $[PbI_6]^{4-}$ cluster: a) zero-dimensional system and a 3D perovskite structure [55], b) the models depict the composition of the top valence band (TVB) and the bottom conduction band (BCB) in accordance with the bonding diagram, as obtained from molecular simulation[56].

3.3.1.2 Electrical properties

Throughout several studies, it was found that perovskites exhibit outstanding optical properties and interesting electrical properties[57]. These properties define the accuracy of generating charge carriers, moving them along the film, and extracting them to generate photocurrent. Several authors have focused on the study and understanding of these properties. Because of the different techniques that allow the determination of the electrical properties, no punctual values are referring to each property but a certain range of values.

Figure 15 depicts some electrical properties determined by Hall measurement. Because of the high resistivity of perovskite thin films, previous photoexcitation was required to make possible appropriate measurements. It can be noticed that the charge

carrier mobility remains constant at around $8 \text{ cm}^2\text{V}^{-1}\text{s}^{-1}$, as observed in Figure 15a. On the other hand, photoconductivity is plotted in Figure 15b along with the charge carrier density.

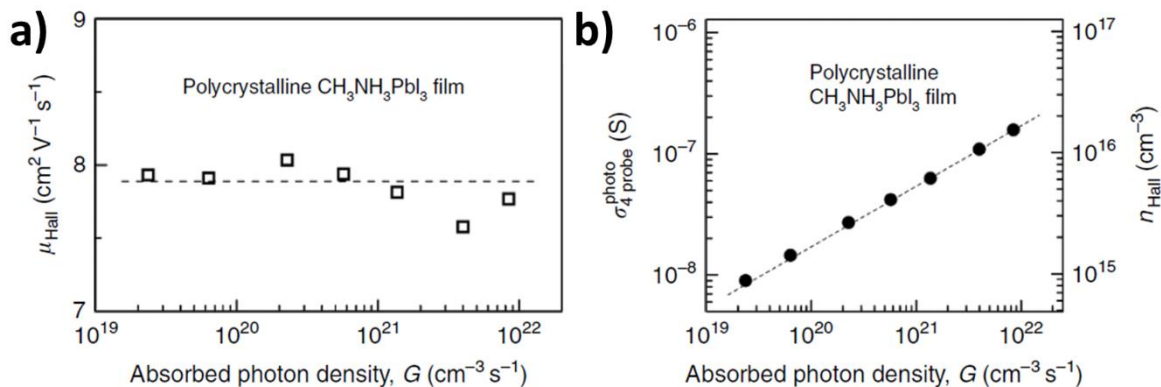


Figure 15 Steady-state photoconductivity and Hall effect measurements in $\text{CH}_3\text{NH}_3\text{PbI}_3$ films: a) μ_{Hall} in a vapor-grown 100 nm thick polycrystalline $\text{CH}_3\text{NH}_3\text{PbI}_3$ film measured at different photoexcitation densities, is narrowly constant (the dashed lines show an average $\approx 8 \text{ cm}^2\text{V}^{-1}\text{s}^{-1}$, b) photoconductivity and Hall carrier density measured as a function of absorbed photon density[58].

Al-Dainy et. al.[54] reported a series of values for the diffusion coefficient and diffusion length of the photogenerated species (see Table 1) for different hybrid perovskite materials. It can be noticed that there is a large variation depending on the material studied. Even though the diffusion length for the classic perovskite MAPbI_3 is quite small, it can be compensated with its absorption coefficient. Mixing different halide ions enhances the diffusion length of the charge carrier species up to 1 micrometer, which is an impressive value for this kind of material.

Table 1 Electron and hole diffusion lengths (L_D) and diffusion coefficients (D) for different perovskite structures[54] .

Perovskite structure	Species	D (cm ² /sec)	L_D (nm)
FAPbI ₃	Electrons	0.004 ± 0.001	177 ± 20
	Holes	0.091 ± 0.009	813 ± 72
CH ₃ NH ₃ PbI _{3-x} Cl _x	Electrons	0.042 ± 0.016	1069 ± 204
	Holes	0.054 ± 0.022	1213 ± 243
CH ₃ NH ₃ PbI ₃	Electrons	0.017 ± 0.011	129 ± 41
	Holes	0.011 ± 0.007	105 ± 32
CH ₃ NH ₃ PbBr ₃	Electrons	0.2198 ± 0.02	1058 ± 48
	Holes	0.2301 ± 0.02	1083 ± 47

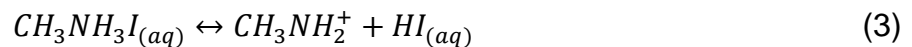
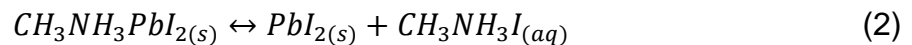
3.3.2 Chemical properties

Hybrid perovskites seem to have the potential to be applied in photovoltaic products. As previously explained, the optical and electrical properties make these materials excellent prospects to compete with well-established technologies like silicon solar cells. However, even though the physical properties seem to categorize the hybrid perovskites as excellent materials, the major drawback and reason why these materials are still under laboratory tests are their chemical properties. Since its first application by Miyasaka et. al.[10], hybrid perovskites were known for their poor stability in humid conditions. For this reason, hybrid perovskites started to be synthesized under dry conditions and another solar cell assembling under the same environment.

Because hybrid perovskites are materials meant for photovoltaic applications, it is important to solve the instability problems. Knowing that solar cells are devices that work outside buildings and that weather conditions cannot be controlled, it is important to guarantee long-term stability under different conditions[59]. For this reason, a brief explanation about chemical stability will be mentioned, along with the thermal stability of hybrid perovskite thin films.

3.3.2.1 Chemical stability

An important component of hybrid perovskites is the organic cation, located in the A position, which gives stability to the crystal structure. Moreover, this cation acts as a counter-ion to equilibrate the electrical charge of the octahedral sphere. Usually, methylammonium is employed to perform this task. However, due to the presence of the amine group, this molecule is prone to be decomposed by losing the proton, then the complete perovskite structure starts to decompose. Niu et al. [60] studied this phenomenon and proposed the following chemical reactions to describe the perovskite decomposition in the presence of moisture:



As observed from these reactions, the product for the complete decomposition of a hybrid perovskite is PbI_2 , and methylammonium completely decomposes to form a methylamine molecule and hydroiodic acid, which volatilize from the material.

There are various ways to identify how and when a perovskite thin-film starts degradation. The most direct form is by physical changes. Figure 16a-c shows the change in color of a perovskite thin-film, after being exposed to an atmosphere of 80% relative humidity. Following the example shown in Figure 16a, a $MAPbI_3$ thin-film exhibit a dark-brown color, which gradually turns yellow when the film is exposed to an atmosphere with a certain amount of moisture (see Figure 16b). Moreover, when the film is taken out from the moisture atmosphere, it regenerates to some extent, which means the degradation process is somewhat reversible, as shown in Figure 16c. However, some degraded parts remain in coexistence in the thin-film. This can be observed by optical microscopy (showed in Figure 16d-e) where the degraded parts of PbI_2 can be clearly identified due to the characteristic yellow color of the compound.

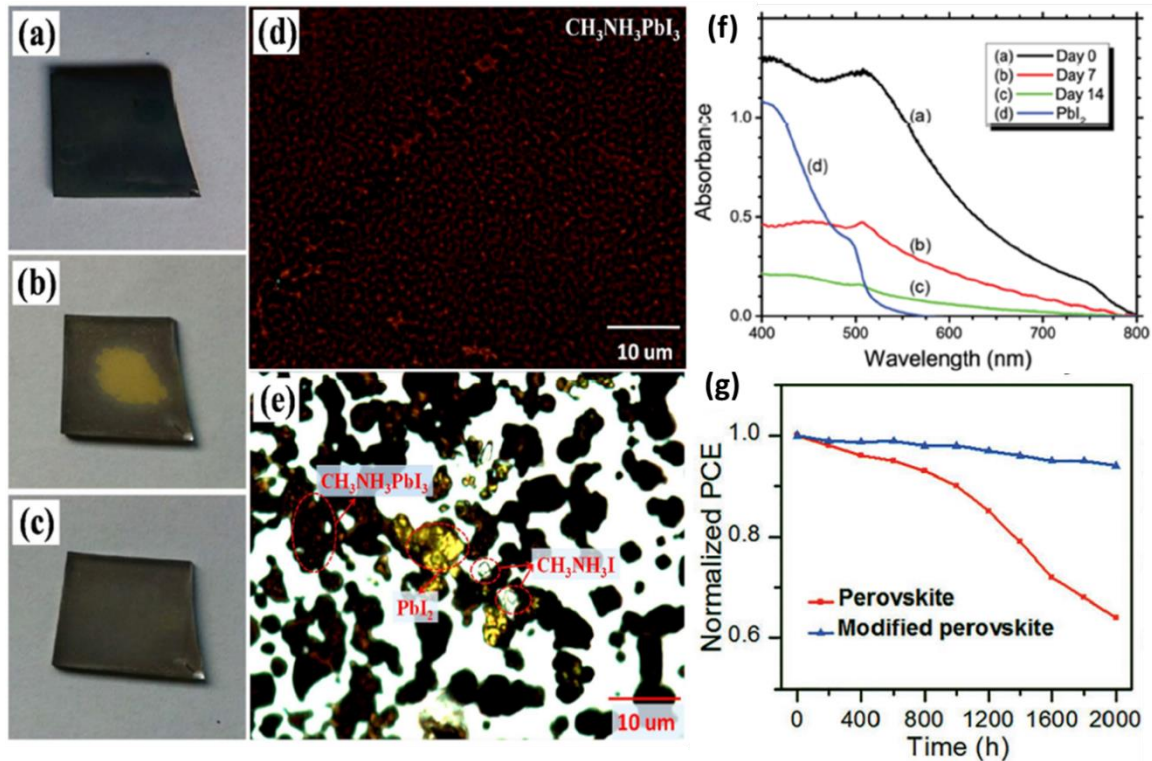


Figure 16 Physical appearance of perovskite thin-films before and after degradation: a) photographs of the as-synthesized $\text{CH}_3\text{NH}_3\text{PbI}_3/\text{FTO}$ film and (b,c) the degraded films after the exposure with moisture. (d) optical micrograph of the as-grown perovskite film and (e) the degraded $\text{CH}_3\text{NH}_3\text{PbI}_3$ film [61]. (f) degradation of perovskite thin-films kept in dark at room temperature with 90% relative humidity and a pristine PbI_2 film. [14] (g) moisture stability of a perovskite solar cell measured with a humidity of 45% [62].

The perovskite degradation can also be tracked by optical absorption. Figure 16f depicts the degradation process over time for a MAPbI_3 thin-film stored in a dark room with 80% R.H. It can be noticed how the optical absorption dramatically decreases after 14 days, as a reference, a spectrum of PbI_2 was recorded to identify common features between the degraded sample and the final product.

The impact of a humid atmosphere on the optical properties of a perovskite thin-film clearly affects the performance of a solar cell. Figure 16g illustrates how the power conversion efficiency of a perovskite solar cell decreases over time after being exposed to an atmosphere of 45% R.H. Although the case for solar cell stability is more complex

and the perovskite itself is not the only factor affecting the performance, it is considered the main contributor.

3.3.2.2 *Thermal stability*

Along with moisture, heat is another major issue that prevents using hybrid perovskites in the long term. Although heat treatment is usually necessary to evaporate the residual solvent after the thin-film deposition, this treatment involves exposure to temperatures up to 150 °C, during 30 min in some cases. After this treatment, no degradation was observed on the thin-films. This fact can be explained with the thermogram in Figure 17a, according to Dualeh et. al.[63] the MAPbI₃ perovskite starts degradation after ~280 °C, so that annealing treatments under this temperature do not degrade the thin-films. Moreover, it can be concluded that exposing the thin-films to an annealing treatment for some minutes does not affect the structure of the material.

Long-term exposure, on the other hand, drastically affects the hybrid perovskites, Conings et. al.[64] observed that after exposing a perovskite thin-film to an ambient atmosphere, with a temperature of 85 °C for 24 h, the only remaining product was PbI₂. This result was obtained after analyzing the samples by X-ray diffraction, by comparing the diffraction peaks of the pristine perovskite, and after being stored at 85 °C it was found that only diffraction peaks from PbI₂ were detected in this sample, which means a complete decomposition of the hybrid perovskite occurred (see Figure 17b).

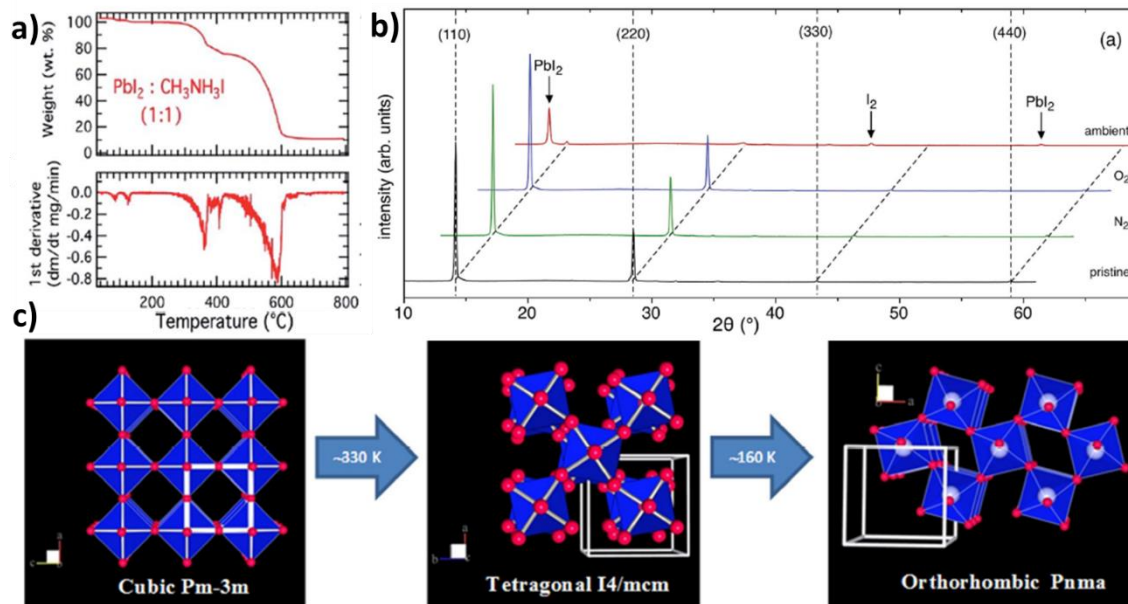


Figure 17 Thermal behavior of $\text{CH}_3\text{NH}_3\text{PbI}_3$ perovskite : a) TGA heating curve and corresponding 1st derivative of a perovskite powder obtained with an equimolar ratio of precursors PbI_2 and $\text{CH}_3\text{NH}_3\text{I}$ in DMF[63], b) X-ray diffractograms of TCO/ TiO_2 /MAPbI₃ films that were subjected to 85 °C for 24 h in different ambient[64], c) crystal phase transitions of MAPbI₃ perovskite, the PbI_6 octahedra are depicted in blue, and the iodide ions are in red[65] .

It is also important to mention that hybrid perovskites exhibit phase transitions at certain temperatures. Figure 17c shows these phase transitions already studied by Whitfield et. al. [65,66] and Oku et. al.[66] MAPbI₃ perovskite exists in tetragonal phase at room temperature. However, over 330 K exhibits a phase transition to cubic phase, and under lower temperatures (~160 K) the structure changes to orthorhombic. These phase transitions also affect other properties of the material, which in turn reflects on the final performance in a solar cell.

The study of perovskite instability and how to overcome this problem is a current strong research field. Several reviews summarize the efforts to achieve the best solar cell performance for the longest time possible[62,67–69]. However, because there are no standardized aging procedures, the results vary from one laboratory to another, making it impossible to establish a good reference for stability and, more importantly, the current progress achieved during these years.

3.4 Solar cells

A solar cell, also known as a photovoltaic cell or photovoltaic device, can be defined as an electrical device that uses light energy to generate electrical energy through the photovoltaic effect. A basic solar cell is composed of two types of semiconductors, a p-type and an n-type semiconductor. These semiconductors can be from the same material (which form a homojunction solar cell) or from different materials (called heterojunction solar cell).

Perovskite solar cells belong to a different kind of heterojunction solar cells, called p-i-n heterojunction solar cells. In this type, an intrinsic semiconductor is placed between the p-type and n-type semiconductor to achieve the photovoltaic effect. Figure 18 shows a sketch of the composition of a basic and a perovskite solar cell.

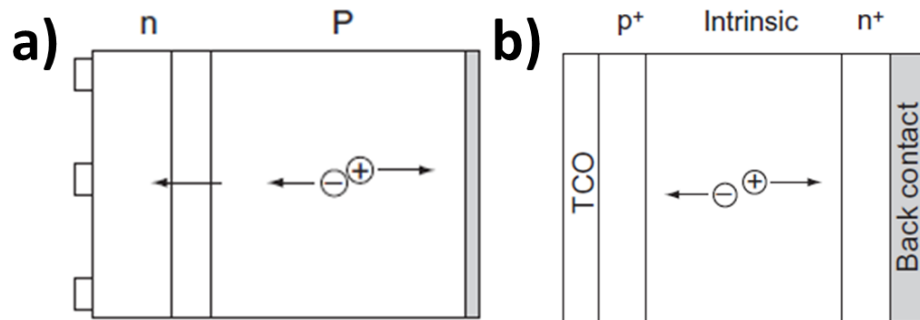


Figure 18 Structures of solar cells with different configurations: a) structure of a silicon solar cell, composed by a thick p-type semiconductor which absorbs most of the incident light and most of the power is generated. After radiation absorption, the minority carriers (electrons) diffuse to the junction, where they are swept across by a strong built-in electric field. The electrical current is extracted by metal contacts at the front and back of the cell. b) structure of a p-i-n junction, this cell contains a layer of intrinsic semiconductor that separates the p-type and n-type semiconductors. Generation of charge carriers occurs mainly within the space charge region. Additionally, the built-in electric field enhances the charge separation, which is reflected in the collection efficiency. Usually transparent conducting oxide (TCO) and a metal layers are used as contacts at the top and back of the solar cell[70].

Photovoltaic energy conversion in solar cells consists of two main steps. The first one involves the absorption of light to generate an electron-hole pair. Then, these exciton species are separated by the solar cell structure, which is explained below.

3.4.1 Working principle of solar cells.

To better explain how a solar cell produce electrical energy, the example of a silicon solar cell will be taken as reference[71], which is depicted in Figure 19.

As previously mentioned, a basic solar cell is composed of an n-type and a p-type semiconductor (in this case an homojunction of silicon semiconductors). N-type semiconductor characterizes for having an excess of electrons while p-type characterizes for the excess of holes, which are vacancies due to the lack of valence electrons in the material. When the two semiconductors are jointed, the electrons from the n-type semiconductor move toward the vacancies from the p-type semiconductor. This process occurs at the zone where the two layers are in close contact, creating an area called the depletion zone in which the electrons fill the holes (process depicted in the close-up figure left).

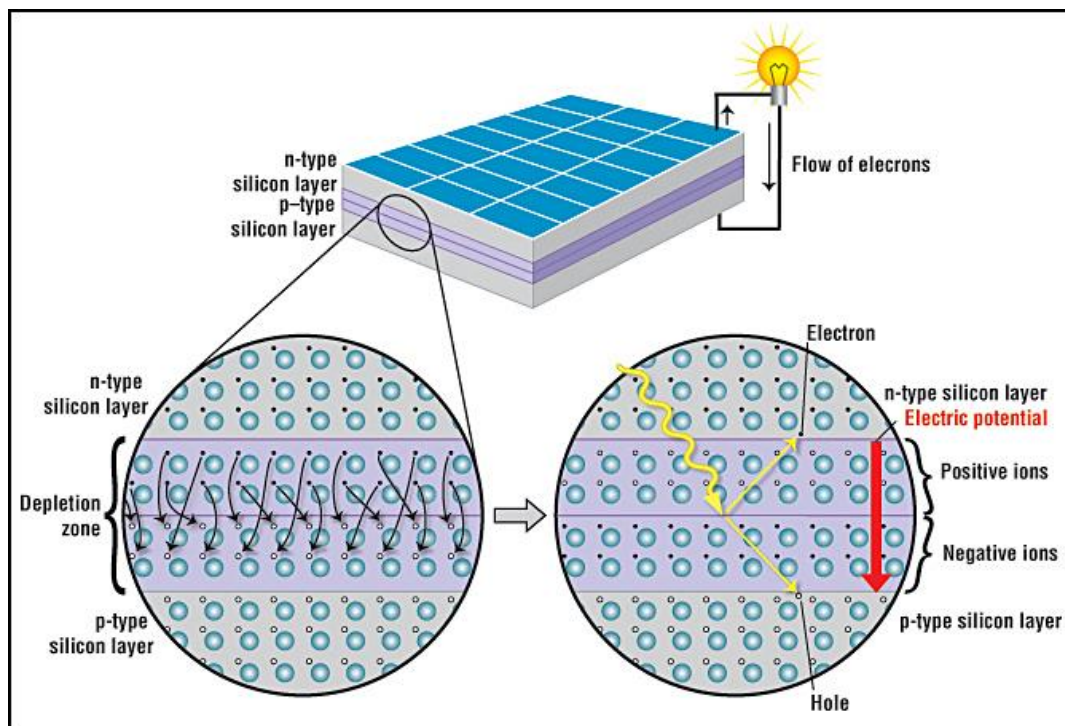


Figure 19 Schematic representation of a solar cell, the close-up shows the depletion zone around the junction between the n-type and p-type layers [71].

As a consequence of the depletion zone formation, a region in the n-type layer now contains holes, conversely a region in the p-type layer contains electrons, and this state in the depletion zone creates an electric field which avoids that electrons from the n-type layer recombine with the holes from the p-type semiconductor. So that, when sunlight reaches the p-n junction, the energy contained in the form of photons supplies sufficient energy to create electron-hole pairs. And by means of the electric field, electrons move towards the n-type region, while holes go to the p-type layer. If the layers are connected by a metallic wire with a small load, the generated electrons will flow from the n-type semiconductor to the back of the p-type layer generating a small flow of electricity.

A similar process occurs in p-i-n heterojunctions, which is showed in Figure 20. In this case, the perovskite material is the intrinsic-type semiconductor, which absorbs electromagnetic radiation generating the electron-hole pair (1). After that, electrons are collected by the electron transport layer (ETL) and holes in the hole transport layer (HTL), respectively (2). Finally, the electrons are extracted by means of electrodes and recombine with the holes in the back metal contact (3), see Figure 20a.

There are some events that avoid the correct electron and hole transitions, which in turn decrease the maximum efficiency in a perovskite solar cell. Figure 20b illustrates these processes (in red lines). Soon after the electron-hole generation, recombination can be produced (4), decreasing the number of electrons generating electrical energy. The recombination can also happen between layers, as shown in processes (5) and (6) in which a back charge transfer at the interface of the ETL or the HTL with the perovskite can occur. An additional recombination process between the ETL and the HTL can be produced when the perovskite layer does not completely cover the previous layer (7).

All these processes define the characteristics of a solar cell, which are important to know to understand the synergy of the materials, the quality of the thin-films and the limitations of the solar cell.

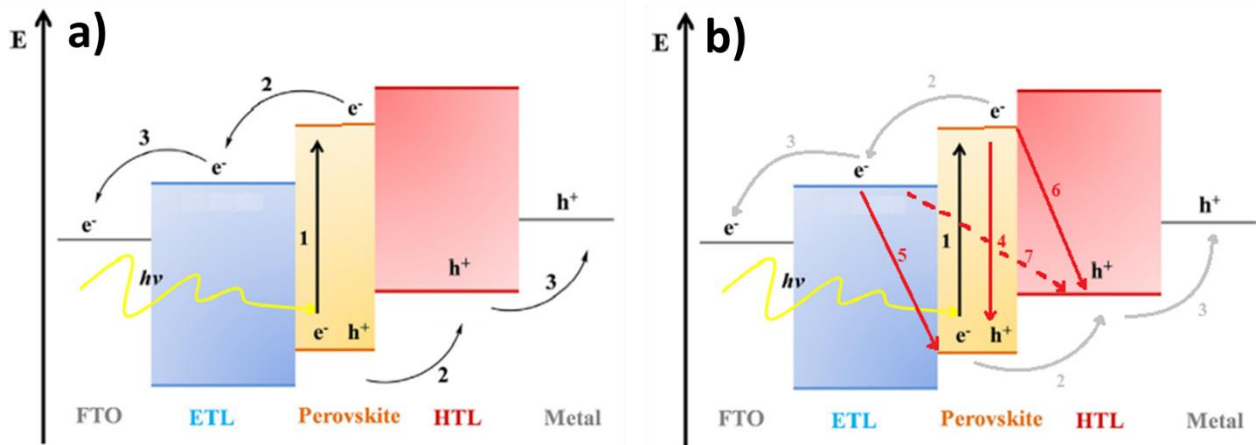


Figure 20 Band diagram with different processes occurring in perovskite solar cells: a) main process: (1) generation, (2) charge transport and (3) charge extraction, b) undesirable processes (marked in red): (4) recombination of the photogenerated species, (5,6) back charge transfer at the interfaces of ETL and HTL and (7) charge recombination between the ETL and HTL [72].

3.4.2 Characteristics of solar cells[70]

An ideal photovoltaic device can be described as a current source connected in parallel with a rectifying diode, Figure 21 depicts this representation in terms of electric circuit. Based on this model, the behavior of a solar cell can be depicted with a current-voltage curve (I-V curve), which is described with the Shockley solar cell equation:

$$I = I_{ph} - I_0 \left(e^{\frac{qV}{k_B T}} - 1 \right) \quad (4)$$

Where k_B is the Boltzmann constant, T is the absolute temperature, q (>0) represents the electron charge, and V is the voltage at the terminals of the cell. The I_0 is the diode saturation current, which is a reminder that a solar cell in dark conditions is similar to a semiconductor current rectifier, or diode. Additionally, the I-V curve can be transformed into a J-V curve by using current density instead of electrical current when measuring a solar cell.

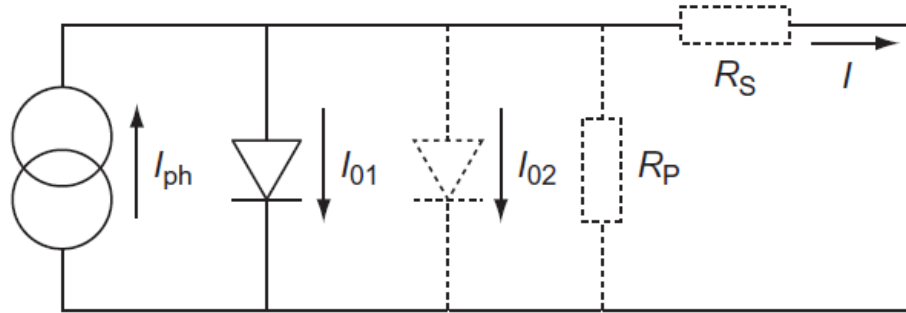


Figure 21 The equivalent circuit of an ideal solar cell (full lines). Nonideal components are shown by the dotted line [70].

In a diode, the current injected in the dark is the difference between recombination current and dark generation current I_0 . However, in a solar cell, an extra term is added, the photocurrent I_{ph} , which comes from the excess radiation that impacts the solar cell. So that for a solar cell, the current balance is described as follows:

$$I = I_{ph} - I_{rec} + I_0 \quad (5)$$

This is the current that flows in the external circuit in terms of electrons leaving the excited state through their selective contact and entering the ground state through the hole selective contact. Figure 22a depicts the shape a current density-voltage curve, corresponding to the ideal diode performance (equation 4). It can be observed that under illumination, the dark characteristic is shifted up in the current density axis.

In the ideal case, the short-circuit current I_{sc} is equal to the photogenerated current I_{ph} , and the open-circuit voltage V_{oc} is given by:

$$V_{oc} = \frac{k_B T}{q} \ln \left(1 + \frac{I_{ph}}{I_0} \right) \quad (6)$$

Usually, the current in the solar cell grows very rapidly when V departs from V_{oc} toward lower voltages (as observed in Figure 22a), but when the voltage further decreases, the current becomes stabilized to $j \approx j_{ph}$. This is because at $V \approx V_{oc}$ a large internal recombination current is induced that compensates the photogeneration, but when V decreases considerably, the recombination current is negligible with respect to j_{ph} .

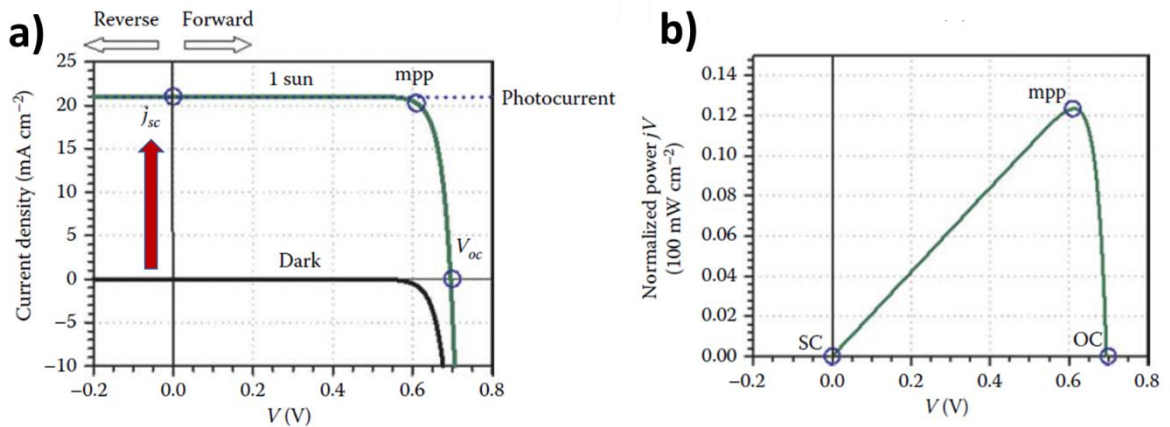


Figure 22 characteristics of a solar cell: a) current density-potential measurement of a solar cell that consists of a fundamental diode with dark saturation current $j_0 = 4.34 \times 10^{-11}$ mA/cm², the short circuit current and open circuit voltage are noted by circles. b) The electrical power supplied by the solar cell as a function of voltage. The power is normalized at 100 mW/cm² (corresponding to 1 sun of light intensity). The maximum power is noted by a circle [73].

A solar cell is designed to be a power supply which generates electricity by absorbing sunlight of ambient light. Then, to verify the solar cell performance, the electrical power that can be extracted from the available radiation level needs to be measured. In a solar cell, the electrical power at a given voltage operation point is calculated by:

$$P = I \cdot V \quad (7)$$

Figure 22b shows the power supplied by the solar cell as a function of the voltage. The power is zero at both open and short circuit points. Between these states, the maximum power point (mpp) is identified, which determines at which voltage (V_{mp}) the solar cell

should operate for electricity production. The maximum power provided by the solar cell is:

$$P_{\max} = I_{\text{mp}}V_{\text{mp}} \quad (8)$$

For the characterization of energy converter devices, which includes solar cells, the maximum conversion efficiency, or PCE, is considered the most important feature. This characteristic represents the electrical power supplied at the mpp with respect to the incoming photon energy and is described by the equation:

$$\eta_{PCE} = \frac{J_{\text{mp}}V_{\text{mp}}}{\Phi_{E,\text{tot}}^{\text{source}}} \quad (9)$$

The PCE is influenced by the operation conditions. For this reason, this measurement is carried out under regulated illumination, which is defined by the standard terrestrial spectrum AM1.5G. Under these conditions, the solar cell is exposed to an integrated power of 1000 W/m² or 100 mW/cm², which is the illumination power of “1 sun”.

In general, if the electrons are extracted at high useful energy (voltage), there is a price in lowering of the number of electrons that can be extracted. The parameter that tracks this property is the fill factor (FF), defined as:

$$FF = \frac{J_{\text{mp}}V_{\text{mp}}}{J_{\text{ph}}V_{\text{oc}}} \quad (10)$$

The I-V characteristics of a real solar cell usually differ to some extent from the ideal behavior (modeled with equation 11). To represent the behavior of a real solar cell, a two-diode model is often employed. In this model an “ideality factor” of 2 is added in the denominator of the argument of the exponential term, corresponding to the second

diode. The solar cell (see Figure 21, dotted lines) may also experiment electric current losses, which are related to the series (R_s) and parallel (or shunt, R_p) resistances. Taking all these issues, the model to determine the behavior of a real solar cell is expressed as:

$$I = I_{ph} - I_{01} \left[\exp\left(\frac{V+IR_s}{k_B T}\right) \right] - I_{02} \left[\exp\left(\frac{V+IR_s}{2k_B T}\right) - 1 - \frac{V+IR_s}{R_p} \right] \quad (11)$$

The effects of the second diode and the series and parallel resistances on the I-V curve of the solar cell are shown in Figure 23 and Figure 24, respectively. Some strategies to determine these parameters from the I-V curve are well explained by Hegedus et.al.[74]

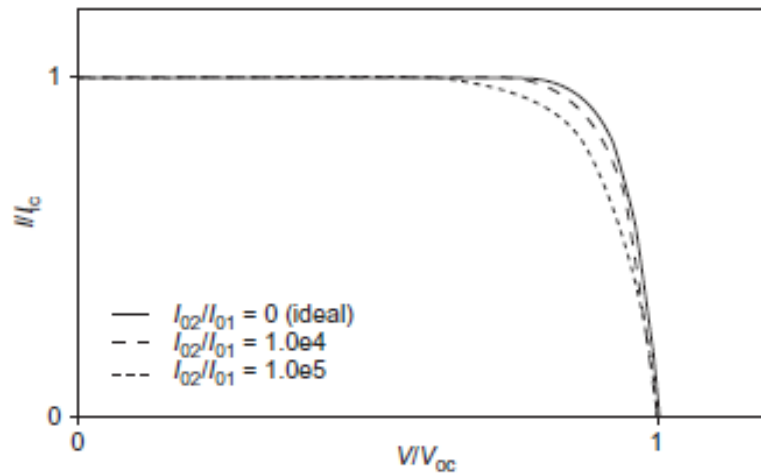


Figure 23 The I-V characteristic of the solar cell in the two-diode model for three values of the ratio I_{02}/I_{01} [70].

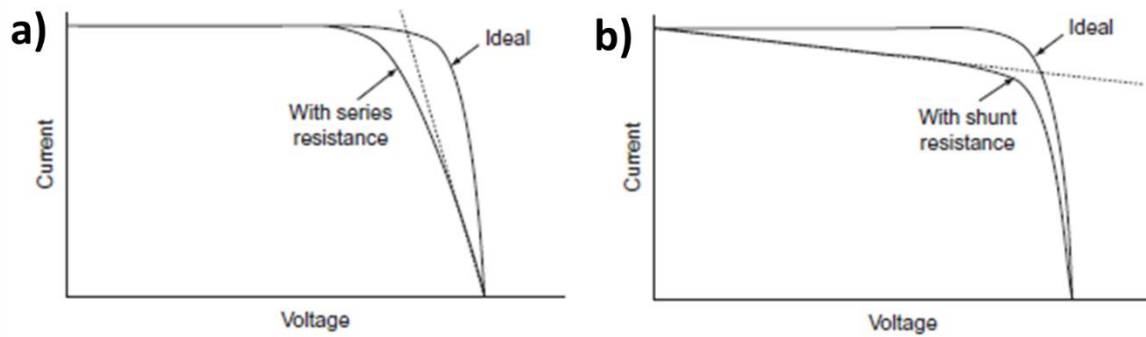


Figure 24 The effect of series (a) and parallel (b) resistance on the I-V characteristics of a solar cell[70].

Overall, these are the basic elements required to understand a solar cell behavior and operation. From these, usually the V_{oc} , J_{sc} , FF and PCE are the most reported values to identify and compare from one solar cell to another. Although in-depth studies require the determination of additional parameters such like the resistances and the spectral conversion to understand the behavior and limitations.

3.4.3 State of the art of perovskite solar cells

The research field focused on perovskite materials for photovoltaic applications is highly active. With more than three thousand publications on each of the last three years(see Figure 25). There is a huge number of studies where hybrid perovskites are employed to fulfill specific requirements. In general, the goal of these studies can be divided into three big approaches: the seek for high-efficiency solar cells, the development of large-area solar cells employing scalable deposition techniques, and the advances in more stable perovskite solar cells. In fact, due to the number of papers published throughout the year, it is very common to find various reviews of the categories previously mentioned. Here, a brief discussion on the three categories will be performed along with the respective conclusions.

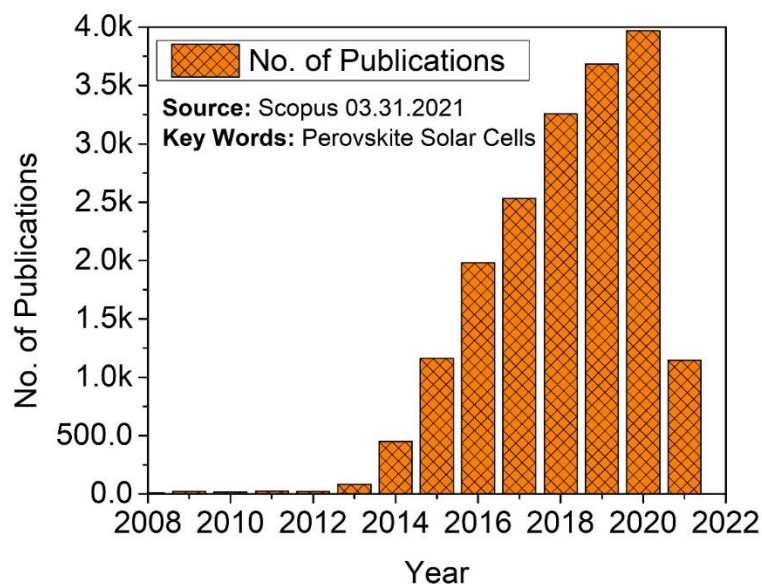


Figure 25 An overview of publications of perovskite solar cells. Data is taken from Scopus in March 2021 using the keywords "perovskite solar cells".

4.4.3.1 High-efficiency perovskite solar cells

It is quite common to relate the phrase "hybrid perovskite solar cells" with "high efficiency". Because of the properties of this kind of material, it is possible to build photovoltaic devices with such efficiency. Figure 26a depicts the improvement in the solar cell efficiency employing hybrid perovskite materials, reported by Kim et al. [75]. The highest efficiency reported is around 25% which was accomplished employing the basic perovskite MAPbI_3 according to Table 2.

Various strategies are recommended to obtain the highest efficiency, starting with the basics of the perovskites: properties, synthesis, type of solar cell structures (Figure 26b), etc. The optimization becomes a complex combination of factors so that to date, there is no specific rule to guarantee success after the development of a perovskite solar cell. Although Saliba et. al.[76] published a series of recommendations established in their research group that claim to guarantee the obtention of perovskite solar cells with efficiencies over 20%.

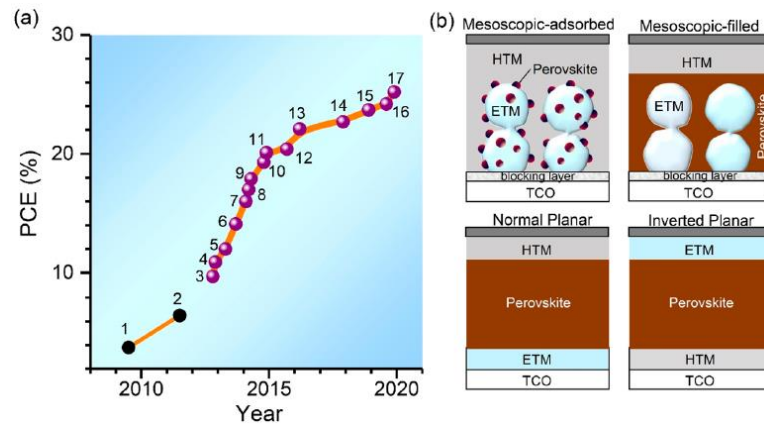


Figure 26 Historical evolution of the power conversion efficiency (PCE) of perovskite solar cells (PSCs), the graphic is composed by the data in Table 2. (b) Different device architectures in PCSs: the mesoscopic, which contains a mesoporous electron-transporting material (ETM) layer, the normal-planar, and the inverted-planar structure[75].

Table 2. PCEs depicted in Figure 26a, perovskite composition and device structures [75]

No.	PCE (%)	Perovskite composition	Device structure (coating procedure)	Institute ^c (year)
1	3.8	MAPbI ₃	Liquid junction	Toin U (2009)
2	6.5	MAPbI ₃	Liquid junction	SKKU (2011)
3	9.7	MAPbI ₃	Solid-state mesoscopic TiO ₂	SKKU (2012)
4	10.9	MAPbI ₃	Solid-state mesoscopic Al ₂ O ₃	Oxford U (2012)
5	12	MAPbI ₃	Solid-state mesoscopic TiO ₂	KRICT (2013)
6	14.1 ^b	MAPbI ₃	Solid-state mesoscopic TiO ₂ (two step)	EPFL (2013)
7	16	FAPbI ₃	Solid-state mesoscopic TiO ₂	SKKU (2014)
8	17	MAPbI ₃	Solid-state mesoscopic TiO ₂ (two step)	SKKU (2014)
9	17.9 ^b	(FAPbI ₃) _{0.85} (MAPbI ₃) _{0.15}	Solid-state mesoscopic TiO ₂	KRICT (2014)
10	19.3	MAPbI ₃	Normal, planar Y:TiO ₂ ETM	UCLA (2014)
11	20.1 ^b	(FAPbI ₃) _{0.95} (MAPbI ₃) _{0.05}	Solid-state mesoscopic TiO ₂	KRICT (2014)
12	20.4	MAPbI ₃	Solid-state mesoscopic TiO ₂	SKKU (2015)
13	22.1 ^b	(FAPbI ₃) _{0.95} (MAPbI ₃) _{0.05}	Solid-state mesoscopic TiO ₂	KRICT (2016)
14	22.7 ^b	(FAPbI ₃) _{0.95} (MAPbI ₃) _{0.05}	Solid-state mesoscopic TiO ₂ , fluorene-terminated HTM	KRICT (2017)
15	23.7 ^b	MAPbI ₃	Normal, planar SnO ₂ ETM	ISCAS (2018)
16	24.2 ^b	MAPbI ₃		KRICT/UNIST (2019)
17	25.2 ^b	MAPbI ₃		KRICT/MIT (2019)

^aThe devices structures are displayed in figure XXb. ^bCertified value. ^cInstitutes: SKKU: Sungkyunkwan University; KRICT: Korea Research Institute of Science and Technology, ISCAS: Institute of Semiconductors, Chinese Academy of Sciences.

Ma and Guo[77] on the other hand, have carried out a systematic analysis of several data of perovskite solar cell devices with the aim to find certain trends related with the obtention of high efficiency perovskite photovoltaic devices. As a result, most of the highest efficiencies are obtained by using spin-coating methodologies, either with the mesoporous or the planar architecture. Regarding the type of perovskite, the basic perovskite MAPbI_3 can reach efficiencies up to 20%, but in order to obtain higher efficiencies, a combination with FAPbI_3 and/or Cs in certain proportions is required. On the other hand, the ETL is usually a TiO_2 based compound, either in the mesoporous or in the solid form. Although sometimes SnO_2 and organic compounds are also employed. Regarding the HTM, Spiro-OMeTAD is the most common material employed with alternatives like PTAA or polythiophene.

Finally, a general conclusion for this area involves the quest for scalable deposition techniques, as the spin coating results in an effective method, but that is hard to industrialize.

3.4.3.2 Large area perovskite solar cells

The mass production of perovskite solar cells is still a challenge because there are various difficulties when the thin-film deposition is scaled. However, due to various years of research and the concern to achieve large-area solar cells that include a perovskite material, there are various methodologies (previously explained in section 2.2.2) that prove the possibility to scale the thin-film deposition.

Table 3 summarizes the latest results regarding large-area perovskite solar cells obtained with different deposition procedures. As observed from these data, the PCE broadly differs depending on the methodology employed. Moreover, some methodologies allow bigger areas than others. Additionally, Figure 27 displays the trajectory of some deposition methodologies and how the efficiency has been

upgraded over the last five years. It can also be observed that blade coating is a promising method to reach efficiencies over 20%.

Table 3. Summary of coating technologies for large -area perovskite films[78]

Method	Material	Largest coating area ^a (cm ²)	PCE ^b (%)
D-bar	MAPbI ₃	20 x 20	~17
Blade	MAPbI ₃	6 x 15	20.3 (14.8 for a 57.8 cm ² module)
Slot-die	MAPbI ₃	-	~12
Spray	MAPbI ₃	7.5 x 7.5	16.4
Stamping	FAPbI ₃	10 x 10	20
	FAPbI ₃	10 x 10	18
Vacuum evaporation		8 x 8	14.2

FA, formamidinium; MA methylammonium; PCE, power conversion efficiency; ^aThe values correspond to the largest coating areas reported. ^bUnless otherwise stated, the PCE values were measured for small-area cells using pieces of large-area coated perovskite films

One major concern discussed by Park et. al.[19] is the adaptation of the precursor solutions to the deposition procedures. Because large area deposition is intended for continuous production, it is necessary that the solvent evaporates quickly to obtain the perovskite thin-film, which is not always the case for the conventional solvents previously discussed sometimes, post-treatments are required to obtain a pure or solvent-free perovskite thin-film.

Liu et. al.[79], on the other hand, discussed the crystallization process involved in these large area deposition techniques, highlighting the necessity of understanding the impact of thin-film growth on the resulting perovskite films. They recommend avoiding long-time crystallization procedures and accelerate the nucleation step to obtain large grain-size perovskite thin-film.

As a general conclusion, the authors agree with the fast development of scalable deposition methodologies, which is a good perspective for large-area photovoltaic devices. However, there is still hard work to do regarding the efficiency because there is a recognizable gap between the efficiencies of small and large-area solar cells.

Additionally, in order to commercialize this kind of photovoltaic product the stability is a problem that must be solved first.

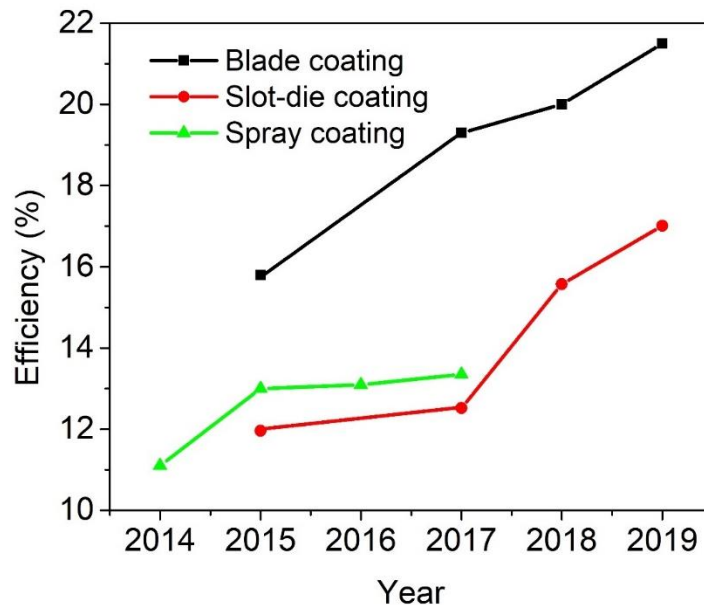


Figure 27 Progress of the efficiency of recently reported large-area perovskite solar cells fabricated by various deposition methods[80].

3.4.3.3 Stable perovskite photovoltaic devices

Despite the advances in efficiency and large area thin-film deposition, device stability has resulted in the definitive challenge to be overcome in order to industrialize perovskite photovoltaic devices. It is well known that hybrid perovskite materials are very sensitive to moisture, temperature, illumination, and other environmental conditions that for photovoltaic devices in a real-life application cannot be controlled. For this reason, several research groups have focused on finding different strategies to extend the life of perovskite solar cells. Table 4 summarizes some relevant results of different perovskite devices tested under different degradation conditions reported by Wali et. al.[81]

From these results, it can be noticed that depending on the degradation factor. A perovskite solar cell can last from 120 h up to 12,000 h when the device is encapsulated. However, despite the relevant durability of the tested devices, it can also be observed that the device composition is not the same. Even the test conditions are not the same for a given degradation factor. It is common to find that different research laboratories have different test conditions, which is an important concern discussed by Christians et. al.[82]

Table 4. Device configuration, their PV parameters and long-term stability of perovskite solar cells[81]

Degradation Factor	Test Conditions	Device configuration	PCE	Loss in PCE	Stability time
Humidity	Unsealed devices and stored in dark with relative humidity <30%	FTO/TiO ₂ -Cl/MAPbI ₃ /Spiro-OMeTAD/Au	21%	4%	2000 h
	Exposed to air at ambient humidity ~55%	FTO/doped C ₆₀ /mixed perovskite /Spiro-OMeTAD/Au	17.6%	20%	650 h
	Exposed to air at ambient humidity 50%	GlassITO/PEDOT:PSS/MAPbI ₃ /PCBM/EFGnP _s -F/Au	14.3%	~10%	30 days
Illumination	Unencapsulated devices in a nitrogen-filled chamber with a constant device temperature of 25 °C and illumination with UV radiation	FTO/LBSO/MAPbI ₃ /PTAA/Au	21.2%	<10%	120 h
	Encapsulated devices tested in open air by including UV radiation	FTO/LBSO/MAPbI ₃ /NiO/Au	-	6.7%	1000 h
	N ₂ atmosphere, LED white light equivalent to 1 sun, and at 60 °C	GlassITO/c-TiO ₂ /mp-TiO ₂ /perovskite / Spiro-OMeTAD-SWCNT	15.5%	20%	580 h
Temperature	The temperature of cells was set at 45 °C in a sealed cell holder with a glass cover	FTO/c-TiO ₂ /mp-TiO ₂ /perovskite / Spiro-OMeTAD/Au	14.6%	40%	300 h
	Sealed under ambient environment and kept at of 55 °C (1 full sun)	FTO/c-TiO ₂ /mp-TiO ₂ /perovskite / ZrO ₂ /Carbon	11.9%	0	12,000 h

The existence of non-standardized conditions makes difficult the comparison of results from one laboratory to another. Also, it makes it impossible to define an appropriate advance regarding long-term stability. For this reason, Christians et. al.[82] proposed a systematic guide to study the stability of hybrid perovskite devices, which is depicted in Figure 28. In this guide, the authors recommend first the study solely of the perovskite material, even under non-standardized conditions, with the aim to understand the degradation phenomena. After that, complete photovoltaic devices must be tested under standardized conditions so that the results can serve as a reference for other research groups. This is the problematic step because, as reported in Table 4, the test conditions cannot be compared most of the time. Finally, a major test carried out under internationally approved test conditions is required to accept the commercialization of a certain photovoltaic device.

Table 5 reports some relevant results of perovskite solar cells tested under standard conditions of the EIC 61215 norm regarding the third step of stability studies. Surprisingly, the devices show good stability for three months under outdoor conditions. These results show the work that needs to be done to obtain long-term stability devices obtained by continuous deposition methods finally.

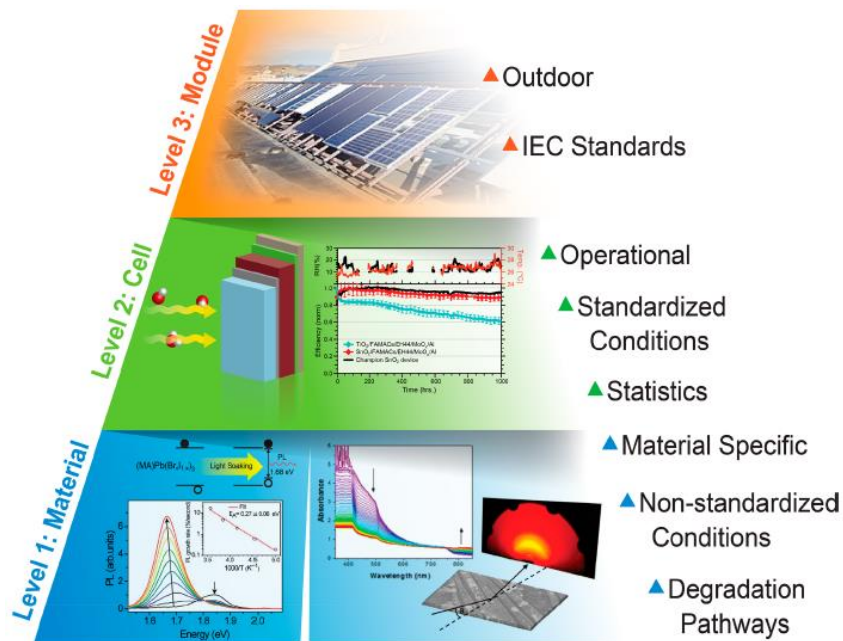


Figure 28 Scheme with the most important studies relating the stability of perovskite materials. At the base, there are localized studies focused on the material and understanding of the nature of stability. Followed by studied on operating cells and finally module-level studies at the pinnacle. The terms at the right represent key aspects of studies at each level[82].

Table 5 The summary of some single tests of the IEC 61215 standard for PCSs[83]

Test	Perovskite component	Encapsulation	Test condition	Lifetime
Damp heat	$FA_{1-x}Cs_xPbI_{1-y}Br_y$	Yes	85 °C, 85% RH	1000 h with no decay
Thermal cycle	FAPbI ₃	Yes	-40 to 85 °C dwell 15 min at -40 and 85 °C	200 thermal cycles with no decay
UV irradiation	$FA_{1-x}Cs_xPbI_{1-y}Br_y$	Yes	UV irradiation (5 mA cm ⁻²) in Ar then UV irradiation (5 mA cm ⁻²) in Air (50% RH)	6 months with 98% PCE retention
Outdoor condition	$FA_{1-x}Cs_xPbI_{1-y}Br_y$	Yes	On the terrace of Politecnico di Torino building in Turin (Italy)	3 months with 95% PCE retention
Hall Impact	$FA_{0.93}Cs_{0.07}PbI_3$	Yes	Dropping a metal ball on top of the perovskite solar modules ^a	Perovskite solar modules stayed as one piece with star-shaped cracks at the attacked position

^aThis test is not the IEC 61215 standard, but is similar to the approval standard for rigid photovoltaic modules (FM 44787)

3.5 Conclusions and outlook

Hybrid perovskite materials show exceptional properties and characteristics, which make them ideal for photovoltaic applications. From its first application in a dye-sensitized solar cell, the development of perovskite photovoltaic devices increased dramatically, allowing the enhancement in the photovoltaic efficiency, and being recognized as a promising technology. Along with the efficiency enhancement, new deposition techniques were implemented to obtain perovskite depositions or even solar cells in a continuous manner. Additionally, stability concerns were studied, and degradation mechanisms were established, along with some strategies to increase the degradation resistance of the photovoltaic devices. Significant advances have been made since its first application. However, there is still much work to do to make possible the commercialization of perovskite photovoltaic devices.

Regarding the deposition techniques, modifications of the precursor solutions are required to increase the solvent evaporation. Moreover, studies of the stability of these devices are required. Stability tests, on the other hand, need to be standardized. Because perovskite solar cells are a relatively new technology, there are no standardized degradation tests, which makes it difficult to establish a long-term stability reference. The perovskite research field is still growing, so that in the next years possible these aspects will be covered, being one step closer to the first perovskite photovoltaic device available for commercialization.



Chapter 4

ONE-STEP METHOD FOR THE FABRICATION OF HIGH-QUALITY PEROVSKITE THIN- FILMS UNDER AMBIENT CONDITIONS

CESAR MANUEL DEL ANGEL OLARTE

4. ONE-STEP METHOD FOR THE FABRICATION OF HIGH-QUALITY PEROVSKITE THIN-FILMS UNDER AMBIENT CONDITIONS: STABILITY, MORPHOLOGICAL, OPTICAL AND ELECTRICAL EVALUATION

4.1. Introduction

Perovskites for photovoltaic applications are organic-inorganic hybrid materials with the typical formula ABX_3 , where A corresponds to an organic cation (usually methyl ammonium, MA or formamidinium, FA), B represents a heavy metal (Pb or Sn) and X is a halogen (Cl, Br, or I)[84]. The most studied perovskite is methylammonium lead iodide (MAPbI) which stands out for its low energy band gap, high absorption coefficient, long diffusion distance, and high electronic mobility[85]. Moreover, these properties can be modulated by mixing the halogens and the organic cations in certain proportions[14].

Lead halide perovskites were used for the first time in 2009 by Miyasaka as absorbers in dye-sensitized solar cells (DSSC), obtaining an efficiency of 3%[10]. Shortly after this event, a new class of photovoltaic devices known as perovskite solar cells (PKSC) emerged. PKSC rapidly evolved, showing a remarkable breakthrough and achieving efficiencies up to 21% only in seven years[86]. This accomplishment was possible because of their exceptional optic and electrical properties. Perovskite thin-films (PKTF) can be easily obtained from solutions that require simple deposition techniques that can be extended to continuous production[14].

Initially, the most used method to obtain PKTF was spin-coating, which consists of dispersing a solution over a rotating substrate [29]. Spin-coating is a batch technique that also wastes more than 80% of the solution used[87], limiting the production to a low area solar cells with the disadvantage of excessive waste of raw material. Over the years, new methodologies to obtain thin-films have been developed. Some examples are blade-coating[88], ink-printing[89], roller-coating[90], and slot-dye[91] coating. These are scalable techniques that promise to solve the batch problem and the

necessity of using inert atmospheres during the deposition process. In this framework, blow-drying is a novel deposition technique that has the advantage of being a low-cost and simple methodology. It only requires a gas stream to eliminate the solvent and promote the formation of the PKTF[39]. Besides, the blow-drying method offers a negligible waste of reactants and can cover a high surface area. Examples of the application of this technique are the works of Zheng et. al. that used a dry N₂ stream to obtain PKTF[92]. From their studies, the authors reported the obtention of homogeneous morphology and good optical properties; on the other hand, Zhang et. al. utilized compressed air to obtain the PKTF and extended the study fabricating PKSC under ambient conditions[40]. At the same time, Ding et. al. used a modified blow-drying method (air blading) to produce first the PKTF and then the PKSC[93]. Although high efficiencies were obtained for the fabricated solar cells, any degradation or stability studies for the PKSC or PKTF were reported in these works. Therefore, stability still represents a huge problem that prevents the development of PKSC as commercial product [94].

In order to commercialize a photovoltaic product, durability must be assured, but lead halide perovskites are highly unstable to humidity[61]. Some strategies to overcome this degradation problem are the substitution of the organic cation for an inorganic ion[95], the implementation of double-layer deposition[96], and the use of polymer composites either as host matrix or protective layer[97]. All these strategies have been carried out with the spin-coating technique, but no studies on stability using scalable techniques under ambient conditions have been reported.

In this work, for the first time, it is proposed a modified blow-drying method for the production of homogeneous and stable MAPbI thin-films. Our method uses hot air in a one-step deposition procedure under ambient conditions. A systematic study of the influence of air temperature on the chemical composition, stability, and crystallinity of the PKTF was performed. The effect of the concentration of the reactants on the morphology and optical properties of the thin films was determined. Additionally, a careful degradation study was carried out under 25% relative humidity (R.H.), showing

the high stability of PKTF for several days. Finally, the electrical and photovoltaic performance of the obtained thin-films and planar heterojunction solar cells were evaluated respectively, highlighting the reliability of the proposed low-cost deposition method to obtain high-performance PKSC.

4.2 Thin Film Preparation

4.2.1 Materials and precursor solutions

The reagents Lead Iodide (PbI_2 , 99.99 %) and methylammonium Iodide (MAI, 98 %), and the solvent Dimethylformamide (DMF, 99 %) were purchased from Sigma Aldrich and used without further purification. Precursor solutions with different molar concentrations (0.216 M, 0.326 M, and 0.434 M) were prepared to maintain the molar ratio PbI_2 :MAI as 1:1, the reactants were dissolved in 1 mL of DMF and stored under dark conditions.

For the preparation of the thin films, borosilicate glass substrates (Lauka) with 2.5 x 2.5 cm dimensions were employed. Prior to deposition, the substrates were treated in a caustic bath for 24 hours, then the slides were cleaned by sonication in a soap solution (5 %), deionized water and ethanol for 15, 10 and 5 min, respectively.

4.2.2 Deposition procedure

The perovskite thin-film deposition carried out by the standard blow-drying method consisted of dispersing 3, 4, or 5 μL of precursor solution over the glass substrate with the help of a syringe tip. After that, the prepared substrates were exposed to a perpendicular air stream (15 m/s, 25 °C, 25 % R.H.) for 10 min, the graphical procedure can be seen in Figure 29. The thin-films obtained by this method were taken as reference.

The hot air blow-drying (HABD) method was achieved by introducing a heat resistance into the flow system resulting in a hot air stream ($T = 90\text{ }^{\circ}\text{C}$, R.H. $< 25\%$). For this case, the glass substrates containing the dispersed solution were exposed to the same flow rate (15 m/s) for 1 min. After the deposition, the thin-films were stored in closed chambers with constant R.H. of 25% until the degradation analysis.

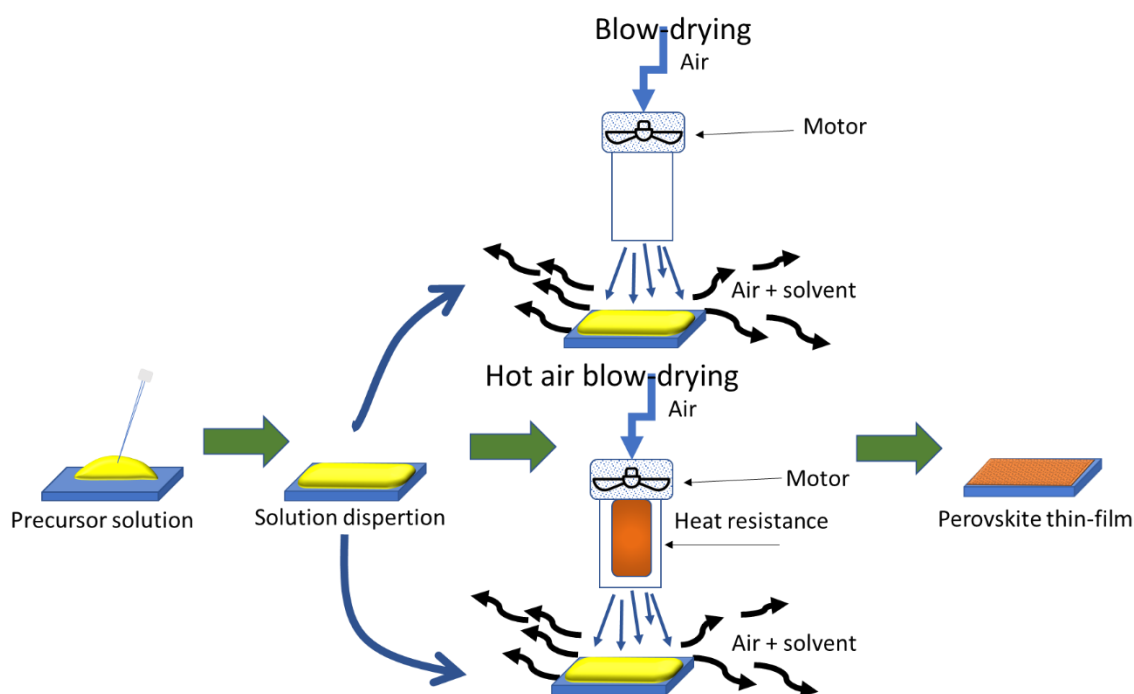


Figure 29. Perovskite preparation by blow-drying deposition under room conditions

4.3 Photovoltaic device preparation

Transparent conductive oxide (TCO) of $\text{SnO}_2:\text{F}$ coated glass substrates ($R = 25\ \Omega\text{cm}$, Aldrich) were cleaned by ultrasonication in a soap solution (5%), deionized water, and ethanol sequentially for 15 min. Next, CdS was deposited as the hole blocking layer (HBL) following the methodology previously reported by Nair et al. and applied in solar cells by Moreno-García [98,99]. Subsequently, MAPbI perovskite was deposited by HABD methodology over the CdS layer. Finally, Colloidal graphite paint (SPI-Chem) was applied and left to dry for 2 h at room temperature. Furthermore, colloidal silver paint (DuPont SP 480) was applied to the graphite electrode and dried at room

temperature overnight. The solar cells were maintained in closed chambers (25 °C, 25% R.H.) until photovoltaic device characterization.

4.4 Thin-film characterization

Surface chemistry was analyzed by Fourier Transform Infrared Spectroscopy (FTIR), the thin-films were characterized in a Cary 600 spectrophotometer (Agilent) coupled with an Attenuated Total Reflection accessory. The analyses were carried out under ambient conditions in the range 4000 – 400 cm^{-1} with a 4 cm^{-1} resolution. For the crystal structure, the X-Ray Diffraction (XRD) analysis was carried out in a D8 DaVinci diffractometer (Bruker). The samples were irradiated with $\text{CuK}\alpha$ ($\lambda = 1.5406 \text{ \AA}$) in the 10° to 50° (2θ) range. The surface morphology was observed by Scanning Electron Microscopy (SEM) in a Philips FEI microscope operated at 20kV. The surface coverage was calculated by using the measurement function in ImageJ software.

Textural properties were studied by Atomic Force Microscopy (AFM). The AFM images were taken in the tapping mode over different areas (Dimension Edge, Bruker). The images were analyzed in NanoScope Analysis 1.5 to obtain the surface morphology and roughness parameters. The optical properties were determined by UV-vis absorption in a Cary 60 (Agilent) spectrophotometer. For this analysis, the thin-films were scanned in the range 950 – 350 nm under ambient conditions.

Furthermore, the degradation of MAPbI thin-films was monitored every 24h by UV-vis absorption. The electrical properties of thin-films were measured at room temperature by Hall effect using the Van der Paw method. For the measurements, a four-probe sample was analyzed without and with a magnetic field (0.17 T) a constant current (30 nA). For the photovoltaic performance, Current-Voltage curves were obtained using a Keithley 4200-SC source meter unit under AM 1.5 solar illumination with an intensity of 100 mW/cm^2 . The effective area of the solar cell was 0.2 cm^2 .

4.4 Results and discussion

4.4.1 Chemical composition

FTIR analyses were conducted to evaluate the effect of the air temperature used to evaporate the solvent during the preparation of MAPbI thin-films. The results are shown in Figure 30. MAPbI is a hybrid material composed of the organic cation MA and an inorganic coordination compound (PbI_3^-). Therefore, some vibrational signals related to the organic part can be detected and identified by this technique. The organic precursor MAI was used as a reference to confirm the formation of MAPbI.

Figure 30a shows the infrared spectrum of dry MAI, the characteristic signals of -NH stretching vibration bands are observed at 3080 and 1500 cm^{-1} , and the C-N at 900 cm^{-1} , confirming the presence of methylammonium molecule. By using regular air, several minutes are required to create the MAPbI thin-film. Figure 30b depicts the infrared spectrum of the sample prepared by using air at $25\text{ }^\circ\text{C}$. The recorded spectrum shows the characteristic vibrations of MA; however, additional features are observed. The -NH stretching vibration previously observed at 3080 cm^{-1} was shifted to 3180 cm^{-1} which was attributed to the chemical interaction of MA with the coordinated PbI_3^- molecule [100]. This signal decreased dramatically when the films became hydrated; at this condition, a new vibration band characteristic of -OH stretching appears at 3500 cm^{-1} . The hydration of the thin-film could be ascribed to the slow rate of solvent evaporation. As the gas phase at standard conditions contains a minimum quantity of humidity, water molecules may interact with the film surface and with the MAPbI internal structure, resulting in the observed partial hydration [100]. This water impurity promotes a premature degradation of MAPbI films since the water quickly degrades the methylammonium cation.

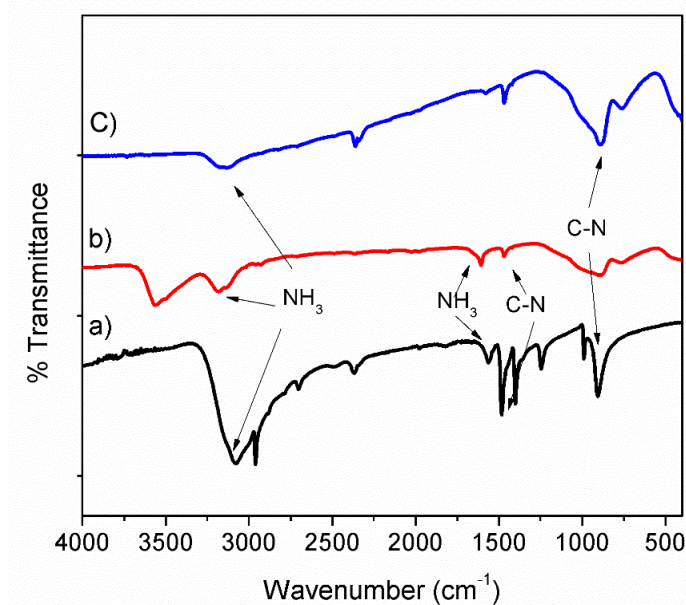


Figure 30 Infrared spectra: a) Methylammonium Iodide powder and MAPbI thin-film obtained by blow-drying methodology using b) air at 25 °C, and c) hot air at 90 °C.

When hot air is used (90 °C), the solvent diffusion increases, resulting in an almost instantaneously film formation. Figure 30c shows the corresponding spectrum of MAPbI thin-film obtained when using hot air to eliminate the solvent. Two critical features can be highlighted: 1) the spectrum shows the characteristic vibrations of MA and 2) there is no vibration of -OH stretching, which means that thin-films formed using hot air do not present water contamination. The use of hot air represents a technical advantage against other deposition techniques because the solvent completely evaporates, eliminating the post-annealing treatment of thin-films usually used after spin-coating deposition [101]. Besides, the air temperature prevents possible water infiltration either at the surface or internal level during the formation of the perovskite films due to the short time required to obtain the thin-films.

4.4.2 Crystallography

MAPbI perovskite is highly sensitive to moisture; the organic cation can be easily deprotonated by water molecules. This reaction corresponds to the first step on the degradation mechanism [102]. With the hydrolysis of MA, the crystalline structure gradually changes, forming two additional crystalline phases. Figure 31 shows the diffractograms of thin-films obtained by the proposed blow-drying method, the crystalline structure of these films was compared with the reference (Figure 31a), previously reported by Oku [66].

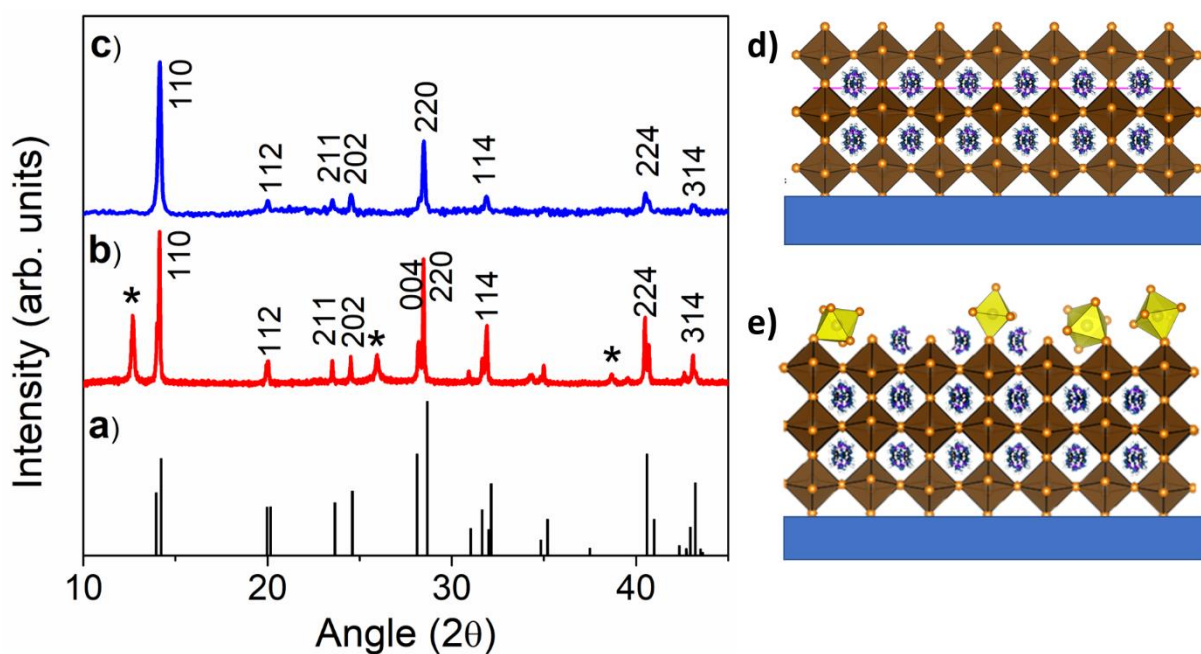


Figure 31 Crystalline structures of MAPbI thin-films obtained by blow-drying, a) calculated diffraction pattern, b) MAPbI perovskite synthesized with air at 25 °C and 25 %R.H. and c) MAPbI thin-film obtained at 90 °C with low humidity atmosphere (<25 %). Schemes of the MSPbI perovskite crystalline structure d) oriented in the 110 direction, and e) partially degraded.

It is observed that both materials show the tetragonal crystalline structure. This result was corroborated by the coincidence of the experimental diffractograms with the calculated diffraction peaks. However, thin-films prepared with air at 25 °C (Figure 31b)

show additional diffraction peaks (12.67° , 25.84° , and 38.7°), assigned to (001), (002), and (003) diffraction planes of PbI_2 . The coexistence of MAPbI and PbI_2 phases in the thin-film confirms the partial degradation of the material. When the air flows through the solution and evaporates the solvent, some molecules of water can get trapped on the internal structure of the as-synthesized film. Subsequently, these molecules could start the degradation process changing the crystalline structure of the material. Figure 31e shows a sketch of the possible coexistence of PbI_2 and MAPbI phases drawn with the software VESTA [103].

On the other hand, when hot air is used to obtain MAPbI thin-films, the high temperature boosts the solvent vapor pressure and increases the diffusion, letting the formation of pure MAPbI in a matter of seconds. As can be seen in Figure 31c, there is no signal of diffraction planes of PbI_2 , indicating the presence of pure perovskite material. Table 6 summarizes the lattice constants of each sample. Moreover, the crystallite size was calculated by using the Debye-Scherrer equation

$$D = \frac{0.9 \lambda}{\beta \cos \theta} \quad (12)$$

Where D is the crystallite size in nm, λ is the diffraction wavelength, β is the full width at half maximum, and θ is the angle of diffraction. According to these data, the unit cell was not affected by the type of methodology employed. The crystallite size, on the other hand, showed a remarked difference, being up to three times bigger the obtained with regular air in comparison with the obtained by HABD. This outcome is in accordance with the evaporation rate itself. A low rate needs long exposure time, allowing the crystal to grow bigger. In the case of instant evaporation, the crystallite grow is limited resulting in small crystallite size.

Table 6 Summary of lattice constants and crystallite size for perovskite thin-films obtained by blow-drying methodology

Sample conditions	Lattice constants (Å)		Crystallite size ^a (nm)
	a	c	
Regular Air (25 °C)	8.85	12.65	145.2
Hot Air (90 °C)	8.85	12.64	51.5

^aCrystallite size calculated by the Debye-Scherrer equation using the XRD information

Another important feature of this result is the absence of diffraction peaks located at 13.95° and 28.11° corresponding to (002) and (004) planes, and the high-intensity and well-located diffraction peaks belonging to (110) and (220) planes, which seems to indicate the preferential growth of the PKTF in the 110 direction.

4.4.3 Thin Film Morphology

The blow-drying method involves using an inert gas stream to evaporate the solvent and promote the crystallization of PKTF. The inert gas is recommended to avoid premature degradation during the synthesis of thin-films [104]. However, in some cases, the air has also been used to enhance the solvent evaporation in gas-assisted spin coating procedures [38]. With this base, we adapted the blow-drying method to use air to evaporate the solvent. Figure 29 depicts the procedure to obtain the MAPbI thin-films by air blowing at different temperatures. As a control, regular air (25 °C, 25 %R.H.) was used to prepare PKTF, which showed irregular film coverage (see Figure 32a). The films took several minutes to be obtained, mainly due to the high boiling point of the solvent (DMF, 153 °C).

The impact of using air blowing to fabricate smooth PKTF was determined by Gao et al. [12]. From their work, the authors concluded that an important factor to be

considered during the film formation is the rate of solvent diffusion, which is strongly influenced by the solvent concentration gradient g in the gas phase:

$$g = \frac{\partial C}{\partial h} \quad (13)$$

Where C is the solvent gas concentration, and h is the distance to the liquid surface.

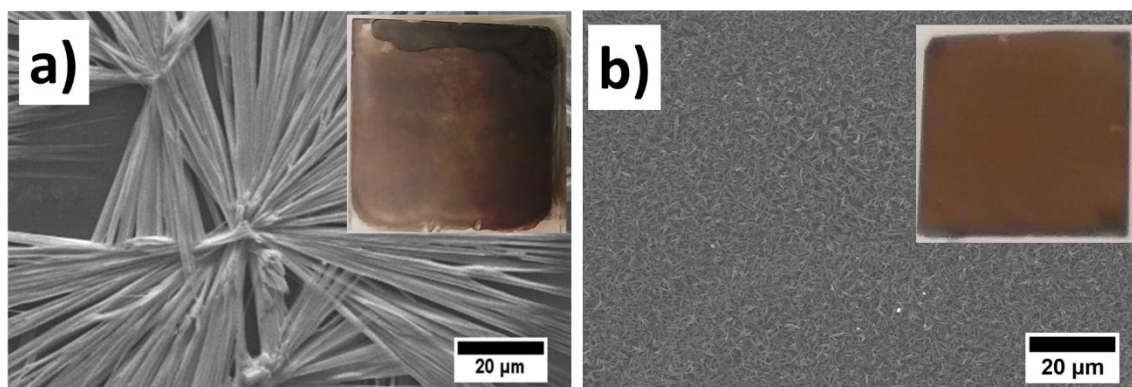


Figure 32 Surface morphology of perovskite thin-films obtained by blow-drying deposition methodology using: a) regular air(25 °C,25 %R.H.), and hot air(90 °C).

By using an air stream, the evaporated solvent molecules leave the liquid surface at the airflow rate, increasing the solvent concentration gradient due to a low concentration of evaporated solvent in the air. However, as the solvent evaporates, the perovskite formation takes place simultaneously, making it very sensitive to the rate of solvent evaporation. Consequently, when the evaporation rate is not fast enough, isolated large crystals grow, as can be seen in Figure 32a, where large dendritic structures with some void spaces covered the surface. Moreover, a rough surface can be easily seen by the naked eye (see inset in Figure 32a) due to poor film deposition. Thus, the morphological characteristics of the films obtained by using regular air do not meet the requirements for being used in the construction of thin-film solar cells.

Despite using an air stream to promote solvent diffusion, it seems that environmental condition is not enough to achieve a good quality thin-film. According to Fick diffusion law, presented in equation (14)

$$J_A = -D_{AB} \frac{\partial C_A}{\partial h} \quad (14)$$

The mass flow rate (J_A) is not only affected by the concentration gradient but also by the diffusion coefficient (D_{AB}), which is temperature and pressure-dependent. A simple correlation for temperature and pressure correction can be derived from the equation proposed by Fuller et. al. [105]:

$$D_{AB}^* = \left(\frac{T^*}{T}\right)^{1.75} \left(\frac{P}{P^*}\right) D_{AB} \quad (15)$$

The corrected diffusion coefficient (D_{AB}^*) is calculated at the given temperature and pressure (T^* , P^*). As can be seen in equation (15), the diffusion coefficient is strongly influenced by temperature and inversely proportional to pressure. Moreover, by increasing the temperature, the solvent vapor pressure rises exponentially, contributing to a faster evaporation rate. This analysis suggests that the use of a hot air flow promotes fast solvent evaporation. Figure 32b shows the thin-film obtained with this procedure. By blowing hot air, just some seconds are necessary to obtain the thin-film. Additionally, the homogeneity was enhanced dramatically, which can be noticed in the SEM micrograph (Figure 32b); also, the film coverage along the glass surface

was complete. Based on the previous results, hot air was used as a promoter of the solvent evaporation during the construction of the PKTF reported in this study.

The concentration of precursors and the volume of solution selected are essential parameters to consider during the synthesis of MAPbI thin-films. In the usual spin coating techniques, high solution concentrations are used (~ 1.5 M), not to mention the volume of solution (up to 100 μ L) [76]. Unfortunately, the spin coating procedure wastes more than 70 % of the precursor solution, which is a significant concern because of the toxicity of the reactants. With the HABD method proposed in this work, the amount of reagents used is drastically reduced and fully exploited. Figure 33 shows photographs of the thin-films obtained by HABD. By eye, it can be observed that all the PKTF are semitransparent (Figure 33a), with a mirror-like appearance (Figure 33b).

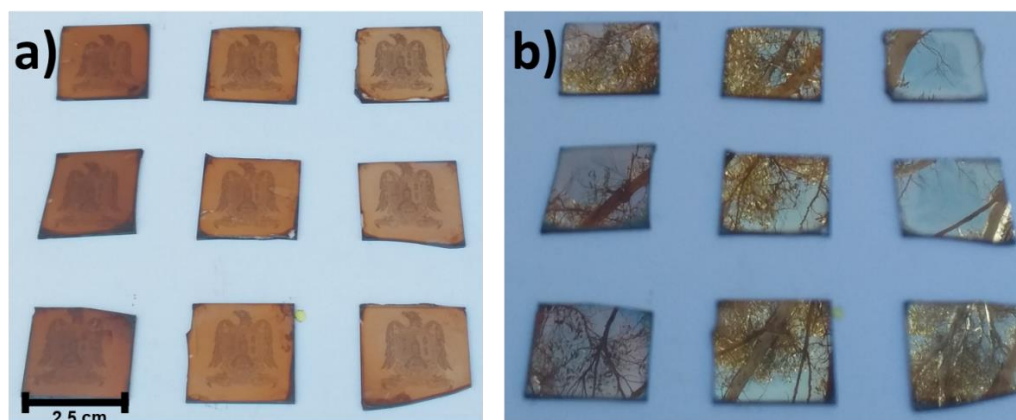


Figure 33 Photographs of MAPbI perovskite thin-films obtained by hot air blow-drying method (air-flow = 10 m/s, $T = 90$ °C) at different solutions' volume and precursors' concentration: a) degree of transparency, b) mirror-like appearance denoting the macroscopic homogeneity.

In general, all the films obtained with the HABD methodology showed a needle-like morphology (Figure 34), which can be explained with XRD results. The needle-like morphology of perovskite is induced by the PbI_2 precursor [22], which grows with preferential orientation in the z-axis, producing long-strip crystals. During the

perovskite film formation, the DMF solvent first coordinates in the 001 interplanar space of PbI_2 ; after that, it is replaced by the MAI molecule. A rearrangement of crystal structure occurs without altering the growth orientation. Figure 34 sketches the orientation of the crystal structure. According to XRD analysis, the film grows in the (110) direction vertically (diffraction plane in pink), and the z-axis is perpendicular to this plane (diffraction plane highlighted with a green line). Therefore, the preferential orientation of the MAPbI thin-film was induced by the PbI_2 during the formation.

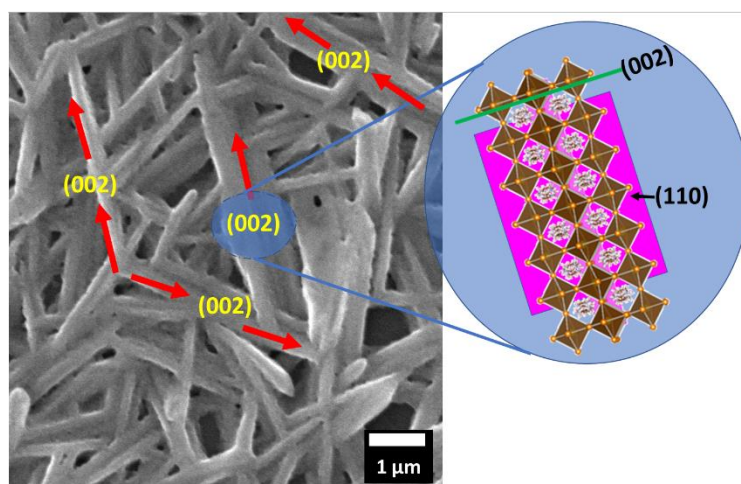


Figure 34 Morphology of MAPbI perovskite thin-film related with the crystal orientation obtained by XRD. The crystal grows in the z-direction resulting in a needle-like morphology observed by SEM.

On the other hand, the surface coverage was directly affected by the concentration of the precursor solution. Figure 35a shows the morphology of a thin-film obtained when using a 0.216 M solution, and the inset is a magnification of a selected area showing uncovered spaces. When the concentration was increased to 0.32 M, more linear microstructures covered the surface (Figure 35b); however, the inset shows a less uncovered area that the obtained at low precursor concentration. Finally, at using a 0.454 M precursor solution (see Figure 35c) almost total coverage was achieved on

the surface, the number of microstructures increased dramatically and just a few uncovered sites could be detected in the inset image.

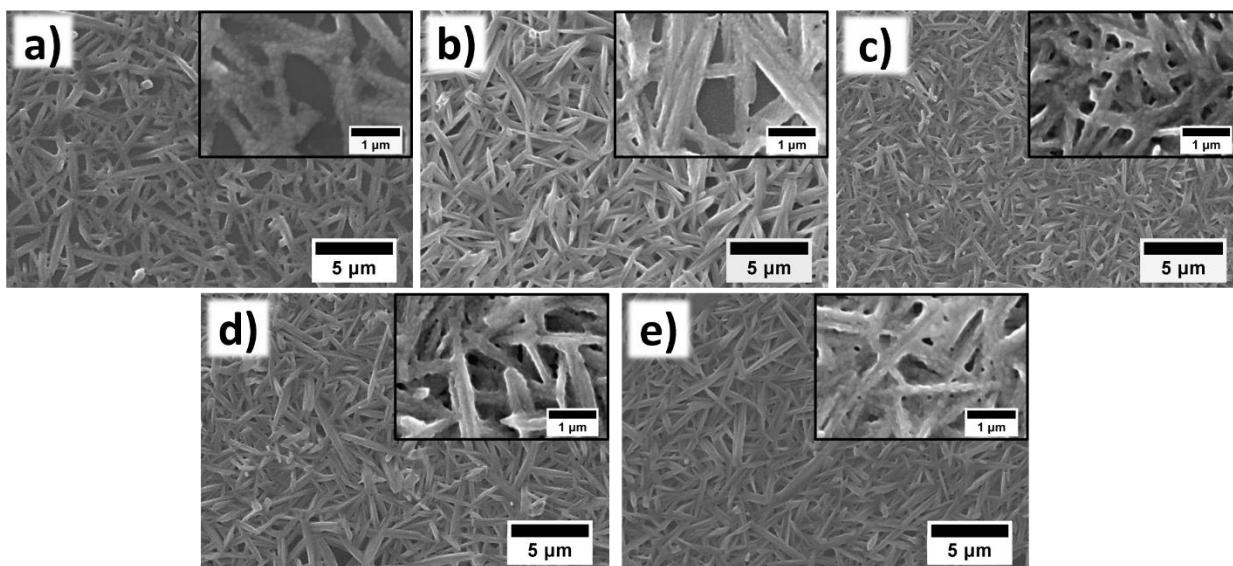


Figure 35 Effect of concentration and volume of precursor solutions in the morphology of MAPbI₃ thin-films. Morphology obtained with 3 μL of: a) 0.216 M, b) 0.32 M, and c) 0.434 M precursor concentration, d) 4 μL , and e) 5 μL of 0.434 M precursor solution.

It is important to notice that the volume of solution used in the previous studies was 3 μL , which is much smaller than the conventional volume utilized to obtain PKTF. Moreover, all the volume dispersed in the substrate was transformed into the thin-film with no waste of precursor solution. This is an important advantage of our proposed HADB methodology. In order to improve the surface coverage of the PKTF, the volume of the 0.434 M solution dispersed in the substrate was increased to 4 μL . The obtained morphology is shown in Figure 35d. In this case, the linear microstructures formed a compact layer by interconnecting each other, which can be seen in the inset. Finally, the morphology obtained using 5 μL of precursor solution (Figure 35e) showed an apparent fully covered substrate, with linear structures merged, resulting in a crosslinked microstructure (inset Figure 35e). Based on these results, it can be

concluded that the holes and surface defects are produced during the crosslinking of the linear structures. Moreover, during the film formation the solvent creates pathways to evaporate from the solid film [106,107], also inducing some morphological defects on the surface .

In our method, we optimized the conditions to reduce surface defects, which was corroborated after surface coverage calculation (Table 7, from SEM images).

Table 7 Surface coverage and film thickness of MAPbI perovskite thin-films obtained with different precursors' concentration and solutions' volume by the HABD deposition method.

Concentration (M)	Volume (μL)	% Covered area	Thickness (nm)
0.216	3	84	120
0.320	3	89.3	150
0.434	3	95.5	150
0.434	4	96.5	160
0.434	5	97.2	180

It can be seen that surface coverage was enhanced dramatically despite the nature of the thin-film growth, achieving a 97% surface coverage for the highest concentration and volume. Similar results were obtained by Ouafi et. al., who investigated the crystal growth of MAPbI thin-films obtained by hot-air flow assisted spin-coating [38].

Another important feature observed was the composition of the microstructures that form the film. At low magnifications, the morphology resembles stacked linear structures. The insets reveal that these linear structures are conformed by tiny micro grains. As the solution concentration raised, the crosslinked structures increase.

4.4.4 Textural properties

A more in-depth study of the PKTF thin-film surface morphology was performed to understand the perovskite crystal growth. AFM analysis was performed on samples

with better film coverage (those obtained with 0.434 M precursor solution). It was found a more detailed surface morphology (Figure 36), mainly due to the capability of the AFM technique to determine the real surface texture of the films with higher resolution. Figure 36a-c show the morphology of thin-films obtained with 3, 4, and 5 μL of precursor solution, respectively. By comparing the morphology of these films with those obtained by SEM (Figure 35c-e) it can be noticed that the linear appearance of the microstructures disappears, and only a granular crosslinked structure is observed. Moreover, the granular surface was barely noticed by SEM analysis, in Figure 36d-f a detailed surface morphology is depicted, revealing that the MAPbI thin-films are composed of stacked micro grains with homogeneous size. This technique allows us to confirm the increase in surface coverage.

The film thickness is shown in Figure 36g-i. The cross-sectional height indicates that film thickness is slightly affected by the volume of the precursor solution used to obtain the PKTF. However, important is to notice that HBD methodology is capable of produce thin-films of ~ 180 nm thickness and ~ 29 nm surface roughness (Figure 36b), in agreement with previous results [37,108], with the advantage of using a minimum volume of precursor solution and no waste of chemical precursors.

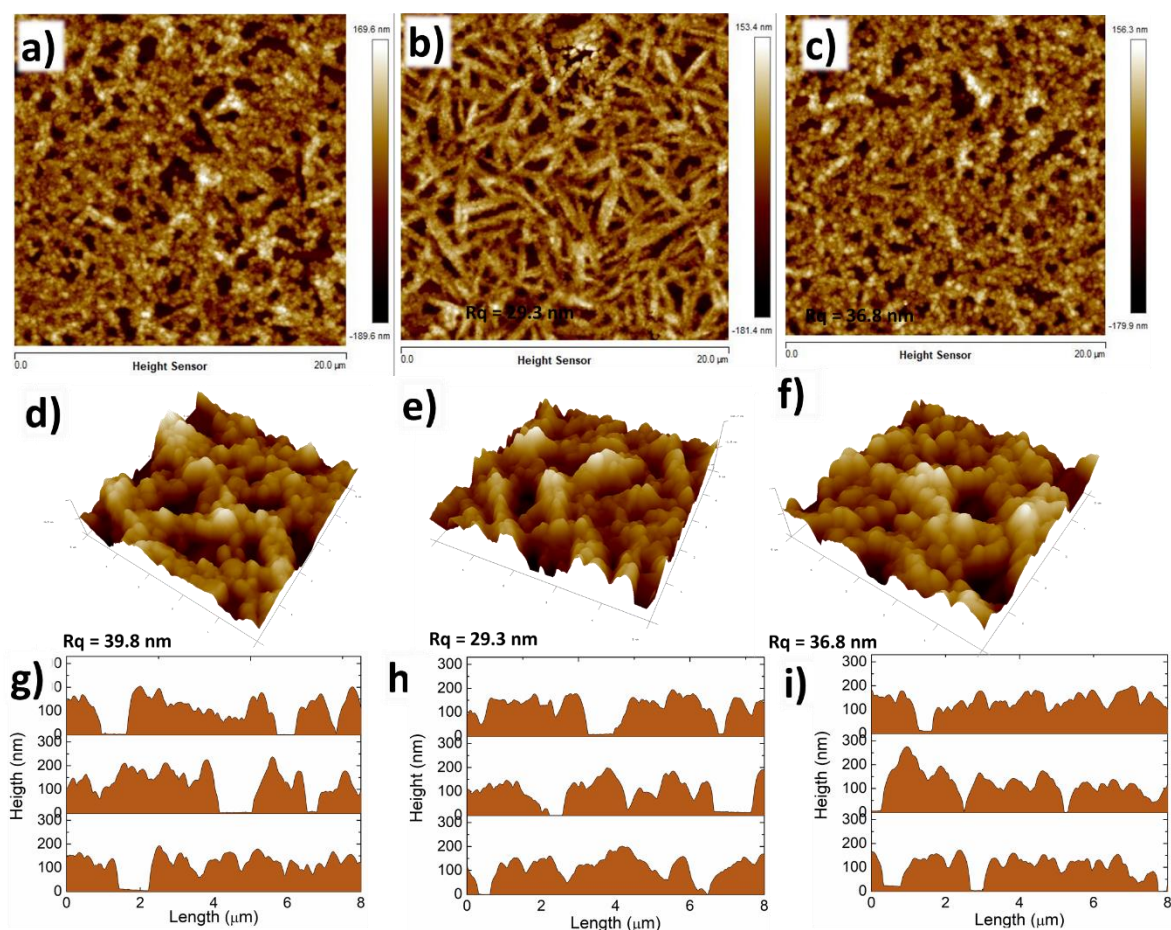


Figure 36 Textural analysis carried out by AFM. Perovskite films (a-c) obtained with 3 μL , 4 μL and 5 μL of precursor solution, respectively. 3D perspective (d-f) of the thin-films. Cross-sectional height in three different areas of the same thin-films (g-i). The solution concentration was 0.434 M.

4.4.5 Optical properties

Figure 37a shows the absorption spectrum of the obtained MAPbI thin-films with optimized conditions. For this analysis, hot air at 90 °C and 0.434 M precursor solution were used. The analysis was conducted in different regions along the film to show the homogeneity. MAPbI perovskite has an energy gap of 1.56 eV and shows an absorption band below 790 nm [109]. This feature is used as a reference to determine the presence of the MAPbI perovskite material; as the degradation proceeds, the absorption decreases until disappear [102]. Additionally, the absorption coefficient of

the MAPbI thin-films was calculated. Figure 37b shows a comparison between absorption coefficients of MAPbI perovskite and silicon (which is a useful reference in the solar cell field). Moreover, Table 8 summarizes the absorption coefficient of MAPbI at 750 nm and silicon at the same wavelength along with some data from bibliography.

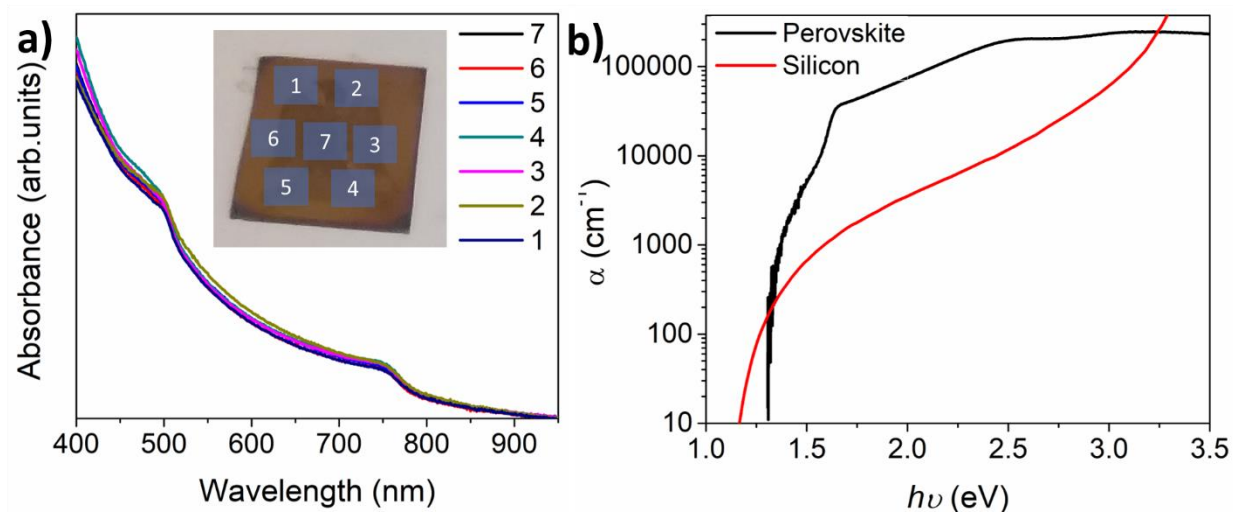


Figure 37 Optical properties of synthesized MAPbI thin-films by blow-drying methodology, using hot-air at 90 °C: a) Absorbance spectra of different sections of the thin-film and b) calculated absorption coefficient of MAPbI compared with the silicon.

According to these data, MAPbI perovskite exhibits a higher absorption coefficient, requiring a thinner thickness to absorb most of the radiative energy of the solar spectrum. Moreover, experimental data obtained from other authors suggest that there is still no standard value for this parameter.

Table 8 The absorption coefficient of MAPbI thin-film and c-silicon at 750 nm.

Material	α ($\times 10^4$ cm^{-1})	Reference
MAPbI ₃	3.5	This work
c-Si	0.1	[110]
MAPbI ₃	1.5	[111]
MAPbI ₃	0.5	[112]
MAPbI ₃	0.4	[109]

4.4.6 Chemical stability

The chemical stability of MAPbI perovskite has been recognized as one of the most important properties to be enhanced in order to make possible the production of perovskite-based photovoltaic products. For this reason, over the past few years, the researchers have focused on studying and understanding how different environmental factors affect the lifetime of perovskite layers and photovoltaic devices. Since the initial studies involving MAPbI perovskite as an absorber layer, the temperature and moisture were identified as essential parameters that promote degradation.

Boyd et. al. suggested that perovskite thin-films degrade upon long-term exposure over 85°C [113]. However, Dualeh et. al. demonstrated through thermogravimetric analysis that MAPbI degradation starts over 234 °C [63]. Other studies used a post-annealing treatment [40,48,114–116] to improve the crystallinity of the material. In this last process, the as-synthesized films are exposed to temperatures ranging from 90 °C to 150 °C for several minutes. No film degradation was observed, indicating that short-term exposure to high temperatures is favorable for the perovskite thin-film formation. This information agrees with the results discussed in sections 4.4.1 and 4.4.2, discarding the possible thermal degradation of the thin-film and enabling the study of chemical degradation by moisture exposure.

A dry atmosphere is always recommended during and after the perovskite formation, mainly due to the perovskite chemical instability. However, with the development of scalable and continuous deposition procedures, ambient conditions have been successfully faced, but there is no information about the thin-film stability after the deposition procedure, which is an important factor to determine if it is known that the deposition method can affect the chemical stability of the thin-films.

In Figure 38, UV-vis spectra of MAPbI thin-films show the degradation process; these materials were stored in a glass chamber under 25 %R.H. conditions. The set of

experiments analyzed show the influence of degradation resistance when 3 μL of different concentration solution is used. In Figure 38a several spectra of the PKTF obtained from a solution 0.216 M are depicted. The characteristic features of a MAPbI UV-vis absorption spectrum are the absorption bands located at 750 and 490 nm, which correspond to the direct absorption and the charge transfer, respectively [117]. The absorption band located at 750 nm was chosen as a reference to follow the degradation process because it is the characteristic absorption of the MAPbI perovskite.

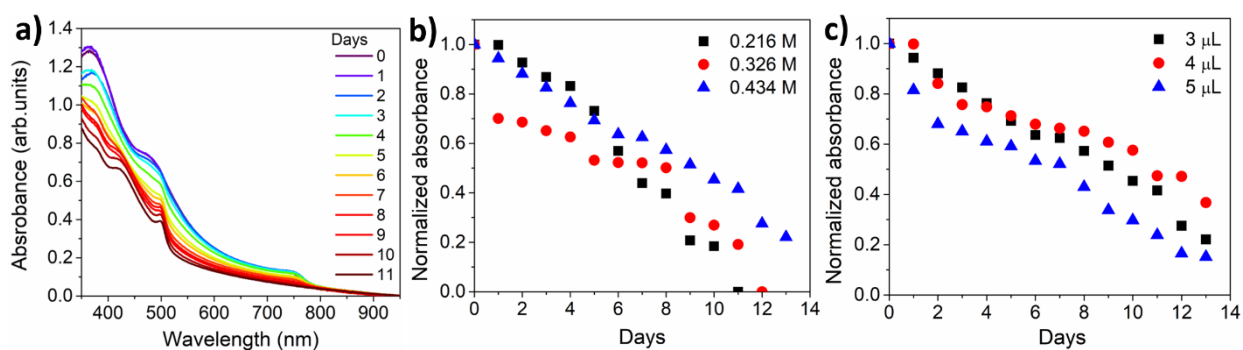


Figure 38 Degradation study under 25 %R.H. of perovskite thin-films. a) Degradation kinetics followed by measuring the UV-Vis absorbance of the thin-films, b) effect of the precursor concentration on the perovskite degradation following the absorption intensity at 750 nm, c) degradation rate of thin films obtained with different volumes of a 0.434 M precursor solution.

As depicted in Figure 38a, the intensity of the characteristic absorption of the MAPbI perovskite decreases slowly; after 10 days, the absorption has wholly disappeared. Simultaneously, a new absorption band arises at 500 nm, which is the characteristic absorption of PbI_2 . In Figure 38a, this feature is slightly noticed on the fifth day and completely evident on the seventh day. Finally, after 10 days, this absorption becomes a peak indicating the complete degradation of the thin-film. The degradation can also be noticed by a change in the color of the thin-film. The dark brown color recognizes the as-synthesized perovskite; over time, this color gradually changes to the light-

yellow characteristic of PbI_2 product. Figure 39 depicts a set of experiments degraded after 10 days; the color change can be easily noticed.

Figure 38b shows the degradation rate for the samples synthesized with different precursor concentrations. By using a 0.326 M concentration, the degradation resistance was not enhanced; after 12 days, the perovskite signal completely banishes. Stability was slightly increased when a 0.434 M precursor solution was used. It can be noticed that after 10 days, the perovskite absorption remains. These results can be related with the surface coverage previously discussed; the uncovered substrate can be considered as a surface defect prone to be attacked by water molecules. Thereby a complete coverage is required not only to avoid chemical degradation but also for a good photovoltaic performance.

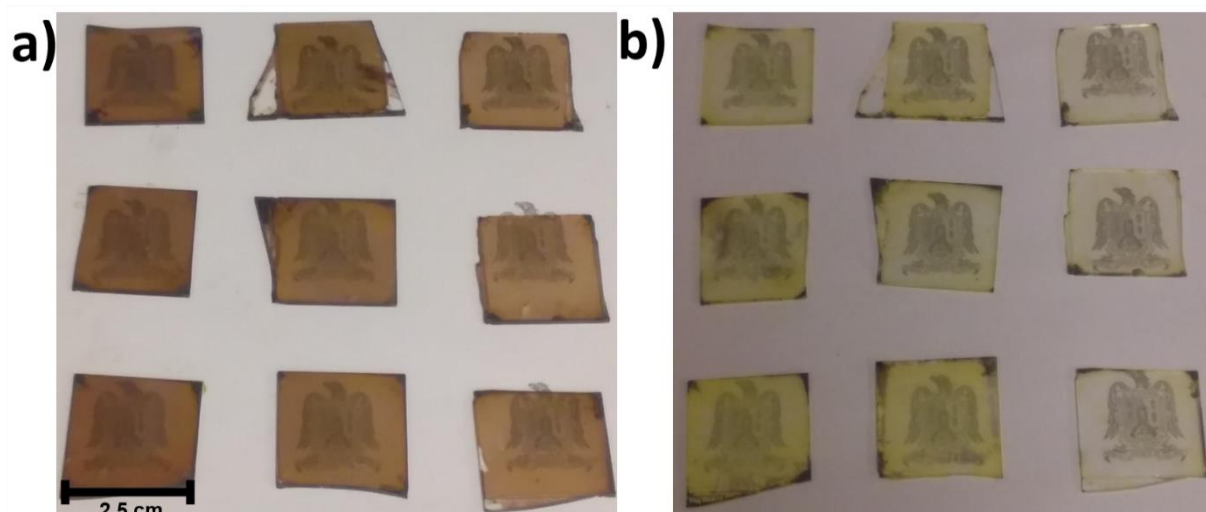


Figure 39 Perovskite thin-films degraded under controlled conditions (25 °C, 25% R.H.): a) as-synthesized MAPbI₃ thin-films obtained by HADB method (air at 90 °C) b) degraded thin-films after several days of exposure at the controlled atmosphere.

In this sense, the PKTF obtained with the highest concentration of precursors showed a better degradation resistance (Figure 38c). The total degradation can be extended

for more than fifteen days, which agrees with the surface coverage. It is important to highlight that the analysis was conducted over bare films under controlled ambient conditions ($T = 25\text{ }^{\circ}\text{C}$, R.H. = 25 %), which is an important approach not showed in previous reports related to alternative methodologies used to obtain PKTF. These results indicate that the PKTF can prevail at least the next five days after the synthesis, without needing strict humidity control or the addition of dopants to extend the chemical resistance. Moreover, the degradation could be reduced when the perovskite is integrated into a solar cell, where the transport layer protects the film from moisture interaction.

4.4.7 Electrical properties

Organic-inorganic perovskites are well known for its impressive optical and electrical properties, which strongly influence the photovoltaic behavior. Therefore, the PKTF obtained by HABD methodology-were assessed in order to explore the impact of the proposed technique in the electrical features. Table 9 summarizes the electrical properties obtained by Hall measurements for the sample obtained with 4 μL of 0.434 M precursor solution. According to these results, the experimental charge carrier concentration is in the order of 10^{20} m^{-3} , which is low in comparison with conventional charge carrier concentrations for n or p-type semiconductors. However, MAPbI perovskite is an intrinsic semiconductor, which means it possesses the same amount of electron and hole species.

Charge carrier mobility, on the other hand, agrees with several results compiled by Herz et. al. [118]. In their work, the authors concluded that mobility results could vary depending on the technique used to determine it and the nature of the sample. Hence this result can be taken as a reference to other experimental data. In the case of resistivity, Chen et. al. [58] discussed the difficulty of measuring electrical properties because of the high resistivity of pure MAPbI perovskite films. They reported resistivities in the range of $\text{G}\Omega$. Our results showed a resistivity six orders of magnitude

lower than the reported, which is attributed to the charge injection previous to the film characterization. As explained by Girtan [119], the conductivity of MAPbI thin-films is highly sensitive to environmental illumination, not to mention that the time required to recover the initial state is quite long. However, despite this, the electrical conductivity and charge carrier concentrations in this work agree with previous reports [120][121].

On the other hand, the charge carrier diffusion coefficient can be calculated according to Einstein relation:

$$\frac{D}{\mu} = \frac{k_B T}{e} \quad (16)$$

At room temperature is reduced to $D = \mu/38.9$ [V^{-1}], where μ is the experimental charge carrier mobility. In this case, the calculated diffusion coefficient agrees with the experimental values obtained by Stranks et. al. [122]. From these results, the electrical properties of the perovskite films obtained by HABD deposition prevail. This outcome demonstrates another advantage of the proposed methodology and its potential to be used in the massive low-cost production of PKTF.

Table 9 Electrical properties of perovskite thin-films obtained by HABD deposition

	$\eta \times 10^{20} (m^{-3})$	$\mu \times 10^4 (m^2V^{-1}s^{-1})$	$\rho (\Omega m)$	$D \times 10^{-5} (m^2s^{-1})$
Experimental	3.95	3.09	51.10	0.79 ^b

^bCalculated from Einstein relation $D = \mu/38.9$ at room temperature.

4.4.8 Photovoltaic performance

The HABD deposition is intended for low-cost production; moreover, the optimized synthesis conditions gave high-quality PKTF for photovoltaic application. For this reason, the performance of the PSC fabricated with PKTF obtained by both HABD and the standard method was compared. The architecture of the PSC was

TCO/CdS/MAPbI/Graphite-Ag. The CdS thin-film was obtained by chemical bath deposition, which is also a cheap and straightforward technique. The configuration of the fabricated planar heterojunction solar cell is shown in Figure 40. In PSC device, CdS was used as a hole blocking layer and perovskite as the absorber. The Current density-Voltage curves in Figure 40 display the typical diode behavior under dark and illumination conditions. This behavior indicates the existence of the photovoltaic effect, hence a solar cell fabricated under ambient conditions.

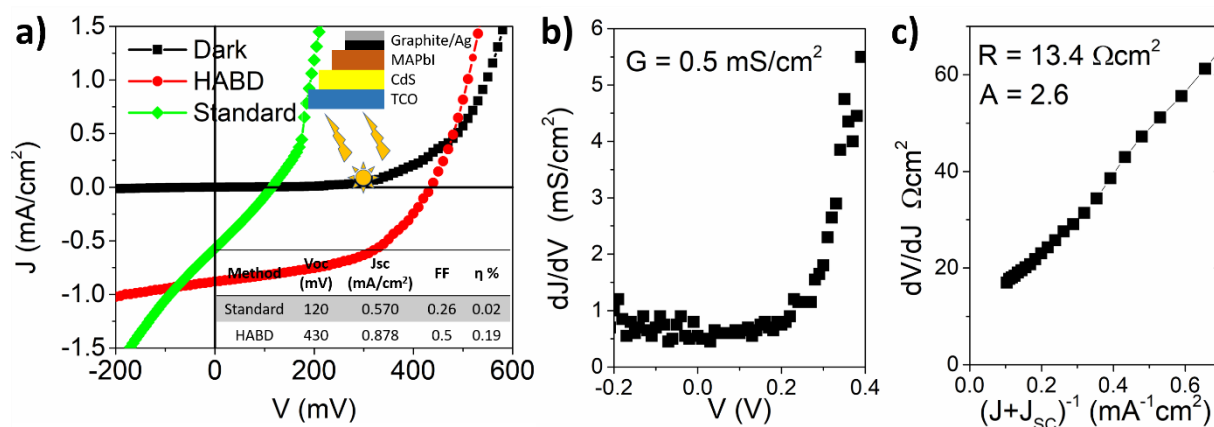


Figure 40 Photovoltaic performance of perovskite solar cells with MAPbI thin-films: a) comparison of the photovoltaic efficiency depending on the type of deposition technique, standard blow-drying, and HADB; b) shunt characterization $g(V)$ and c) $r(J)$ used to obtain R and A factors for the solar cell assembled by HADB methodology. The architecture of the solar cell was TCO/CdS/MAPbI/Graphite-Ag. The measurements were carried out under ambient conditions.

Regarding the photovoltaic performance, low current density was obtained, which can be attributed to the low thickness of the perovskite film and recombination of charge carriers due to the lack of hole transport material (HTM). Gu et. al. [123] studied the effect of the HTM in planar heterojunctions, where CdS nanorods were employed as an electron transport layer. In the absence of HTM, the current density obtained was in the range of 0.01 mA/cm², affecting the photovoltaic efficiency. Another reason for the poor photovoltaic performance can be ascribed to the parasitic losses in the solar

cell device. In order to know these issues, analysis over the current density-voltage curve was conducted [74] to determine the values of series resistance (R), shunt conductance (G), and ideality factor (A). The Figure 40b-c depict the obtained results. According to this procedure, the shunt conductance can be obtained from the derivative of exponential diode equation $g(V) = dJ/dV$ against V, where the flat zone in Figure 40b corresponds to $G = 0.5 \text{ mS/cm}^2$ given that the shunt term can be considered ohmic and J_L constant. Figure 40c, on the other hand, shows a plot of the derivative of exponential diode equation dV/dJ against $(J+J_{sc})^{-1}$. Considering the equation:

$$\frac{dV}{dJ} = R + \frac{AkT}{q} (J + J_L)^{-1} \quad (17)$$

Where

A = ideality factor

k = Boltzman constant

T = Temperature (300 K)

q = electron charge

J = diode current density

And it is considered that $J_L \approx J_{sc}$

This equation can be linearly fitted. R-value corresponds to the intercept and the slope to AkT/q . The obtained values for R and A were $13.4 \text{ } \Omega/\text{cm}^2$ and 2.5, respectively.

The R and G values are associated with parasitic losses in the cell. In our case, these losses are mainly derived from the series resistance(R), which is related to the carrier transport at the interface layer. The shunt conductance(G), on the other hand, refers to the charge recombination. Based on the magnitude of the obtained value, it can be deduced that charge recombination occurs during the photovoltaic generation, affecting the solar cell performance.

Finally, the A values are typically in the range $1.3 < A < 2$, so it can be said that the cell has lost efficiency by recombination through trap states in the space-charge region of the absorber layer as explained by Sah et. al. [124]

On the other hand, a dramatic decrease in both open circuit voltage and short circuit current density was observed in the solar cell produced by the standard blow-drying method. The poor efficiency ($\sim 0.02\%$) of this photovoltaic device can be attributed to perovskite thin-film morphology defects and the inhomogeneous surface coverage produced by this method. To correlate the thin-film quality with the solar cell performance, a comparison on the series and shunt resistance was carried out, table 10 reports the values obtained by calculating the slope at the V_{OC} and I_{SC} points on the I-V curves for the series and shunt resistance, respectively.

It can be noticed that, due to the poor coverage of the film obtained by the standard method, a low shunt resistance was obtained, which indicates that the cell is experiencing current leakages due to alternate pathways that prevent the appropriate collection of electrons. On the other hand, by applying HABD methodology, a complete coverage is achieved, allowing the correct collection of charge carriers, ideally, the shunt resistance value is preferred as high as possible, which is accomplished with the modified deposition procedure.

The series resistance, on the other hand, is related to energetic barriers at the interface and bulk resistances within layers. In this case, the standard method provided rough and thick films, which possibly promoted electron recombination within the film. This undesired process is minimized when synthesizing perovskite films by the HABD method, from Table 10 It can be observed that the resistance was reduced considerably.

Table 10. Shunt and series resistance for the solar cells obtained by different deposition methods*

Deposition method	R_s (Ω)	R_{SH} (Ω)
Standard	1428.571	2000
HABD	588.2353	10000

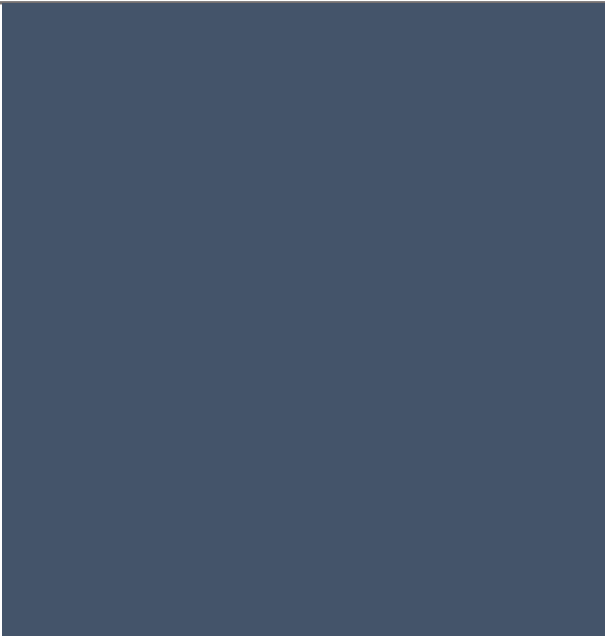
*The values were obtained by calculating the inverse slope at V_{oc} and I_{sc} for series and shunt resistance respectively

The fill factor was another characteristic affected by the quality of the films, notice in Figure 40, that the value was almost doubled when the deposition procedure was changed from the standard to the HABD, which is in accordance with the film properties previously explained.

4.5 Conclusions

The viability of obtaining PKTF by tuning the air temperature at ambient conditions was verified for the first time. The PKTF were obtained using air heated at 90 °C to evaporate the solvent in a one-step deposition without needing of post-annealing treatment. The synthesized MAPbI thin-films exhibited a cross-linked morphology covering the substrate. The presence of some water contamination was found when regular air was used to generate the PKTF. On the contrary, at using hot air, the films showed pure perovskite composition; this was determined by FTIR and XRD. The optical properties of PKTF showed a long-range absorption with a higher absorption coefficient over the visible region in comparison with silicon. In addition, MAPbI thin-films showed slow degradation under environmental conditions (25% R.H). It was found that the electrical properties of the PKTF are similar to those previously reported. HABD methodology was combined with another simple deposition technique to fabricate planar heterojunction solar cells, showing promising results in its photovoltaic performance. With these studies, the viability of obtaining PKTF by tuning the air temperature at ambient conditions was verified for the first time. The PKTF obtained

with this methodology showed good optical properties and improved resistance to degradation which open a new low-cost route for the continuous fabrication of PKSC, with a negligible waste of reagent and without compromising the optical and electrical properties of the perovskites.



Chapter 5

General Conclusions

CESAR MANUEL DEL ANGEL OLARTE

5. GENERAL CONCLUSIONS

In this work, the methodology of blow-drying to synthesize perovskite thin-films was successfully implemented. Additionally, the procedure was modified by adding hot-air to obtain homogeneous depositions on glass substrates.

The perovskite thin-films synthesized by the conventional blow-drying method showed certain water contamination, as observed by infrared spectroscopy. Moreover, this hydration represented the partial degradation of the perovskite thin-films soon after its synthesis, which was detected by X-ray diffraction. This problem was corrected using hot air to obtain the thin-films. The perovskite materials obtained with the modified method showed a pure crystalline perovskite phase. No signal of hydration was detected in infrared spectroscopy.

Regarding the physical appearance, the synthesized thin-films exhibited a dark brown coloration, which is the appearance characteristic of a MAPbI₃ perovskite thin-film. Additionally, it was observed through scanning electron microscopy that the films were composed of large, cross-linked structures. By atomic force microscopy, the surface was observed as homogenous grains with minimal uncovered space resulting in a covered area of 97%.

The perovskite materials showed a broad optical absorption, covering the visible spectrum up to the near-infrared at 800 nm. Additionally, the calculated absorption coefficient and electrical properties determined at room environmental conditions agreed with previous reports. This confirms that the methodology implemented in this work did not affect the perovskite thin-films optical and electrical properties, which are essential for their application in photovoltaic devices.

The stability tests proved that perovskite thin-films could resist up to 15 days exposed at room temperature and humidity of 25%. This is a new result that contrasts with the common opinion that MAPbI₃ perovskite thin-films are highly unstable. According to our

results, the perovskite thin-films obtained with a precursor solution 0.454 M showed the best resistance to degradation.

The thin-films were successfully tested in a solar cell, with the architecture TCO/CdS/perovskite/graphite-Ag. The solar cell was obtained under ambient conditions, and no special equipment was required to be assembled. Moreover, a PCE of 0.91% was obtained under 1 sun of illumination.

APPENDIX. CHARACTERIZATION TECHNIQUES

In order to determine the properties of the perovskite thin-films different characterization techniques are required. Some of them (optical and infrared spectroscopy, X-ray diffraction) correlate properties of the material with the interaction with electromagnetic radiation. For this reason, a brief explanation about this topic is included. Some other properties (such like morphology, roughness, film thickness) are obtained by microscopy, and the determination of electrical properties are carried out by Hall effect and current-voltage measurements. All the characterization techniques employed in this project are explained below.

Electromagnetic radiation

Electromagnetic radiation is a form of energy that propagates as both electrical and magnetic waves traveling in packets of energy called photons. Some sources of electromagnetic radiation include sources in the cosmos (like the sun or stars), radioactive elements, and manufactured devices.

Electromagnetic radiation travels in a wave form at constant speed. The wave characteristics of electromagnetic radiation are described according to the following expression:

$$C = \lambda \nu \quad (1)$$

Where c = velocity, λ = wavelength and ν = frequency

Because the velocity is constant, from this formula can be deduced that wavelength and frequency are inversely proportional. Additionally, the amount of energy in a photon can be calculated with the frequency (ν) and the Planck's constant (h) as follows:

$$E = h\nu \quad (2)$$

Photon energy is measured in eV and depends directly on the photon frequency, so that all the forms of electromagnetic radiation can be grouped to build the electromagnetic spectrum, as depicted in Figure 41. Depending on the wavelength range or energy, every form of electromagnetic radiation has a different name.

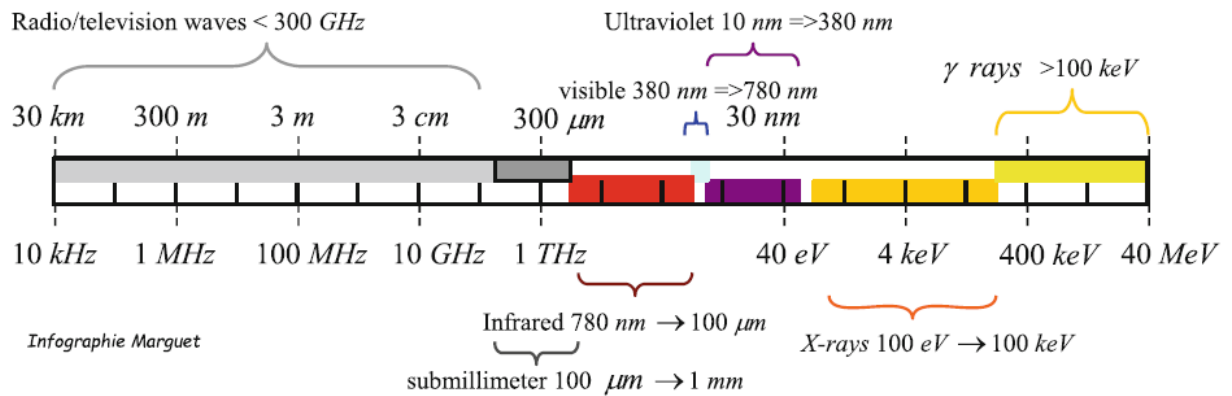


Figure 41. Types of electromagnetic radiation by wavelength range and energy[125]

Electromagnetic radiation can interact with matter in different ways, which are illustrated in Figure 42. Moreover, depending on the photon energy, the effects caused on matter can differ from ionization of atoms to molecule vibration, among others.

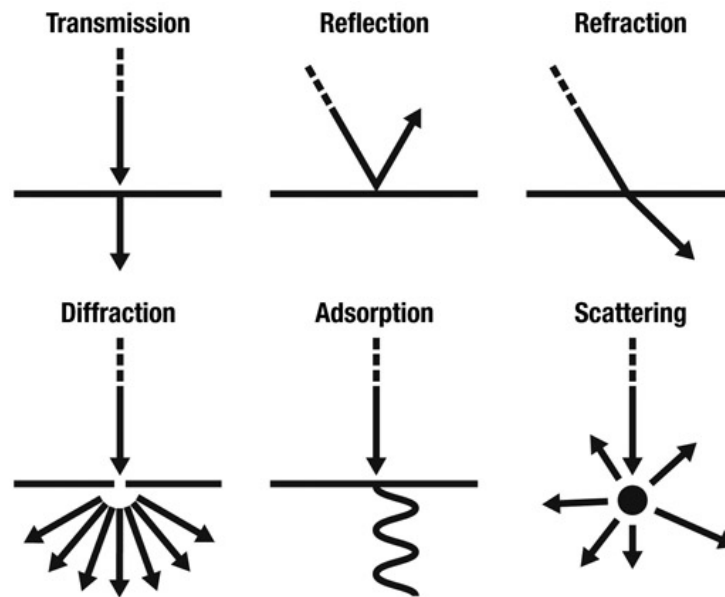


Figure 42. Interactions of electromagnetic radiation with matter[126].

The interactions of electromagnetic radiation with matter are useful to obtain information about the material properties, such as the optical absorption, surface composition, crystal structure, these interactions are important in the characterization techniques described below.

Optical absorption spectroscopy

Absorption spectroscopy measures the absorption of radiation of a material, as a function of wavelength. Materials have the capacity to absorb radiation at certain extent. Additionally, all the materials differ in absorption capacity, so that this characteristic can be employed to identify a material based on its absorption spectrum, which is the absorption intensity as a function of wavelength.

In optical absorption spectroscopy, the energy used to irradiate materials can range from the UV to the near infrared region, generally from 300 nm to 1100 nm. And the equipment employed to carry out this measurement is called spectrophotometer. The basic components of a spectrophotometer include a radiation source, a

monochromator to modulate the energy radiation for the measurement, the sample space, and a detector.

During the measurement, the sample is exposed to different radiation energies, so that if the irradiated energy matches with the energy gap of the material, the radiation is absorbed to promote an electronic transition. This absorption results in changes on the radiation intensity before and after the sample, making possible the absorption quantification through the following expression:

$$A = \log (I/I_0) \quad (3)$$

Where A is the absorbance of the material (in arbitrary units), I is the intensity after the radiation passes the sample and I_0 is intensity of the incident radiation.

In this project, optical absorption spectroscopy was employed to identify the characteristic absorbance spectrum of a perovskite material, which also allows the determination of the energy gap. Moreover, the optical absorption can be used to track the chemical degradation of perovskites, because as the material gradually decomposes, the absorption spectrum changes according to the decomposition products.

Fourier Transformed Infrared Spectroscopy

Infrared spectroscopy is a technique employed to determine the chemical composition of organic compounds, in particular, functional groups. In this case, the materials are irradiated with energies ranging from 2500 nm to 16,000 nm. At this level, the energy is not sufficient to promote electronic transitions, but may induce vibrations of covalently bonded atoms. This phenomenon is possible because covalent bonds are not rigid, but rather their nature resembles springs that can bend or stretch.

Molecules can experience a wide variety of vibrational motions, characteristic of their component atoms. As a result, virtually all organic compounds can absorb infrared radiation, which translates in different molecular vibrations. Figure 43 depicts different range of appearance of molecular vibrations through the common infrared region of analysis. In this graphic, the stretching vibrations are colored in blue, while the bending vibrations are colored in green. The section between 1450 cm^{-1} to 600 cm^{-1} is called the fingerprint region, because in this section specific patterns can be identified. On the other hand, the section from 4000 cm^{-1} to 1450 cm^{-1} is known as the group region, because in this section, the absorption bands usually correspond to stretching vibrations of diatomic atoms.

The equipment required to perform this characterization is known as infrared spectrophotometer, which in principle operates as the optical spectrophotometer explained above. However, the Fourier transformed infrared spectroscopy differs from this approach in the energy irradiated over the sample, while in the conventional analysis, monochromatic radiation is employed. In the Fourier transform methodology, a beam containing many frequencies of light is irradiated. Then the equipment measures the amount of the beam absorbed. After that, the beam is modified to contain another combination of frequencies, and the process is repeated. The data is processed to transform the radiation absorption of each beam into the appropriate infrared spectrum. The process employed to transform the data is the Fourier transform.

The FTIR technique was employed to determine the presence of the perovskite compound, because the material is composed of an organic part, its vibrations can be detected by this characterization method, confirming the successful formation of the material. Moreover, additional information can be obtained depending on the vibration bands detected, which can also be related to the organic solvent employed or water impurities in the as-synthesized material.

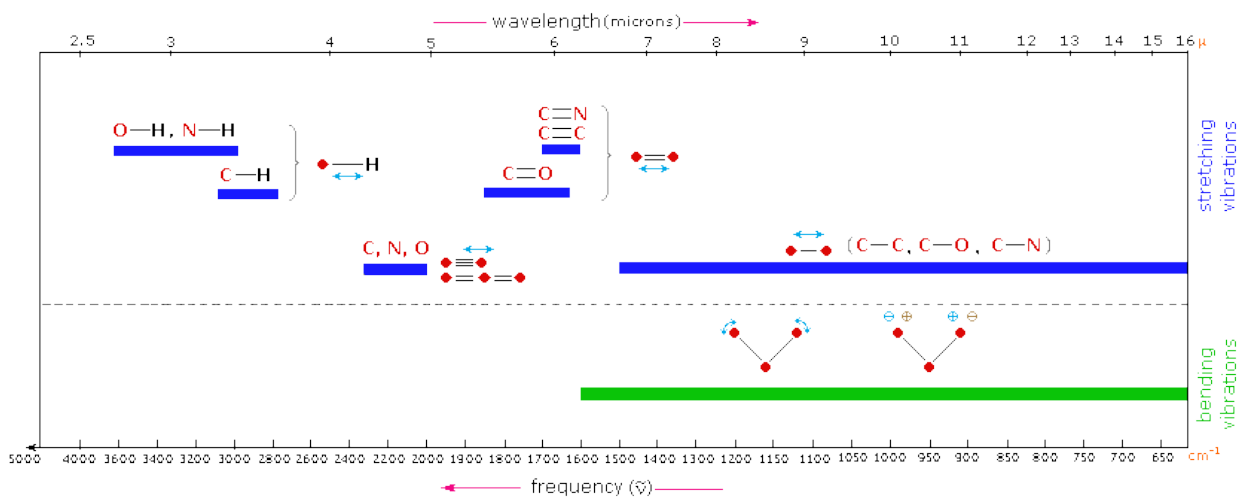


Figure 43. Molecular vibrations and the range in which they are detected over the infrared spectrum[127].

X-ray diffraction

X-ray diffraction is a technique that relies on the interaction of electromagnetic radiation in the range 0.05 nm – 0.3 nm with the matter in the crystalline form. It is a common characterization in materials sciences to determine the crystallographic structure of a material. Moreover, as the materials crystalize in different forms, X-ray diffraction can be useful to identify and differentiate materials based on their diffraction pattern.

A crystal is an array of atoms that repeats itself symmetrically to fill space. Moreover, atoms can scatter X-rays because the energy is sufficient to interact with the electrons. This phenomenon is known as elastic scattering so that in a crystal arrangement, the scattered X-rays interfere with each other either constructively or destructively (see Figure 44). In particular, the constructive interference occurs when the scattering in specific directions follow the Bragg's Law:

$$n\lambda = 2d \sin\theta \quad (4)$$

Where d is the spacing between diffraction planes, θ is the incident angle, λ is the beam wavelength and n is an integer. As the wavelength of radiation is known and the angles at which constructive interference occurs are measured, the Bragg's law allow the calculation of the distance between planes in a crystalline material. The result of the measurements is called diffractogram, which is a plot of X-ray intensity on the y-axis against the angle 2θ in the x-axis.

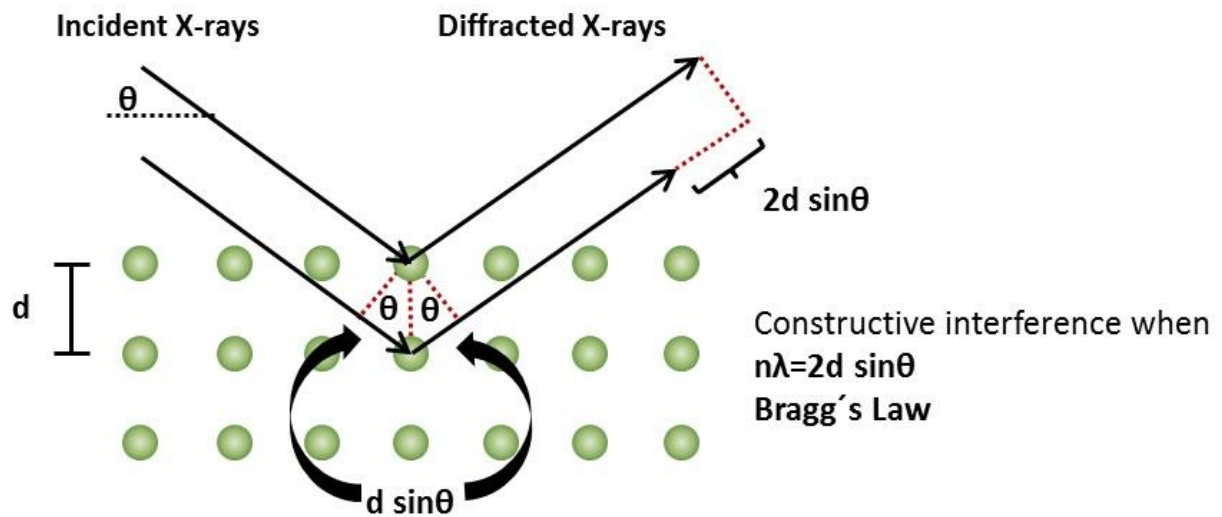


Figure 44. Schematic representation of the Bragg's Law[128]

The equipment used to carry out this assessment is a diffractometer, which consists of an X-ray source, a monochromator to adjust the wavelength of the incident radiation, a sample holder, and a detector. Additionally, modern equipment also has a goniometer which helps in the sample and detector positions.

The objective of using this characterization technique in the project was to determine the crystalline structure of the studied material. Because the methodology employed to obtain the material was applied for the first time in our research group, it was

necessary to determine the effects of the synthesis procedure on the final structure of the material. Additional information like the presence of different crystal phases, grain size or crystal orientation, can also be determined from the resulting diffractograms. The crystal structure information is important to corroborate composition results obtained by other techniques like absorption spectroscopy or infrared spectroscopy.

Scanning electron microscopy

Scanning electron microscopy is a technique that uses a focused electron beam to generate a diversity of signals at the surface of a solid sample. Figure 45 depicts a comparison between the operation principle of an optical microscope and a scanning electron microscope. Two important differences between these techniques are the illumination source, which are accelerated electrons for the case of SEM instead of light, and that the illumination beam collides with the sample in the SEM technique while in the optical microscopy, the illumination passes through the sample.

Accelerated electrons contain significant amounts of kinetic energy, and when these electrons collide with the sample, different interactions occur, generating specific signals. Some of these signals are secondary electrons, backscattered electrons (BSE), diffracted backscattered electrons (EBSD), X-ray photons, visible light, and heat.

Secondary electrons and backscattered electrons allow the construction of an image of the sample surface. Secondary electrons are more valuable in constructing details of morphology and topography, while BSE allows the differentiation between phases in samples with different compositions. X-ray photons, on the other hand, determine the elemental composition of the sample.

In the development of this project, the SEM characterization played an important role in studying the surface morphology of the samples, detecting surface defects of the material, and surface coverage over the substrate. Due to the limitations of this

technique's resolution, specific details like grain composition or film thickness were hardly observed.

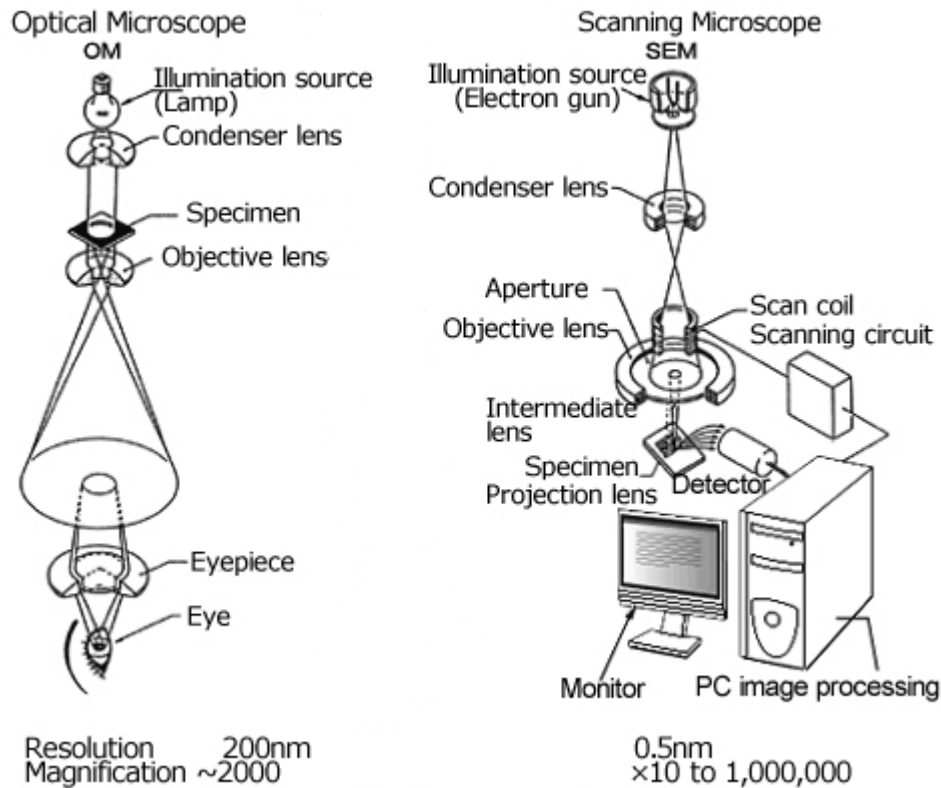


Figure 45. Differences between the optical microscopy and scanning electron microscopy[129].

Atomic force microscopy

Atomic force microscopy is considered an advanced imaging technique. It relies on the interaction of atomic forces to reconstruct the topology of a sample. A sharp tip is raster-scanned over a surface using a feedback loop to adjust parameters to image a surface to achieve this. When the tip interacts with the surface sample, it is subjected to attraction or repulsion forces (see Figure 46a), which can be obtained according to the Hooke's law:

$$F = -kz \quad (5)$$

Where F is the force, k the stiffness of the lever, and z the distance the lever is bent. As can be seen from this equation, the force is not measured directly, instead is calculated by measuring the deflection of the lever, knowing the stiffness of the cantilever.

The feedback loop uses a laser beam deflection. This laser is reflected from the back of the cantilever. As the tip interacts with the surface, the laser position on the photodetector is used in the feedback loop to track the surface for imaging, as depicted in Figure 46b.

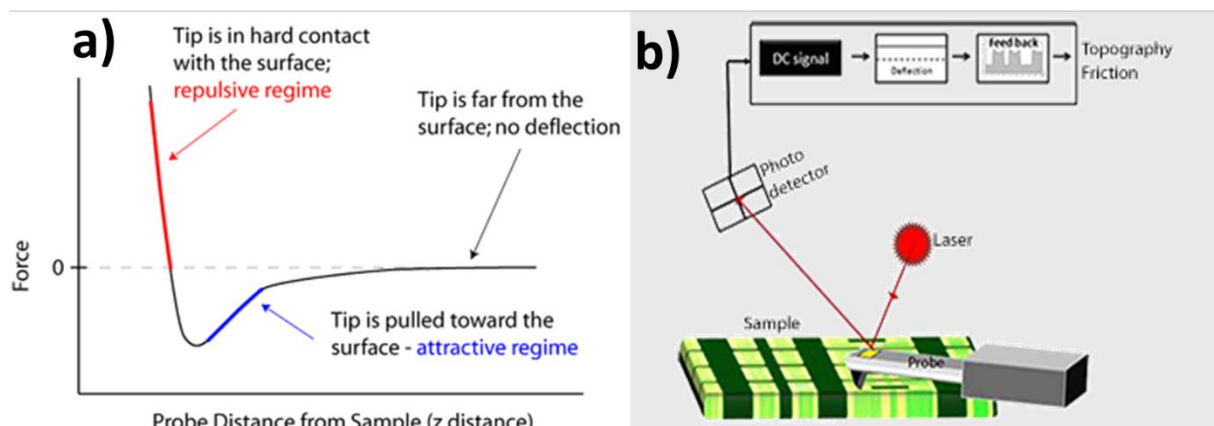


Figure 46. AFM operation principle: a) attraction/repulsion forces experimented by the tip measured by AFM and b) the feedback loop of an AFM equipment to construct the analyzed surface[130].

Because the technique measures surface forces experimented by the tip of the cantilever, not only topographic information can be obtained, but also friction, electrical forces, capacitance, conductivity, viscoelasticity, surface potential, resistance, among others.

In this project, the AFM characterization helped in the observation of details like surface roughness, grain composition and film thickness on the surface of the material synthesized, complementing the morphological results obtained by SEM. Moreover, it

allowed the determination of the film thickness and the surface roughness of the films obtained.

Hall-effect measurement

The Hall effect measurement is an important technique applied to determine the carrier density, electrical resistivity, and mobility of carriers in semiconductors. It relies on the Lorentz force, which is an effect experimented by an electron when it moves along a direction perpendicular to an applied magnetic field. Figure 47 depicts the Hall effect in a bar-shaped sample. A constant current I flows through the bar while a uniform magnetic field is applied perpendicular to the current flow. Since the electrons are traveling through the magnetic field, they experiment with an upwards Lorentz force that makes them drift to the top of the bar while maintaining their horizontal motion. As a result, a negative buildup charge concentrates on one side of the bar and a positive charge on the opposite side due to the lack of electrons. This leads to a potential difference between the two sides, which can be measured as the Hall voltage (V_H).

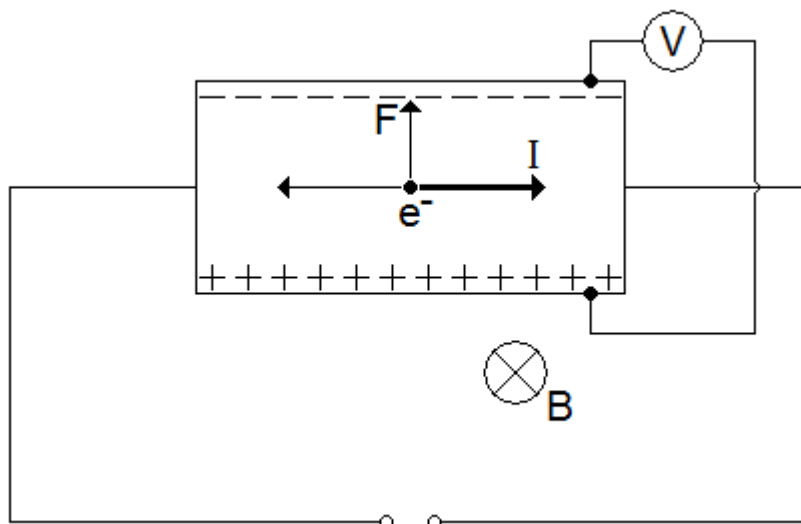


Figure 47. Hall effect experimented by a bar sample of a conducting material[131].

The Hall voltage is related to the bulk density of charge carriers with the expression:

$$V_H = \frac{IB}{qnd} \quad (6)$$

Where I is the current density applied, B is the magnetic field, q is the elementary charge, n is the bulk density, and d is the sample thickness. However, it is convenient to use a layer or sheet density ($n_s = nd$) instead of bulk density. By measuring the Hall voltage and knowing the value of I, B and q can determine the sheet density of charge carriers.

Since the sheet resistance (R_S) relates both sheet density (n_s) and mobility (μ) according to the formula:

$$\mu = \frac{|V_H|}{R_S IB} = \frac{1}{qn_s R_S} \quad (7)$$

A modification of the Hall measurement is required to determine these properties. Conveniently, the Van der Paw resistivity measurement allows the determination of the sheet resistance by employing the same sample.

According to Van der Paw, two characteristic resistances (R_A and R_B) are associated to the sheet resistance (R_S) through the expression:

$$e^{-\frac{\pi R_A}{R_S}} + e^{-\frac{\pi R_B}{R_S}} = 1 \quad (8)$$

The characteristic resistances can be calculated by the following expressions:

$$R_A = \frac{V_{43}}{I_{12}} \text{ and } R_B = \frac{V_{14}}{I_{23}} \quad (9)$$

The measurement of the voltage V_{43} from contact 4 to contact 3 (see Figure 48) when applying a DC current from the contact 1 to contact 2 is required. Along with the measurement of the voltage V_{14} (from contact 1 to contact 4) when the current from contact 2 to contact 3 is applied.

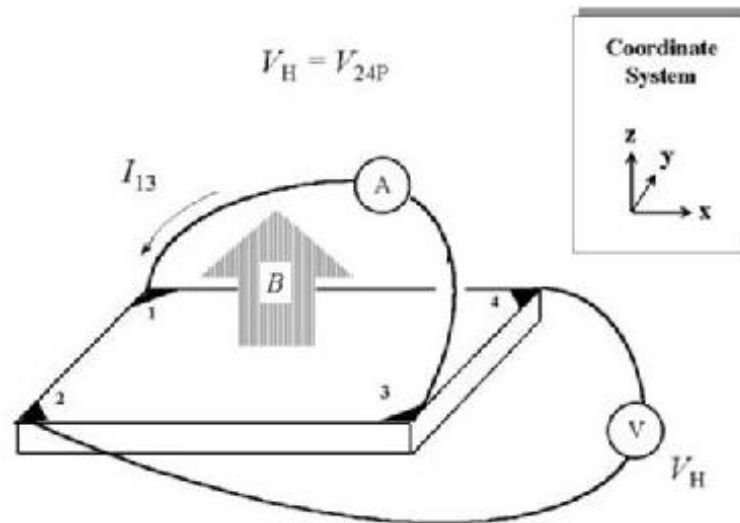


Figure 48. Film sample prepared for the Van der Pauw resistivity and Hall measurements[132].

The determination of R_s is achieved by the numerical solution of equation (8)

I-V curve measurement

The current-voltage (I-V) measurement of an electrical device enables determining how it works in a circuit. Moreover, by analyzing the shape of the curve obtained, detailed information about the device operation can be deduced. Depending on the electronic device analyzed, a characteristic curve can be obtained.

An I-V curve measurement is performed by applying a series of voltages to the device. At each voltage, the current flowing through the device is measured. To measure the voltage applied and the current obtained, a voltmeter is placed in parallel to the circuit

and an ammeter is connected in series, as sketched in Figure 49. Alternatively, a source measure unit can be employed, which is a device capable of supplying voltage and measuring current simultaneously.

For a solar cell characterization, an additional device is required, which is the illumination source. The source must satisfy the power requirements to simulate the sun irradiance. That is, provide a power of 1000 W/m^2 which corresponds to one sun of illumination.

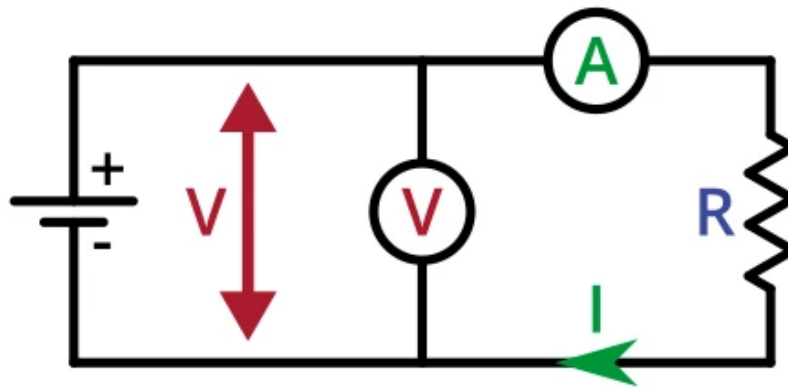


Figure 49. Circuit diagram for a current-voltage (I-V) measurement of a solar cell[133].

When characterizing a solar cell, it is necessary to measure an I-V curve in dark, in order to corroborate the characteristic behavior of a solar cell in dark conditions, which are similar to a diode. After that, the measurement under illumination is carried out under the same voltage range.

In this project, I-V curve measurements were required to verify the functionality of a solar cell, which was build with the material of study. The measurements were carried out in ambient conditions under dark and illumination. Moreover, measurements along time allowed the verification of solar cell stability, which is an important parameter to be compared with the intrinsic stability of the material.

The information obtained from the I-V curves allowed the determination of the characteristic properties of a solar cell, such as the open-circuit voltage (V_{OC}), short circuit current (I_{SC}), the fill factor(FF), and the power conversion efficiency(PCE). This information helps to correlate the intrinsic properties of the material being applied in a solar cell device.

6. BIBLIOGRAPHY

- [1] M. Petrović, V. Chellappan, S. Ramakrishna, Perovskites: Solar cells & engineering applications – materials and device developments, *Sol. Energy*. 122 (2015) 678–699. <https://doi.org/10.1016/j.solener.2015.09.041>.
- [2] W. Li, Z. Wang, F. Deschler, S. Gao, R.H. Friend, A.K. Cheetham, Chemically diverse and multifunctional hybrid organic–inorganic perovskites, *Nat. Rev. Mater.* 2 (2017) 16099. <https://doi.org/10.1038/natrevmats.2016.99>.
- [3] C.-X. Zhang, T. Shen, D. Guo, L.-M. Tang, K. Yang, H.-X. Deng, Reviewing and understanding the stability mechanism of halide perovskite solar cells, *InfoMat*. 2 (2020) 1034–1056. <https://doi.org/10.1002/inf2.12104>.
- [4] S. Sundaram, K. Shanks, H. Upadhyaya, 18 - Thin Film Photovoltaics, in: T.M. Letcher, V.M. Fthenakis (Eds.), *Compr. Guide Sol. Energy Syst.*, Academic Press, 2018: pp. 361–370. <https://doi.org/10.1016/B978-0-12-811479-7.00018-X>.
- [5] J.P. Attfield, P. Lightfoot, R.E. Morris, Perovskites, *Dalton Trans.* 44 (2015) 10541–10542. <https://doi.org/10.1039/C5DT90083B>.
- [6] R.M. Hazen, Perovskites, *Sci. Am.* 258 (1988) 74–81.
- [7] K. Kato, K. Mimura, F. Dang, H. Imai, S. Wada, M. Osada, H. Haneda, M. Kuwabara, BaTiO₃ nanocube and assembly to ferroelectric supracrystals, *J. Mater. Res.* 28 (2013) 2932–2945. <https://doi.org/10.1557/jmr.2013.299>.
- [8] A. Bhattacharya, S.J. May, S.G.E. te Velthuis, M. Warusawithana, X. Zhai, B. Jiang, J.-M. Zuo, M.R. Fitzsimmons, S.D. Bader, J.N. Eckstein, Metal-Insulator Transition and Its Relation to Magnetic Structure in $(\text{LaMnO})_3_{2n}/(\text{SrMnO})_3_{n}$ Superlattices, *Phys. Rev. Lett.* 100 (2008) 257203. <https://doi.org/10.1103/PhysRevLett.100.257203>.
- [9] D.B. Mitzi, S. Wang, C.A. Feild, C.A. Chess, A.M. Guloy, Conducting Layered Organic-inorganic Halides Containing Pb^{2+} -Oriented Perovskite Sheets, *Science*. 267 (1995) 1473. <https://doi.org/10.1126/science.267.5203.1473>.
- [10] A. Kojima, K. Teshima, Y. Shirai, T. Miyasaka, Organometal Halide Perovskites as Visible-Light Sensitizers for Photovoltaic Cells, *J. Am. Chem. Soc.* 131 (2009) 6050–6051. <https://doi.org/10.1021/ja809598r>.
- [11] H.J. Snaith, Perovskites: The Emergence of a New Era for Low-Cost, High-Efficiency Solar Cells, *J. Phys. Chem. Lett.* 4 (2013) 3623–3630. <https://doi.org/10.1021/jz4020162>.
- [12] N.-G. Park, Perovskite solar cells: an emerging photovoltaic technology, *Mater. Today*. 18 (2015) 65–72. <https://doi.org/10.1016/j.mattod.2014.07.007>.
- [13] M. Saliba, J.-P. Correa-Baena, M. Grätzel, A. Hagfeldt, A. Abate, Perovskite Solar Cells: From the Atomic Level to Film Quality and Device Performance, *Angew. Chem. Int. Ed.* 57 (2018) 2554–2569. <https://doi.org/10.1002/anie.201703226>.

- [14] J.S. Manser, M.I. Saidaminov, J.A. Christians, O.M. Bakr, P.V. Kamat, Making and Breaking of Lead Halide Perovskites, *Acc. Chem. Res.* 49 (2016) 330–338. <https://doi.org/10.1021/acs.accounts.5b00455>.
- [15] A. Sharma, N.B. Chaure, Studies on CH₃NH₃PbI₃ prepared by low-cost wet chemical technique, *Appl. Phys. A.* 125 (2019) 767. <https://doi.org/10.1007/s00339-019-3047-1>.
- [16] X. Dai, Y. Deng, C.H. Van Brackle, J. Huang, Meniscus fabrication of halide perovskite thin films at high throughput for large area and low-cost solar panels, *Int. J. Extreme Manuf.* 1 (2019) 022004. <https://doi.org/10.1088/2631-7990/ab263e>.
- [17] S. Wang, X. Li, J. Wu, W. Wen, Y. Qi, Fabrication of efficient metal halide perovskite solar cells by vacuum thermal evaporation: A progress review, *Environ. Electrochem. • Sol. Cells.* 11 (2018) 130–140. <https://doi.org/10.1016/j.coelec.2018.10.006>.
- [18] J. Sun, J. Wu, X. Tong, F. Lin, Y. Wang, Z.M. Wang, Organic/Inorganic Metal Halide Perovskite Optoelectronic Devices beyond Solar Cells, *Adv. Sci.* 5 (2018) 1700780. <https://doi.org/10.1002/advs.201700780>.
- [19] N.-G. Park, Research Direction toward Scalable, Stable, and High Efficiency Perovskite Solar Cells, *Adv. Energy Mater.* 10 (2020) 1903106. <https://doi.org/10.1002/aenm.201903106>.
- [20] J.C. Hamill, J. Schwartz, Y.-L. Loo, Influence of Solvent Coordination on Hybrid Organic–Inorganic Perovskite Formation, *ACS Energy Lett.* 3 (2018) 92–97. <https://doi.org/10.1021/acsenenergylett.7b01057>.
- [21] L. Shimoni-Livny, J.P. Glusker, C.W. Bock, Lone Pair Functionality in Divalent Lead Compounds, *Inorg. Chem.* 37 (1998) 1853–1867. <https://doi.org/10.1021/ic970909r>.
- [22] K. Yan, M. Long, T. Zhang, Z. Wei, H. Chen, S. Yang, J. Xu, Hybrid Halide Perovskite Solar Cell Precursors: Colloidal Chemistry and Coordination Engineering behind Device Processing for High Efficiency, *J. Am. Chem. Soc.* 137 (2015) 4460–4468. <https://doi.org/10.1021/jacs.5b00321>.
- [23] M. Jung, S.-G. Ji, G. Kim, S.I. Seok, Perovskite precursor solution chemistry: from fundamentals to photovoltaic applications, *Chem. Soc. Rev.* 48 (2019) 2011–2038. <https://doi.org/10.1039/C8CS00656C>.
- [24] Y. Zhao, K. Zhu, Organic-inorganic hybrid lead halide perovskites for optoelectronic and electronic applications, *Chem. Soc. Rev.* 45 (2016) 655–689. <https://doi.org/10.1039/C4CS00458B>.
- [25] L. Chao, T. Niu, W. Gao, C. Ran, L. Song, Y. Chen, W. Huang, Solvent Engineering of the Precursor Solution toward Large-Area Production of Perovskite Solar Cells, *Adv. Mater.* 33 (2021) 2005410. <https://doi.org/10.1002/adma.202005410>.
- [26] R. Swartwout, M.T. Hoerantner, V. Bulović, Scalable Deposition Methods for Large-area Production of Perovskite Thin Films, *ENERGY Environ. Mater.* 2 (2019) 119–145. <https://doi.org/10.1002/eem2.12043>.

- [27] K. Liao, C. Li, L. Xie, Y. Yuan, S. Wang, Z. Cao, L. Ding, F. Hao, Hot-Casting Large-Grain Perovskite Film for Efficient Solar Cells: Film Formation and Device Performance, *Nano-Micro Lett.* 12 (2020) 156. <https://doi.org/10.1007/s40820-020-00494-2>.
- [28] D.N. FERIA, C.-Y. Chang, K.P.O. Mahesh, C.-L. Hsu, Y.-C. Chao, Perovskite solar cells based on a perovskite film with improved film coverage, *Synth. Met.* 260 (2020) 116283. <https://doi.org/10.1016/j.synthmet.2019.116283>.
- [29] N. Sahu, B. Parija, S. Panigrahi, Fundamental understanding and modeling of spin coating process: A review, *Indian J. Phys.* 83 (2009) 493–502. <https://doi.org/10.1007/s12648-009-0009-z>.
- [30] C. Jiang, S.L. Lim, W.P. Goh, F.X. Wei, J. Zhang, Improvement of CH₃NH₃PbI₃ Formation for Efficient and Better Reproducible Mesoscopic Perovskite Solar Cells, *ACS Appl. Mater. Interfaces.* 7 (2015) 24726–24732. <https://doi.org/10.1021/acsami.5b07446>.
- [31] W. Kong, G. Wang, J. Zheng, H. Hu, H. Chen, Y. Li, M. Hu, X. Zhou, C. Liu, B.N. Chandrashekar, A. Amini, J. Wang, B. Xu, C. Cheng, Fabricating High-Efficient Blade-Coated Perovskite Solar Cells under Ambient Condition Using Lead Acetate Trihydrate, *Sol. RRL.* 2 (2018) 1770153. <https://doi.org/10.1002/solr.201770153>.
- [32] R. Patidar, D. Burkitt, K. Hooper, D. Richards, T. Watson, Slot-die coating of perovskite solar cells: An overview, *Mater. Today Commun.* 22 (2020) 100808. <https://doi.org/10.1016/j.mtcomm.2019.100808>.
- [33] J.E. Bishop, J.A. Smith, D.G. Lidzey, Development of Spray-Coated Perovskite Solar Cells, *ACS Appl. Mater. Interfaces.* 12 (2020) 48237–48245. <https://doi.org/10.1021/acsami.0c14540>.
- [34] A.T. Barrows, A.J. Pearson, C.K. Kwak, A.D.F. Dunbar, A.R. Buckley, D.G. Lidzey, Efficient planar heterojunction mixed-halide perovskite solar cells deposited via spray-deposition, *Energy Environ. Sci.* 7 (2014) 2944–2950. <https://doi.org/10.1039/C4EE01546K>.
- [35] B. Xia, Z. Wu, H. Dong, J. Xi, W. Wu, T. Lei, K. Xi, F. Yuan, B. Jiao, L. Xiao, Q. Gong, X. Hou, Formation of ultrasoft perovskite films toward highly efficient inverted planar heterojunction solar cells by micro-flowing anti-solvent deposition in air, *J. Mater. Chem. A.* 4 (2016) 6295–6303. <https://doi.org/10.1039/C6TA00253F>.
- [36] S.S. Mali, J.V. Patil, C.K. Hong, Hot-Air-Assisted Fully Air-Processed Barium Incorporated CsPbI₂Br Perovskite Thin Films for Highly Efficient and Stable All-Inorganic Perovskite Solar Cells, *Nano Lett.* 19 (2019) 6213–6220. <https://doi.org/10.1021/acs.nanolett.9b02277>.
- [37] J. Su, H. Cai, X. Ye, X. Zhou, J. Yang, D. Wang, J. Ni, J. Li, J. Zhang, Efficient Perovskite Solar Cells Prepared by Hot Air Blowing to Ultrasonic Spraying in Ambient Air, *ACS Appl. Mater. Interfaces.* 11 (2019) 10689–10696. <https://doi.org/10.1021/acsami.9b01843>.

- [38] M. Ouafi, L. Atourki, L. Laânab, E. Vega, B. Mari, M. Mollar, B. Jaber, Hot airflow deposition: Toward high quality MAPbI₃ perovskite films, *J. Alloys Compd.* 790 (2019) 1101–1107. <https://doi.org/10.1016/j.jallcom.2019.03.187>.
- [39] L.-L. Gao, C.-X. Li, C.-J. Li, G.-J. Yang, Large-area high-efficiency perovskite solar cells based on perovskite films dried by the multi-flow air knife method in air, *J. Mater. Chem. A* 5 (2017) 1548–1557. <https://doi.org/10.1039/C6TA09565H>.
- [40] M. Zhang, H. Yu, J.-H. Yun, M. Lyu, Q. Wang, L. Wang, Facile preparation of smooth perovskite films for efficient meso/planar hybrid structured perovskite solar cells, *Chem. Commun.* 51 (2015) 10038–10041. <https://doi.org/10.1039/C5CC02534F>.
- [41] J. Chen, Z. Wan, J. Liu, S.-Q. Fu, F. Zhang, S. Yang, S. Tao, M. Wang, C. Chen, Growth of Compact CH₃NH₃PbI₃ Thin Films Governed by the Crystallization in PbI₂ Matrix for Efficient Planar Perovskite Solar Cells, *ACS Appl. Mater. Interfaces* 10 (2018) 8649–8658. <https://doi.org/10.1021/acsami.7b18667>.
- [42] X. Guo, C. McCleese, C. Kolodziej, A.C.S. Samia, Y. Zhao, C. Burda, Identification and characterization of the intermediate phase in hybrid organic–inorganic MAPbI₃ perovskite, *Dalton Trans.* 45 (2016) 3806–3813. <https://doi.org/10.1039/C5DT04420K>.
- [43] K. Sveinbjörnsson, K. Aitola, J. Zhang, M.B. Johansson, X. Zhang, J.-P. Correa-Baena, A. Hagfeldt, G. Boschloo, E.M.J. Johansson, Ambient air-processed mixed-ion perovskites for high-efficiency solar cells, *J. Mater. Chem. A* 4 (2016) 16536–16545. <https://doi.org/10.1039/C6TA06912F>.
- [44] M. Yang, T. Zhang, P. Schulz, Z. Li, G. Li, D.H. Kim, N. Guo, J.J. Berry, K. Zhu, Y. Zhao, Facile fabrication of large-grain CH₃NH₃PbI₃-xBr_x films for high-efficiency solar cells via CH₃NH₃Br-selective Ostwald ripening, *Nat. Commun.* 7 (2016) 12305–12305. <https://doi.org/10.1038/ncomms12305>.
- [45] C. Aranda, C. Cristobal, L. Shooshtari, C. Li, S. Huettnner, A. Guerrero, Formation criteria of high efficiency perovskite solar cells under ambient conditions, *Sustain. Energy Fuels* 1 (2017) 540–547. <https://doi.org/10.1039/C6SE00077K>.
- [46] Y. Zhao, K. Zhu, CH₃NH₃Cl-Assisted One-Step Solution Growth of CH₃NH₃PbI₃: Structure, Charge-Carrier Dynamics, and Photovoltaic Properties of Perovskite Solar Cells, *J. Phys. Chem. C* 118 (2014) 9412–9418. <https://doi.org/10.1021/jp502696w>.
- [47] A. Babayigit, J. D’Haen, H.-G. Boyen, B. Conings, Gas Quenching for Perovskite Thin Film Deposition, *Joule* 2 (2018) 1205–1209. <https://doi.org/10.1016/j.joule.2018.06.009>.
- [48] J. Troughton, K. Hooper, T.M. Watson, Humidity resistant fabrication of CH₃NH₃PbI₃ perovskite solar cells and modules, *Nano Energy* 39 (2017) 60–68. <https://doi.org/10.1016/j.nanoen.2017.06.039>.
- [49] Y. Zhou, M. Yang, W. Wu, A.L. Vasiliev, K. Zhu, N.P. Padture, Room-temperature crystallization of hybrid-perovskite thin films via solvent-solvent

- extraction for high-performance solar cells, *J. Mater. Chem. A.* 3 (2015) 8178–8184. <https://doi.org/10.1039/C5TA00477B>.
- [50] X. Zheng, B. Chen, C. Wu, S. Priya, Room temperature fabrication of $\text{CH}_3\text{NH}_3\text{PbBr}_3$ by anti-solvent assisted crystallization approach for perovskite solar cells with fast response and small J–V hysteresis, *Nano Energy.* 17 (2015) 269–278. <https://doi.org/10.1016/j.nanoen.2015.08.023>.
- [51] M. Yin, F. Xie, H. Chen, X. Yang, F. Ye, E. Bi, Y. Wu, M. Cai, L. Han, Annealing-free perovskite films by instant crystallization for efficient solar cells, *J. Mater. Chem. A.* 4 (2016) 8548–8553. <https://doi.org/10.1039/C6TA02490D>.
- [52] M.M. Byranvand, S. Song, L. Pyeon, G. Kang, G.-Y. Lee, T. Park, Simple post annealing-free method for fabricating uniform, large grain-sized, and highly crystalline perovskite films, *Nano Energy.* 34 (2017) 181–187. <https://doi.org/10.1016/j.nanoen.2017.02.017>.
- [53] J.H. Noh, S.H. Im, J.H. Heo, T.N. Mandal, S.I. Seok, Chemical Management for Colorful, Efficient, and Stable Inorganic–Organic Hybrid Nanostructured Solar Cells, *Nano Lett.* 13 (2013) 1764–1769. <https://doi.org/10.1021/nl400349b>.
- [54] G.A. Al-Dainy, S.E. Bourdo, V. Saini, B.C. Berry, A.S. Biris, Hybrid Perovskite Photovoltaic Devices: Properties, Architecture, and Fabrication Methods, *Energy Technol.* 5 (2017) 373–401. <https://doi.org/10.1002/ente.201600486>.
- [55] T. Umebayashi, K. Asai, T. Kondo, A. Nakao, Electronic structures of lead iodide based low-dimensional crystals, *Phys. Rev. B.* 67 (2003) 155405. <https://doi.org/10.1103/PhysRevB.67.155405>.
- [56] M.R. Filip, G. Volonakis, F. Giustino, Hybrid Halide Perovskites: Fundamental Theory and Materials Design, in: W. Andreoni, S. Yip (Eds.), *Handb. Mater. Model. Appl. Curr. Emerg. Mater.*, Springer International Publishing, Cham, 2018: pp. 1–30. https://doi.org/10.1007/978-3-319-50257-1_23-1.
- [57] J. Huang, Y. Yuan, Y. Shao, Y. Yan, Understanding the physical properties of hybrid perovskites for photovoltaic applications, *Nat. Rev. Mater.* 2 (2017) 17042. <https://doi.org/10.1038/natrevmats.2017.42>.
- [58] Y. Chen, H.T. Yi, X. Wu, R. Haroldson, Y.N. Gartstein, Y.I. Rodionov, K.S. Tikhonov, A. Zakhidov, X.-Y. Zhu, V. Podzorov, Extended carrier lifetimes and diffusion in hybrid perovskites revealed by Hall effect and photoconductivity measurements, *Nat. Commun.* 7 (2016) 12253. <https://doi.org/10.1038/ncomms12253>.
- [59] T. Leijtens, K. Bush, R. Cheacharoen, R. Beal, A. Bowring, M.D. McGehee, Towards enabling stable lead halide perovskite solar cells; interplay between structural, environmental, and thermal stability, *J. Mater. Chem. A.* 5 (2017) 11483–11500. <https://doi.org/10.1039/C7TA00434F>.
- [60] G. Niu, W. Li, F. Meng, L. Wang, H. Dong, Y. Qiu, Study on the stability of $\text{CH}_3\text{NH}_3\text{PbI}_3$ films and the effect of post-modification by aluminum oxide in all-solid-state hybrid solar cells, *J Mater Chem A.* 2 (2013). <https://doi.org/10.1039/C3TA13606J>.

- [61] J. Zhao, B. Cai, Z. Luo, Y. Dong, Y. Zhang, H. Xu, B. Hong, Y. Yang, L. Li, W. Zhang, C. Gao, Investigation of the Hydrolysis of Perovskite Organometallic Halide $\text{CH}_3\text{NH}_3\text{PbI}_3$ in Humidity Environment, *Sci. Rep.* 6 (2016) 21976.
- [62] R. Wang, M. Mujahid, Y. Duan, Z.-K. Wang, J. Xue, Y. Yang, A Review of Perovskites Solar Cell Stability, *Adv. Funct. Mater.* 29 (2019) 1808843. <https://doi.org/10.1002/adfm.201808843>.
- [63] A. Dualeh, P. Gao, S.I. Seok, M.K. Nazeeruddin, M. Grätzel, Thermal Behavior of Methylammonium Lead-Trihalide Perovskite Photovoltaic Light Harvesters, *Chem. Mater.* 26 (2014) 6160–6164. <https://doi.org/10.1021/cm502468k>.
- [64] B. Conings, J. Drijkoningen, N. Gauquelin, A. Babayigit, J. D'Haen, L. D'Olieslaeger, A. Ethirajan, J. Verbeeck, J. Manca, E. Mosconi, F.D. Angelis, H.-G. Boyen, Intrinsic Thermal Instability of Methylammonium Lead Trihalide Perovskite, *Adv. Energy Mater.* 5 (2015) 1500477. <https://doi.org/10.1002/aenm.201500477>.
- [65] P.S. Whitfield, N. Herron, W.E. Guise, K. Page, Y.Q. Cheng, I. Milas, M.K. Crawford, Structures, Phase Transitions and Tricritical Behavior of the Hybrid Perovskite Methyl Ammonium Lead Iodide, *Sci. Rep.* 6 (2016) 35685. <https://doi.org/10.1038/srep35685>.
- [66] T. Oku, Crystal Structures of $\text{CH}_3\text{NH}_3\text{PbI}_3$ and Related Perovskite Compounds Used for Solar Cells, in: L.A. Kosyachenko (Ed.), *Sol. Cells - New Approaches Rev.*, InTech, Rijeka, 2015: p. Ch. 03. <https://doi.org/10.5772/59284>.
- [67] S.N. Habisreutinger, D.P. McMeekin, H.J. Snaith, R.J. Nicholas, Research Update: Strategies for improving the stability of perovskite solar cells, *APL Mater.* 4 (2016) 091503. <https://doi.org/10.1063/1.4961210>.
- [68] Q. Fu, X. Tang, B. Huang, T. Hu, L. Tan, L. Chen, Y. Chen, Recent Progress on the Long-Term Stability of Perovskite Solar Cells, *Adv. Sci.* 5 (2018) 1700387. <https://doi.org/10.1002/advs.201700387>.
- [69] L.K. Ono, Y. Qi, S. (Frank) Liu, Progress toward Stable Lead Halide Perovskite Solar Cells, *Joule.* 2 (2018) 1961–1990. <https://doi.org/10.1016/j.joule.2018.07.007>.
- [70] T. Markvart, L. Castañer, Chapter I-1-A - Principles of Solar Cell Operation, in: S.A. Kalogirou (Ed.), *McEvoy's Handb. Photovolt.* Third Ed., Academic Press, 2018: pp. 3–28. <https://doi.org/10.1016/B978-0-12-809921-6.00001-X>.
- [71] How a solar cell works, *Am. Chem. Soc.* (n.d.). <https://www.acs.org/content/acs/en/education/resources/highschool/chemmatters/past-issues/archive-2013-2014/how-a-solar-cell-works.html>.
- [72] N. Marinova, S. Valero, J.L. Delgado, Organic and perovskite solar cells: Working principles, materials and interfaces, *J. Colloid Interface Sci.* 488 (2017) 373–389. <https://doi.org/10.1016/j.jcis.2016.11.021>.
- [73] J. Bisquert, *The Physics of Solar Cells: Perovskites, Organics, and Photovoltaic Fundamentals*, 1st ed., CRC Press, Boca Raton, 2017.
- [74] S.S. Hegedus, W.N. Shafarman, Thin-film solar cells: device measurements and analysis, *Prog. Photovolt. Res. Appl.* 12 (2004) 155–176. <https://doi.org/10.1002/pip.518>.

- [75] J.Y. Kim, J.-W. Lee, H.S. Jung, H. Shin, N.-G. Park, High-Efficiency Perovskite Solar Cells, *Chem. Rev.* 120 (2020) 7867–7918. <https://doi.org/10.1021/acs.chemrev.0c00107>.
- [76] M. Saliba, J.-P. Correa-Baena, C.M. Wolff, M. Stolterfoht, N. Phung, S. Albrecht, D. Neher, A. Abate, How to Make over 20% Efficient Perovskite Solar Cells in Regular (n–i–p) and Inverted (p–i–n) Architectures, *Chem. Mater.* 30 (2018) 4193–4201. <https://doi.org/10.1021/acs.chemmater.8b00136>.
- [77] J. Ma, D. Guo, A data review on certified perovskite solar cells efficiency and I–V metrics: Insights into materials selection and process scaling up, *Sol. Energy.* 209 (2020) 21–29. <https://doi.org/10.1016/j.solener.2020.08.090>.
- [78] N.-G. Park, K. Zhu, Scalable fabrication and coating methods for perovskite solar cells and solar modules, *Nat. Rev. Mater.* 5 (2020) 333–350. <https://doi.org/10.1038/s41578-019-0176-2>.
- [79] C. Liu, Y.-B. Cheng, Z. Ge, Understanding of perovskite crystal growth and film formation in scalable deposition processes, *Chem. Soc. Rev.* 49 (2020) 1653–1687. <https://doi.org/10.1039/C9CS00711C>.
- [80] X. Dai, K. Xu, W. Fanan, Recent progress in perovskite solar cells: the perovskite layer, *Beilstein J. Nanotechnol.* 11 (2020) 51–60. <https://doi.org/10.3762/bjnano.11.5>.
- [81] Q. Wali, F.J. Iftikhar, M.E. Khan, A. Ullah, Y. Iqbal, R. Jose, Advances in stability of perovskite solar cells, *Org. Electron.* 78 (2020) 105590. <https://doi.org/10.1016/j.orgel.2019.105590>.
- [82] J.A. Christians, S.N. Habisreutinger, J.J. Berry, J.M. Luther, Stability in Perovskite Photovoltaics: A Paradigm for Newfangled Technologies, *ACS Energy Lett.* 3 (2018) 2136–2143. <https://doi.org/10.1021/acsenergylett.8b00914>.
- [83] N. Li, X. Niu, Q. Chen, H. Zhou, Towards commercialization: the operational stability of perovskite solar cells, *Chem. Soc. Rev.* 49 (2020) 8235–8286. <https://doi.org/10.1039/D0CS00573H>.
- [84] Abd.R. bin M. Yusoff, M.K. Nazeeruddin, Organohalide Lead Perovskites for Photovoltaic Applications, *J. Phys. Chem. Lett.* 7 (2016) 851–866. <https://doi.org/10.1021/acs.jpcclett.5b02893>.
- [85] G. Xing, N. Mathews, S. Sun, S.S. Lim, Y.M. Lam, M. Grätzel, S. Mhaisalkar, T.C. Sum, Long-Range Balanced Electron- and Hole-Transport Lengths in Organic-Inorganic CH₃NH₃PbI₃, *Science.* 342 (2013) 344. <https://doi.org/10.1126/science.1243167>.
- [86] M.A. Green, Y. Hishikawa, E.D. Dunlop, D.H. Levi, J. Hohl-Ebinger, M. Yoshita, A.W.Y. Ho-Baillie, Solar cell efficiency tables (Version 53), *Prog. Photovolt. Res. Appl.* 27 (2019) 3–12. <https://doi.org/10.1002/pip.3102>.
- [87] M. Remeika, Y. Qi, Scalable solution coating of the absorber for perovskite solar cells, *J. Energy Chem.* 27 (2018) 1101–1110. <https://doi.org/10.1016/j.jechem.2017.10.005>.
- [88] J.H. Kim, S.T. Williams, N. Cho, C.-C. Chueh, A.K.-Y. Jen, Enhanced Environmental Stability of Planar Heterojunction Perovskite Solar Cells Based on

- Blade-Coating, *Adv. Energy Mater.* 5 (2015) 1401229.
<https://doi.org/10.1002/aenm.201401229>.
- [89] F. Guo, W. He, S. Qiu, C. Wang, X. Liu, K. Forberich, C.J. Brabec, Y. Mai, Sequential Deposition of High-Quality Photovoltaic Perovskite Layers via Scalable Printing Methods, *Adv. Funct. Mater.* 0 (2019) 1900964.
<https://doi.org/10.1002/adfm.201900964>.
- [90] S.-M. Park, Y.-J. Noh, S.-H. Jin, S.-I. Na, Efficient planar heterojunction perovskite solar cells fabricated via roller-coating, *Sol. Energy Mater. Sol. Cells.* 155 (2016) 14–19. <https://doi.org/10.1016/j.solmat.2016.04.059>.
- [91] J. Ciro, M.A. Mejía-Escobar, F. Jaramillo, Slot-die processing of flexible perovskite solar cells in ambient conditions, *Sol. Energy.* 150 (2017) 570–576.
<https://doi.org/10.1016/j.solener.2017.04.071>.
- [92] J. Zheng, M. Zhang, C.F.J. Lau, X. Deng, J. Kim, Q. Ma, C. Chen, M.A. Green, S. Huang, A.W.Y. Ho-Baillie, Spin-coating free fabrication for highly efficient perovskite solar cells, *Sol. Energy Mater. Sol. Cells.* 168 (2017) 165–171.
<https://doi.org/10.1016/j.solmat.2017.04.029>.
- [93] J. Ding, Q. Han, Q.-Q. Ge, D.-J. Xue, J.-Y. Ma, B.-Y. Zhao, Y.-X. Chen, J. Liu, D.B. Mitzi, J.-S. Hu, Fully Air-Bladed High-Efficiency Perovskite Photovoltaics, *Joule.* 3 (2019) 402–416. <https://doi.org/10.1016/j.joule.2018.10.025>.
- [94] D. Wang, M. Wright, N.K. Elumalai, A. Uddin, Stability of perovskite solar cells, *Sol. Energy Mater. Sol. Cells.* 147 (2016) 255–275.
<https://doi.org/10.1016/j.solmat.2015.12.025>.
- [95] Liang Jia, Liu Jie, Jin Zhong, All-Inorganic Halide Perovskites for Optoelectronics: Progress and Prospects, *Sol. RRL.* 1 (2017) 1700086.
<https://doi.org/10.1002/solr.201700086>.
- [96] T.M. Koh, J. Huang, I. Neogi, P.P. Boix, S.G. Mhaisalkar, N. Mathews, High Stability Bilayered Perovskites through Crystallization Driven Self-Assembly, *ACS Appl. Mater. Interfaces.* 9 (2017) 28743–28749.
<https://doi.org/10.1021/acsami.7b07780>.
- [97] S.N. Habisreutinger, T. Leijtens, G.E. Eperon, S.D. Stranks, R.J. Nicholas, H.J. Snaith, Carbon Nanotube/Polymer Composites as a Highly Stable Hole Collection Layer in Perovskite Solar Cells, *Nano Lett.* 14 (2014) 5561–5568.
<https://doi.org/10.1021/nl501982b>.
- [98] M.T.S. Nair, P.K. Nair, R.A. Zingaro, E.A. Meyers, Conversion of chemically deposited photosensitive CdS thin films to n-type by air annealing and ion exchange reaction, *J. Appl. Phys.* 75 (1994) 1557–1564.
<https://doi.org/10.1063/1.356391>.
- [99] H.M. Garcia, O. Gómez-Daza, J. Campos, M.T.S. Nair, P.K. Nair, Revisiting CdS-PbS Solar Cell Structure, *MRS Proc.* 1012 (2007) 1012-Y12-31.
<https://doi.org/10.1557/PROC-1012-Y12-31>.
- [100] C. Müller, T. Glaser, M. Plogmeyer, M. Sendner, S. Döring, A.A. Bakulin, C. Brzuska, R. Scheer, M.S. Pshenichnikov, W. Kowalsky, A. Pucci, R. Lovrinčić, Water Infiltration in Methylammonium Lead Iodide Perovskite: Fast and

- Inconspicuous, *Chem. Mater.* 27 (2015) 7835–7841.
<https://doi.org/10.1021/acs.chemmater.5b03883>.
- [101] N.-G. Park, Crystal growth engineering for high efficiency perovskite solar cells, *CrystEngComm.* 18 (2016) 5977–5985.
<https://doi.org/10.1039/C6CE00813E>.
- [102] J. Yang, B.D. Siempelkamp, D. Liu, T.L. Kelly, Investigation of CH₃NH₃PbI₃ Degradation Rates and Mechanisms in Controlled Humidity Environments Using in Situ Techniques, *ACS Nano.* 9 (2015) 1955–1963.
<https://doi.org/10.1021/nn506864k>.
- [103] K. Momma, F. Izumi, VESTA 3 for three-dimensional visualization of crystal, volumetric and morphology data, *J. Appl. Crystallogr.* 44 (2011) 1272–1276.
- [104] H. Hu, Z. Ren, P.W.K. Fong, M. Qin, D. Liu, D. Lei, X. Lu, G. Li, Room-Temperature Meniscus Coating of >20% Perovskite Solar Cells: A Film Formation Mechanism Investigation, *Adv. Funct. Mater.* 29 (2019) 1900092.
<https://doi.org/10.1002/adfm.201900092>.
- [105] E.N. Fuller, P.D. Schettler, J. Calvin. Giddings, NEW METHOD FOR PREDICTION OF BINARY GAS-PHASE DIFFUSION COEFFICIENTS, *Ind. Eng. Chem.* 58 (1966) 18–27. <https://doi.org/10.1021/ie50677a007>.
- [106] L. Atourki, E. Vega, B. Marí, M. Mollar, H. Ait Ahsaine, K. Bouabid, A. Ihlal, Role of the chemical substitution on the structural and luminescence properties of the mixed halide perovskite thin MAPbI₃-xBr_x (0 ≤ x ≤ 1) films, *Appl. Surf. Sci.* 371 (2016) 112–117. <https://doi.org/10.1016/j.apsusc.2016.02.207>.
- [107] M. Ouafi, B. Jaber, L. Atourki, R. Bekkari, L. Laânab, Improving UV stability of MAPbI₃ perovskite thin films by bromide incorporation, *J. Alloys Compd.* 746 (2018) 391–398. <https://doi.org/10.1016/j.jallcom.2018.02.240>.
- [108] D. Liu, Y. Li, B. Shi, X. Yao, L. Fan, S. Zhao, J. Liang, Y. Ding, C. Wei, D. Zhang, Y. Zhao, X. Zhang, Tailoring morphology and thickness of perovskite layer for flexible perovskite solar cells on plastics: The role of CH₃NH₃I concentration, *Sol. Energy.* 147 (2017) 222–227. <https://doi.org/10.1016/j.solener.2017.03.035>.
- [109] E. Mosconi, P. Umari, F. De Angelis, Electronic and optical properties of MAPbX₃ perovskites (X = I, Br, Cl): a unified DFT and GW theoretical analysis, *Phys. Chem. Chem. Phys.* 18 (2016) 27158–27164.
<https://doi.org/10.1039/C6CP03969C>.
- [110] Martin A Green, M.J. Keevers, Optical properties of intrinsic silicon at 300 K, *Prog. Photovolt. Res. Appl.* 3 (1995).
- [111] Y. Yang, M. Yang, D.T. Moore, Y. Yan, E.M. Miller, K. Zhu, M.C. Beard, Top and bottom surfaces limit carrier lifetime in lead iodide perovskite films, *Nat. Energy.* 2 (2017) 16207.
- [112] S. De Wolf, J. Holovsky, S.-J. Moon, P. Löper, B. Niesen, M. Ledinsky, F.-J. Haug, J.-H. Yum, C. Ballif, Organometallic Halide Perovskites: Sharp Optical Absorption Edge and Its Relation to Photovoltaic Performance, *J. Phys. Chem. Lett.* 5 (2014) 1035–1039. <https://doi.org/10.1021/jz500279b>.
- [113] C.C. Boyd, R. Cheacharoen, T. Leijtens, M.D. McGehee, Understanding Degradation Mechanisms and Improving Stability of Perovskite Photovoltaics,

- Chem. Rev. 119 (2019) 3418–3451.
<https://doi.org/10.1021/acs.chemrev.8b00336>.
- [114] Y. Tidhar, E. Edri, H. Weissman, D. Zohar, G. Hodes, D. Cahen, B. Rytchinski, S. Kirmayer, Crystallization of Methyl Ammonium Lead Halide Perovskites: Implications for Photovoltaic Applications, *J. Am. Chem. Soc.* 136 (2014) 13249–13256. <https://doi.org/10.1021/ja505556s>.
- [115] B. Philippe, B.-W. Park, R. Lindblad, J. Oscarsson, S. Ahmadi, E.M.J. Johansson, H. Rensmo, Chemical and Electronic Structure Characterization of Lead Halide Perovskites and Stability Behavior under Different Exposures—A Photoelectron Spectroscopy Investigation, *Chem. Mater.* 27 (2015) 1720–1731. <https://doi.org/10.1021/acs.chemmater.5b00348>.
- [116] S. Yang, Y. Chen, Y.C. Zheng, X. Chen, Y. Hou, H.G. Yang, Formation of high-quality perovskite thin film for planar heterojunction solar cells, *RSC Adv.* 5 (2015) 69502–69508. <https://doi.org/10.1039/C5RA12348H>.
- [117] K.G. Stamplecoskie, J.S. Manser, P.V. Kamat, Dual nature of the excited state in organic-inorganic lead halide perovskites, *Energy Environ. Sci.* 8 (2015) 208–215. <https://doi.org/10.1039/C4EE02988G>.
- [118] L.M. Herz, Charge-Carrier Mobilities in Metal Halide Perovskites: Fundamental Mechanisms and Limits, *ACS Energy Lett.* 2 (2017) 1539–1548. <https://doi.org/10.1021/acsenergylett.7b00276>.
- [119] M. Girtan, On the electrical and photoelectrical properties of CH₃NH₃PbI₃ perovskites thin films, *Sol. Energy.* 195 (2020) 446–453. <https://doi.org/10.1016/j.solener.2019.11.096>.
- [120] P. Basumatary, P. Agarwal, Two-step fabrication of MAPbI₃ perovskite thin films with improved stability, *Bull. Mater. Sci.* 42 (2019) 268. <https://doi.org/10.1007/s12034-019-1959-1>.
- [121] G.-H. Chiao, L.-C. Li, M. Shellaiah, K.W. Sun, Improved morphological characteristics and electronic properties of MAPbI₃ thin film with multiple methylamine spray treatments, *Org. Electron.* 78 (2020) 105556. <https://doi.org/10.1016/j.orgel.2019.105556>.
- [122] S.D. Stranks, G.E. Eperon, G. Grancini, C. Menelaou, M.J.P. Alcocer, T. Leijtens, L.M. Herz, A. Petrozza, H.J. Snaith, Electron-Hole Diffusion Lengths Exceeding 1 Micrometer in an Organometal Trihalide Perovskite Absorber, *Science.* 342 (2013) 341. <https://doi.org/10.1126/science.1243982>.
- [123] Z. Gu, F. Chen, X. Zhang, Y. Liu, C. Fan, G. Wu, H. Li, H. Chen, Novel planar heterostructure perovskite solar cells with CdS nanorods array as electron transport layer, *Sol. Energy Mater. Sol. Cells.* 140 (2015) 396–404. <https://doi.org/10.1016/j.solmat.2015.04.015>.
- [124] C. Sah, R. N. Noyce, W. Shockley, Carrier Generation and Recombination in P-N Junctions and P-N Junction Characteristics, *Proc. IRE.* 45 (1957) 1228–1243. <https://doi.org/10.1109/JRPROC.1957.278528>.
- [125] S. Marguet, Interaction of electromagnetic radiation and charged particles with matter, in: *Phys. Nucl. React.*, Springer, 2018: pp. 153–210.

- [126] D. Clark, When Light meets matter, (n.d.).
<http://weekllysciencequiz.blogspot.com/2011/09/when-light-meets-matter.html>.
- [127] Infrared Spectroscopy, (n.d.).
<https://www2.chemistry.msu.edu/faculty/reusch/virttxtjml/spectrpy/infrared/infrared.htm>.
- [128] X-Ray Diffraction (XRD), (n.d.). <https://wiki.anton-paar.com/es-es/difraccion-de-rayos-x-xrd/>.
- [129] Scanning Electron Microscopes, (n.d.).
<https://www.jeol.co.jp/en/science/sem.html>.
- [130] Atomic Force Macroscopy, (n.d.).
<https://www.nanoscience.com/techniques/atomic-force-microscopy/>.
- [131] Hall effect measurements, (n.d.).
<https://warwick.ac.uk/fac/sci/physics/current/postgraduate/regs/mpagswarwick/ex5/techniques/electronic/hall-effect>.
- [132] The Hall Effect, (n.d.). <https://www.nist.gov/pml/nanoscale-device-characterization-division/popular-links/hall-effect/hall-effect>.
- [133] I-V curve : A Guide To Measurements, (n.d.). <https://www.ossila.com/pages/iv-curves-measurement>.